[^{11}C]ABP688: Optimization of Radiosynthesis and Testing as a PET Tool to Quantify Glutamate Release *In Vivo*

Hussein Bdair, BSc Pharm, RPh, MSc

Integrated Program in Neuroscience

McGill University

Submitted October 2023

A thesis submitted to McGill University in partial fulfillment of the requirements of the degree of Doctoral of Philosophy

To my lovely wife, my parents, and my sister

I wouldn't be able to do it without your support

TABLE OF CONTENTS

LIST OF FIGURES

LIST OF TABLES

LIST OF ABBREVIATIONS

ABP688	3-((6-Methylpyridin-2-yl)ethynyl) cyclohex-2-en-1-one-*O*-methyl oxime
ACC	Anterior cingulate cortex
aCSF	Artificial cerebral spinal fluid
A_m	Molar activity
AMPA	α-amino-3-hydroxy-5-methyl-4-isoazolepropionic acid
AST	Associative striatum
AUC	Area under the curve
α	Alpha particle
BBB	Blood-brain barrier
B_{max}	Density of the target
BOLD	Blood oxygen level dependent
BP_{ND}	Non-displaceable binding potential
C-11 or 11C	Carbon-11
cAMP	Cyclic adenosine monophosphate
CB	Cannabinoid
cDNA	Complementary deoxyribonucleic acid
CNS	Central nervous system
d.e.	Diastereomeric excess
dlPFC	Dorsolateral prefrontal cortex
e^+ or b^+	Positron
e^-	Electron
EAAT	Excitatory amino acid transporter
EDDP	2-ethylene-1,5-dimethyl-3,3-diphenylpyrrolidine
EtOH	Ethanol
F-18 or 18F	Fluoride-18
FCD	Focal cortical dysplasia
FDG	Fluorodeoxyglucose
fMRI	Functional magnetic resonance imaging
FOV	Field of view
GABA	Gamma-aminobutyric acid
Gln	Tissue concentration of glutamine

Glu	Tissue concentration of glutamate
Glx	Tissue concentration of glutamate + glutamine
GM	Grey matter
GPCR	G-protein coupled receptors
HPA	Hypothalamus-pituitary-adrenal
HPLC	High-performance liquid chromatography
HRRT	High resolution research tomograph
ID	Intradermal
iGlu	Ionotropic glutamate receptors
IP	Intraperitoneal
IV	Intravenous
KA	Kainate
K_D	Dissociation constant
LTD	Long-term depression
LTP	Long-term potentiation
MAO	Monoamine oxidase
MAP	Maximum a Posteriori
MDD	Major depressive disorder
mGlu	Metabotropic glutamate receptors
MPEP	2-Methyl-6-(phenylethynyl)pyridine
mPFC	Medial prefrontal cortex
MRI	Magnetic resonance imaging
mRNA	Messenger ribonucleic acid
MRS	Magnetic resonance spectroscopy
MTEP	3-((2-Methyl-4-thiazolyl)ethynyl)pyridine
N-14 or 14N	Nitrogen-14
NAc	Nucleus accumbens
NAC	*N*-acetylcysteine
NAM	Negative allosteric modulator
NHPs	Non-human primates
NMDA	N-methyl-D-aspartate
OCD	Obsessive compulsive disorder
OFC	Orbitofrontal cortex
p	Proton
P-gp	P-glycoprotein
PAM	Positive allosteric modulator
PCP	Phencyclidine
PCR	Polymerase chain reaction

PET	Positron emission tomography
PFC	Prefrontal cortex
PKC	Protein kinase C
PND	Postnatal day
PTSD	Post-traumatic stress disorder
RCI	Radiochemical identity
RCP	Radiochemical purity
rmANOVA	Repeated measures analysis of variance
ROI	Region of interest
SC	Subcutaneous
SCR	Skin conductance response
SMST	Sensorimotor striatum
SPECT	Single photon emission computerized tomography
SRTM	Simplified reference tissue model
STAI	State-trait anxiety inventory
SUD	Substance use disorder
THC	Tetrahydrocannabinol
TTX	Tetrodotoxin
VAS	Visual analog scale
VGLUT	Vesicular glutamate transporter
VST	Ventral striatum
VTA	Ventral tegmental area
WM	White matter

ACKNOWLEDGEMENT

There are many colleagues and collaborators that I am grateful for supporting me throughout this journey. First, I would like to extend my gratitude to my thesis supervisor, Dr. Marco Leyton, for his immense support, guidance, and mentorship throughout the years. His invaluable input has inherently shaped the way I approach and conduct research. Thank you for also giving me the opportunity to pursue my professional development as a pharmacist alongside my PhD research. Second, I would like to extend my thanks and appreciation to my thesis co-supervisor, Dr. Alexey Kostikov, for his great support, mentorship, and training in radiochemistry. Thank you for providing me with the opportunity to be a part of several collaborative research projects. I'm also sincerely thankful to my late supervisor, Dr. Chawki Benkelfat, who took me under his wings during the early stages of my PhD studies and encouraged me to pursue both my clinical and research goals.

I'm also thankful for the members of my PhD advisory committee, Drs. Jean-Paul Soucy and Salah El-Mestikawi, for their support throughout my PhD journey. Additionally, I would like to thank Dr. Gassan Massarweh and his Radiochemistry team, including Robert Hopewell, Karen Ross, Dean Jolly, Arturo Aliaga, Monica Samoila and I-Huang Tsai for guiding me in my training in radiochemistry and supplying me with radiotracers for my experiments. Karen, thank you for the countless talks to encourage me during my lows. Robert, thank you for being a great friend and colleague. Arturo, I cannot thank you enough for showing up to the lab at four in the morning alongside me for some of the experiments. I would also like to thank Chris Hsiao and Reda Bouhachi for their assistance in operating the PET scanner.

I would like to express my deepest appreciation to Dr. Alain Gratton and his lab manager, Luc Moquin, for their collaboration and assistance. Luc, your expertise in microdialysis was instrumental to this project and I am thankful for the countless hours we spent optimizing my experiments. A special thanks to Drs. Sylvia Cox and Atsuko Nagano-Saito for their training in PET image analyses and their insightful discussions; Dr. Thomas Singleton from Kostikov lab for his help in organic chemistry and being the best office-colleague; Drs. Danilo de Gregorio and Luca Posa from Gobbi lab for their training in animal surgery; Dr. Min Su (Peter) Kang for his training and assistance in animal PET image co-registration and analyses; and the Centre for Animal Disease Models (CNDM) team for their assistance and training in animal care.

To my parents and sister who supported me throughout my journey and encouraged me to keep going; I cannot thank you enough for your support. I could not imagine myself being able to complete my PhD without your support.

Last, but not least, to my wife, Thana. Thank you for being by my side and my cheerleader, for supporting me during my tough times and celebrating my accomplishments during my high times. I would not be able to do this without you.

CONTRIBUTION TO ORIGINAL KNOWLEDGE

The research presented in this thesis provides a method that enhances the purity of [^{11}C]ABP688 radiotracer, an allosteric antagonist of metabotropic glutamate type 5 (mGlu5) receptors. Notably, this research also advances the knowledge on this radiotracer's potential in measuring fluctuations in extracellular glutamate concentrations.

The first study, presented in Chapter 2, provides an optimized radiosynthesis purification method that maximizes the content of the active form of the radiotracer, (*E*)-[^{11}C]ABP688, in the final product. This was achieved with high chemical and radiochemical purity, and molar activity, regardless of the precursor diastereomeric enrichment, by using a commercially available semipreparative HPLC column.

The second study presented in Chapter 3 provides a novel contribution to the field of non-invasive quantification of extracellular neurotransmitter levels. Herein, we present a first-in-kind simultaneous *in vivo* microdialysis and microPET study in rodents that examined the sensitivity of (*E*)-[^{11}C]ABP688 in measuring *in vivo* fluctuations of extracellular glutamate in response to low-dose ethanol. The simultaneous dual-technique study demonstrated that low-dose ethanol (20%, 0.5 g/kg, i.p.) resulted in significant increases in ventral striatal extracellular glutamate release, along with significant reductions in striatal [^{11}C]ABP688 binding potentials. Since changes in these two measures were not proportionate, the study indicates that modest changes in [^{11}C]ABP688 binding are influenced by glutamate release but should not be used as a quantitative index of release. These findings underscore the importance of carefully controlling testing conditions during PET imaging of mGlu5 receptor availability.

CONTRIBUTIONS OF AUTHORS

The contributions of the author and each co-author are explicitly stated below.

Chapter 1: Hussein Bdair performed the literature review, wrote and organized each section of the dissertation, and made revisions where needed based on the feedback from Drs. Marco Leyton and Alexey Kostikov.

Chapter 2: Dr. Alexey Kostikov conceived of the project. Hussein Bdair developed the HPLC purification methods and validated the tracer radiosynthesis. I-Huang Tsai contributed to the validation of the tracer radiosynthesis. Hussein Bdair drafted the manuscript in collaboration with Dr. Alexey Kostikov. Drs. Kelly Smart, Chawki Benkelfat and Marco Leyton critically reviewed the manuscript.

Chapter 3: Dr. Marco Leyton conceived of the studies in laboratory animals. Hussein Bdair and Dr. Marco Leyton designed the study. Hussein Bdair wrote the ethics protocol of the animal study and conducted the simultaneous microdialysis–microPET study in rodents, including performing animal surgeries, PET and MRI scanning, and analyzing PET and MRI images. Dr. Chawki Benkelfat conceived of the experiment in humans carried out by Marie Sato-Fitoussi, and she conducted the PET and MRS study and analysed the acquired images. Dr. Leyton conceived of the study conducted by Stéphane Planche, and he carried out the standalone microdialysis study in rodents. Luc Moquin built the microdialysis probes inhouse and analysed the dialysate samples using resources and equipment from the laboratory of Dr. Alain Gratton. Min Su (Peter) Kang assisted in analysing human and animal PET and MRI images using resources from the laboratory of Dr. Pedro Rosa-Neto. Arturo Aliaga assisted in animal microPET and MRI scanning. Atsuko

Nagano-Saito assisted in writing the ethics protocol for the human study, recruiting human participants and analyzing human PET images. Kelly Smart wrote the ethics protocol for the human study. Jamie Near provided assistance in analyzing MRS images. Argel Aguilar-Valles analysed human saliva samples. Dr. Sylvia ML Cox contributed to the writing of ethics protocol for the human study and analysing human PET and MRI images. Drs. Gassan Massarweh, Jean-Paul Soucy, and Alexey Kostikov provided access to the radiotracer, [^{11}C]ABP688. Hussein Bdair drafted the manuscript for the findings of both animal studies, including creation of images and figures. Marie Sato-Fitoussi contributed to the writing of the human study section in the manuscript. Dr. Marco Leyton contributed to the writing of the manuscript and provided critical feedback. All co-authors critically reviewed the manuscript.

Chapter 4: Hussein Bdair wrote the discussion section and included critical feedback from Drs. Marco Leyton and Alexey Kostikov.

ABSTRACT

Glutamate is the primary excitatory neurotransmitter in mammalian brain where it is found in more than half of all brain synapses. In laboratory animals, it plays an essential role in experience-dependent neuroplasticity and the acquisition of new behaviors, *i.e.*, learning. Some preliminary progress has been made in our ability to measure glutamatergic processes in human brain, including development of [^{11}C]ABP688, a positron emission tomography (PET) radiotracer. This labelled ligand is a highly selective allosteric antagonist of metabotropic glutamate type 5 (mGlu5) receptors. Studies using this PET radiotracer have reported group differences between healthy volunteers and people with neuropsychiatric disorders. Despite these encouraging results, the data have exhibited more variability than anticipated. We and others have proposed that this could reflect two features. First, common radiotracer production methods yield two distinct diastereomers: (*E*)- and (*Z*)-[^{11}C]ABP688 isomers, with the former being the active isomer that binds to mGlu5 receptors with higher affinity than the latter. Indeed, we have reported that even modest amounts of the *Z*-isomer in the injected sample can reduce estimates of radiotracer binding *in vivo*. Second, the radiotracer might be responsive to changes in extracellular glutamate. If the first problem can be resolved, we will have reduced a major source of noise in the data. If we can demonstrate that the radiotracer binding response is *proportional* to changes extracellular glutamate, we will have validated the first non-invasive measure of glutamate release in living human brain.

In the present work, we have two main objectives: (i) develop a new radiosynthesis purification method that allows for the quantitative separation of (*E*)-[^{11}C]ABP688 from the

inactive *Z*-isomer, and (ii) demonstrate that changes in extracellular glutamate concentrations are proportional to alterations of (*E*)-[^{11}C]ABP688 binding in response to ethanol (EtOH), a glutamate release inducer, using *simultaneous* microdialysis and microPET imaging in rodents.

The (*Z*)- and (*E*)-[^{11}C]ABP688 isomers were successfully separated using a readily available semipreparative HPLC column, reliably providing *E*-isomer with > 99% radiochemical purity. The *simultaneous* microdialysis and microPET study with pure (*E*)-[^{11}C]ABP688 identified significant EtOH-induced increases in ventral striatal glutamate concentrations along with significant decreases in striatal [^{11}C]ABP688 non-displaceable binding potential (BP_{ND}). Despite these trends, changes in striatal [^{11}C]ABP688 BP_{ND} did not significantly correlate with changes in extracellular glutamate. One interpretation is that [^{11}C]ABP688 binding is not systematically responsive to changes in extracellular glutamate release. A second interpretation is that the glutamate response was too small (~27%) and had too narrow of a range to reveal proportional changes in radiotracer binding.

These studies have provided a new HPLC purification method that produces >99% pure (*E*)-[^{11}C]ABP688 isomer that is suitable to conduct pre-clinical and clinical imaging studies. Using purified isomer in rodents, we have shown that moderate increases in glutamate release result in significant, yet non-proportional, decreases in [^{11}C]ABP688 BP_{ND}, underscoring the need for highly controlled testing conditions during PET studies of mGlu5 receptors.

RÉSUMÉ

Le glutamate est le principal neurotransmetteur excitateur du cerveau des mammifères et se trouve dans plus de la moitié des synapses cérébrales. Chez les animaux de laboratoire, il joue un rôle essentiel dans la neuroplasticité dépendante de l'expérience et l'acquisition de nouveaux comportements, c'est-à-dire l'apprentissage. Des progrès préliminaires ont été réalisés dans notre capacité à mesurer les processus glutamatergiques dans le cerveau humain, notamment grâce à la mise au point du [^{11}C]ABP688, un radiotraceur pour la tomographie par émission de positrons (TEP). Ce ligand marqué est un antagoniste allostérique hautement sélectif des récepteurs métabotropiques du glutamate de type 5 (mGlu5). Les études utilisant ce radiotraceur TEP ont fait état de différences de groupe entre les volontaires sains et les personnes souffrant de troubles neuropsychiatriques. Malgré ces résultats encourageants, les données ont montré plus de variabilité que prévu. Nous avons proposé, avec d'autres, que ces variabilités puissent refléter deux caractéristiques. Premièrement, les méthodes courantes de production de radiotraceurs produisent deux diastéréoisomères distincts : les isomères (*E*)- et (*Z*)-[^{11}C]ABP688, le premier étant l'isomère actif qui se lie aux récepteurs mGlu5 avec une plus grande affinité que le second. En effet, nous avons signalé que même des quantités modestes de l'isomère Z dans l'échantillon injecté peuvent réduire les estimations de la liaison du radiotraceur in vivo. Deuxièmement, le radiotraceur pourrait réagir aux variations du glutamate extracellulaire. Si le premier problème peut être résolu, nous aurons réduit une source importante de bruit dans les données. Ensuite, si nous pouvons démontrer que la réponse de la liaison du radiotraceur est proportionnelle aux changements du glutamate

extracellulaire, nous aurons validé la première mesure non invasive de la libération de glutamate dans le cerveau humain vivant.

Dans le présent travail, nous avons deux objectifs principaux : (i) développer une nouvelle méthode de purification de la radiosynthèse qui permet la séparation quantitative du (*E*)-[^{11}C]ABP688 de l'isomère Z inactif, et (ii) démontrer que les changements dans les concentrations extracellulaires de glutamate sont proportionnels aux modifications de la liaison du (*E*)-[^{11}C]ABP688 en réponse à l'éthanol (EtOH), un inducteur de la libération de glutamate, en utilisant simultanément la microdialyse et l'imagerie microPET chez les rongeurs.

Les isomères (*Z*)- et (*E*)-[^{11}C]ABP688 ont été séparés avec succès à l'aide d'une colonne HPLC semi-préparative facilement disponible, fournissant de manière fiable l'isomère E avec une pureté radiochimique > 99%. L'étude simultanée de microdialyse et de microTEP avec du (*E*)-[^{11}C]ABP688 pur a identifié des augmentations significatives induites par l'EtOH dans les concentrations de glutamate du striatum ventral ainsi que des diminutions significatives du potentiel de liaison non déplaçable (BP_{ND}) du [^{11}C]ABP688 au niveau du striatum. Malgré ces tendances, les changements dans le BP_{ND} [^{11}C]ABP688 striatal n'ont pas été significativement corrélés avec les changements dans le glutamate extracellulaire. Une interprétation possible est que la liaison de l'[^{11}C]ABP688 n'est pas systématiquement sensible aux changements dans la libération de glutamate extracellulaire. Une deuxième interprétation est que la réponse au glutamate était trop faible (~27%) et avait une gamme trop étroite pour révéler des changements proportionnels dans la liaison du radiotraceur.

Ces études ont permis de mettre au point une nouvelle méthode de purification par HPLC qui produit un isomère (*E*)-[^{11}C]ABP688 pur à plus de 99 %, adapté à la réalisation d'études d'imagerie précliniques et cliniques. En utilisant l'isomère purifié chez les rongeurs, nous avons

montré que des augmentations modérées de la libération de glutamate entraînent des diminutions significatives, mais non proportionnelles, du BP_{ND} [^{11}C]ABP688, soulignant la nécessité de conditions d'essai hautement contrôlées lors des études TEP sur les récepteurs mGlu5.

CHAPTER 1: Introduction

Overview

1.1. Glutamatergic Neurotransmission

Glutamate was known to have several effects in the central nervous system (CNS) for over half a century, but it was not recognized as a neurotransmitter until 1984 when Fonnum summarized the evidence that it fulfilled all four required features: (i) it is localized in presynaptic neurons, (ii) it is released in response to physiological stimuli to elicit a postsynaptic response, (iii) it possesses a unique mechanism of action to identify it as a naturally occurring neurotransmitter, and (iv) it has mechanisms to rapidly terminate its transmitting actions (Fonnum, 1984). Under this new classification, glutamate also became the most ubiquitous neurotransmitter in mammalian CNS.

Due to its abundant presence in intracellular compartments, extracellular glutamate levels are tightly regulated to ensure optimal neurotransmission. The tight control of glutamatergic neurotransmission is an energy-consuming process that requires high amounts of glucose oxidation (Shen *et al.*, 1999). Glutamatergic neurotransmission commences with the transmitter in presynaptic cytoplasm crossing into synaptic vesicles *via* vesicular glutamate transporters (VGLUTs) (Takamori, 2006). Glutamate is then released *via* Ca^{2+}-dependent exocytosis into synaptic clefts to elicit effect on postsynaptic receptors (Bollmann, Sakmann, & Borst, 2000; Pang & Sudhof, 2010). Extracellular glutamate is then cleared from synaptic clefts into adjacent astrocytes *via* excitatory amino acid transporters (EAATs) (O'Shea, 2002). Subsequently, cytosolic glutamate in astrocytes is then converted to glutamine *via* glutamine synthetase. Glutamine then crosses from astrocytes to adjacent neurons *via* glutamine transporters and reconverts into glutamate *via* phosphate-specific glutaminase, for subsequent encapsulation into neuronal synaptic vesicles (Shen *et al.*, 1999). Noteworthy, due to the lack of neuronal enzymes necessary for

glutamate synthesis, glial cells are considered the main source of the precursor, glutamine, for glutamate repletion in neurons.

1.1.1. Ionotropic *vs*. Metabotropic Glutamate Receptor Signaling

Glutamate signaling is mediated by two sets of receptors that can be broadly categorized as (i) fast excitatory ligand-gated ion channels known as ionotropic glutamate (iGlu) receptors, and (ii) slow modulatory seven transmembrane domain metabotropic glutamate (mGlu) receptors. Three classes of iGlu receptors have been identified, including *N*-methyl-D-aspartate (NMDA), *α*-amino-3-hydroxy-5-methyl-4-isoazolepropionic acid (AMPA) and kainate (KA) receptors. Contrary to the iGlu receptors that are cation (Na^+, Ca^{2+}) flux dependent, mGlu receptors are G-protein coupled receptors (GPCRs) that upon glutamate binding lead to activation or inhibition of downstream cascade of second messengers (Meldrum, 2000). A total of eight mGlu receptors have been identified to date and are classified into three main groups, based on sequence homology, pharmacological profile and second messenger coupling (Conn, 2003). Group I (mGlu1 and mGlu5) receptors are G_q-coupled that increase hydrolysis of the membrane phosphoinositide by phospholipase C (Conn, 2003; Niciu, Kelmendi, & Sanacora, 2012). Although evidence for presynaptic functions have been reported, Group I mGlu receptors are predominantly located on postsynaptic neurons (Pin, Galvez, & Prezeau, 2003; Pinheiro & Mulle, 2008; Smart *et al.*, 2021). In comparison, Group II (mGlu2 and mGlu3) and Group III (mGlu4, mGlu6, mGlu7 and mGlu8) are $G_{i/o}$-coupled receptors that decrease intracellular cyclic adenosine monophosphate (cAMP) *via* inhibition of adenylyl cyclase (Conn, 2003; Niciu, Kelmendi, & Sanacora, 2012). Group II receptors are located both pre- and post-synaptically, whereas Group III receptors are consistently found at presynaptic sites (Bodzeta, Scheefhals, & MacGillavry, 2021; Pin, Galvez, & Prezeau,

2003). Main components of the tripartite glutamatergic synaptic transmission are illustrated in Figure 1.1. Given that mGlu5 receptors are the target site of the radiotracer used in this research, [^{11}C]ABP688, this dissertation will review these receptors in further detail.

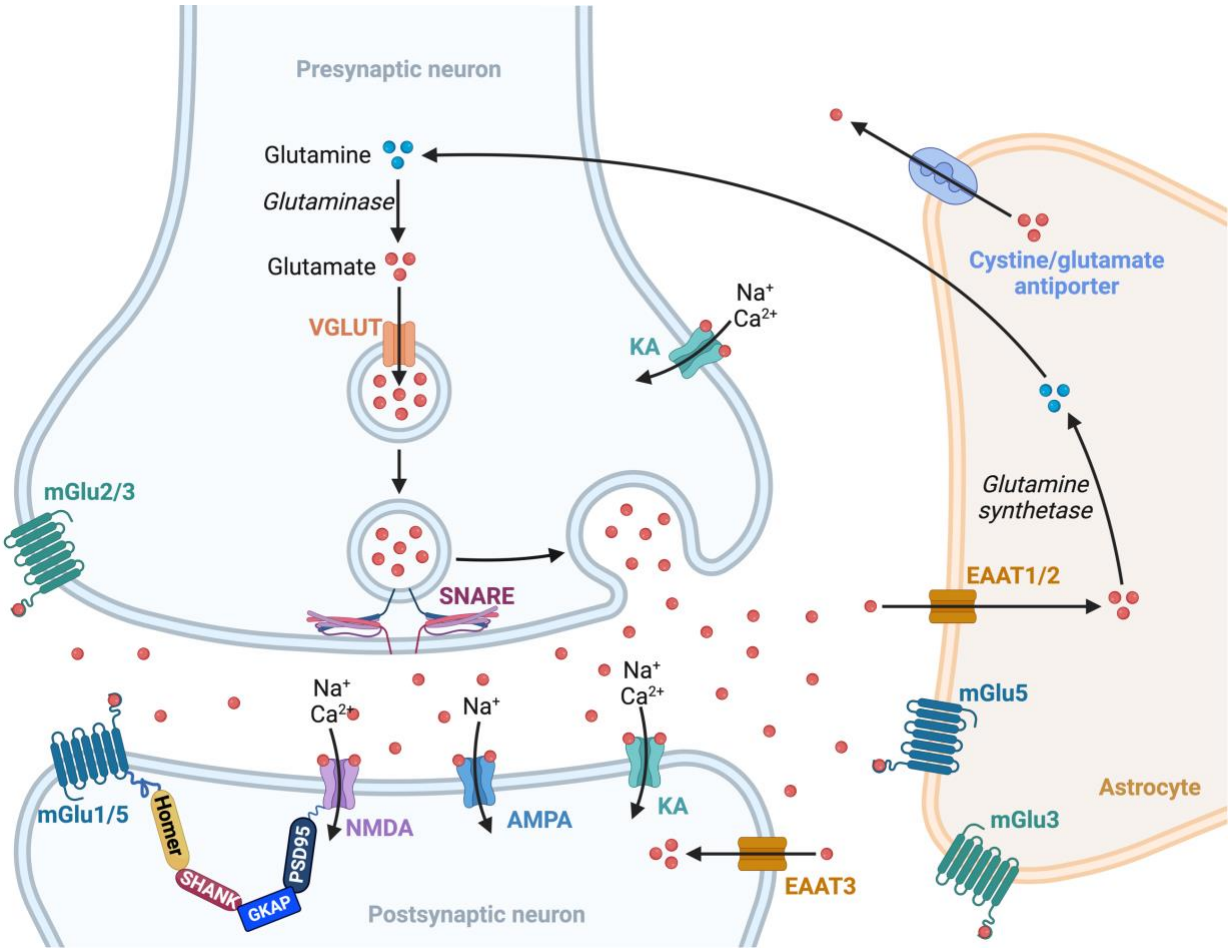

Figure 1.1: Schematic illustration of major components of the glutamatergic synaptic transmission. Neuronal glutamate is synthesized in the presynaptic neurons from glutamine *via* glutaminase. Glutamate is then encapsulated into the synaptic vesicles *via* vascular glutamate transporters (VGLUTs). SNARE proteins mediate the mobilization and fusion of the synaptic vesicles with the membrane of the presynaptic neuron. Neuronal glutamate is then released from the presynaptic neuron into the synaptic cleft where it binds to the ionotropic (AMPA, NMDA, and KA) and metabotropic (mGlu1-8) receptors located on the membranes of both presynaptic and postsynaptic neurons, as well as astrocytes. Extracellular glutamate is then scavenged from synaptic clefts *via* excitatory amino acid transporters (EAATs) into adjacent astrocytes. Glutamate is then converted to glutamine *via* glutamine synthetase, which diffuses back to the presynaptic neurons. Glial glutamate could also be released into the synaptic cleft *via* cystine-glutamate antiporter. mGlu5 receptor is connected indirectly to NMDA receptor *via* Homer, SHANK, GKAP and PSD95 proteins. The figure is created with BioRender.com.

1.1.2. Neuroanatomical Distribution of mGlu5 Receptors

Mapping of mGlu5 receptors in the brain was first attempted by Abe *et al* when they reported cloning of these receptors from a rat brain complementary deoxyribonucleic acid (cDNA) library, using polymerase chain reaction (PCR)-mediated DNA amplification technique (Abe *et al.,* 1992). The hydrophobicity analysis showed that the mGlu5 protein consists of eight hydrophobic segments. One segment is located at the N-terminus and presumed to serve as a signaling domain, whereas the other seven segments are transmembrane-spanning domains located at the C-terminus typical to most GPCR (Abe *et al.,* 1992; Masu *et al.,* 1991). Interestingly, it was found that the extracellular signaling domain at the N-terminus accounts for almost half the amino acid residues in the entire rat mGlu5 protein (560 out of 1171) (Abe *et al.,* 1992). Subsequent cloning of the human mGlu5 receptor demonstrated a large sequence homology (94.9%) to rat mGlu5 receptors, with the extracellular N-terminus being extremely well conserved between species (98.6%) (Minakami *et al.,* 1994). By using in situ hybridization technique, it was shown that mGlu5 messenger ribonucleic acid (mRNA) is highly expressed in the olfactory bulb, anterior olfactory nuclei, olfactory tubercle, dorsal (*i.e.,* caudate/putamen) and ventral (*i.e.,* nucleus accumbens; NAc) striatum. Extensive expression of mGlu5 mRNA was also observed in the granular and pyramidal regions of the hippocampus, thalamic nuclei, and the inferior colliculus. The cerebral cortex exhibited moderate expression levels of mGlu5 mRNA with higher expression in the superficial than in the deeper cortical layers (Abe *et al.,* 1992; Kerner *et al.,* 1997; Testa *et al.,* 1994). Conversely, only a small number of Golgi cells in the cerebellar cortex expressed mGlu5 mRNA, with almost no expression in the pons and medulla (Abe *et al.,* 1992). These findings were later reproduced *via* immunohistochemical techniques, using rodent mGlu5-specific antibodies (Romano *et al.,* 1995; Shigemoto *et al.,* 1993).

These features noted, substantial discrepancies regarding mGlu5 receptor localization existed in early studies. For instance, at the synaptic level, some studies reported significant expression of mGlu5 receptor at presynaptic terminals (Romano *et al.*, 1995), whereas others did not (Hubert, Paquet, & Smith, 2001; Shigemoto *et al.*, 1993). Similarly, at the neuronal level, some studies showed substantial mGlu5 expression on cell bodies (Paquet & Smith, 2003), while other reported negligible amounts at these sites (Romano *et al.*, 1995; Shigemoto *et al.*, 1993). This might be attributed to the variations in species, techniques and brain regions being investigated. Nevertheless, by using a validated mGlu5 receptor antibody, a recent study demonstrated that mGlu5 receptors are predominately expressed on the postsynaptic elements within close proximity to both the postsynaptic scaffold protein PSD95, a protein that physically links mGlu5 to NMDA receptors, and VGLUT1, evidence that the receptor is present at excitatory synapses (Smart *et al.*, 2021). Finally, mGlu5 receptors are also expressed extrasynaptically on glial cells where they play an important role modulating glutamatergic gliotransmission (Aronica *et al.*, 2003; D'Ascenzo *et al.*, 2007).

1.1.3. Role of mGlu5 Receptors in Glutamatergic Signaling

mGlu5 receptors modulate the release of glutamate and other neurotransmitters. Structurally, mGlu5 receptors exist as disulfide-linked dimers (Kunishima *et al.*, 2000; Romano, Yang, & O'Malley, 1996), predominantly in the postsynaptic elements of excitatory glutamatergic synapses, as well as extrasynaptically on astrocytes (Shigemoto *et al.*, 1993; van den Pol, Romano, & Ghosh, 1995). Upon glutamate binding, mGlu5 couples to G_q proteins that activate phospholipase C ultimately leading to an increase in intracellular Ca^{2+} concentration (Abe *et al.*, 1992). The functional interaction between mGlu5 and NMDA receptors, mediated by a protein

scaffold that links these two types of receptors (Naisbitt *et al.*, 1999; Tu *et al.*, 1999), has been widely investigated. The mGlu5 receptors have been found to positively modulate NMDA receptor activity *via* phosphorylation of protein kinase C (PKC) and/or tyrosine kinase, depending on the brain region (Collett & Collingridge, 2004; Kotecha *et al.*, 2003). Additionally, activation of mGlu5 receptors lead to a developmental alteration in NMDA subunit composition, which is essential in experience- and activity-dependent regulation of NMDA receptors (Matta *et al.*, 2011; Paoletti, Bellone, & Zhou, 2013). This functional interaction between mGlu5 and NDMA receptors is believed to mediate the modulatory effect of mGlu5 in long-term potentiation (LTP), a form of synaptic plasticity where repeated activation leads to a persistent strengthening of synapses (Anwyl, 2009). These effects are considered essential in regulating NMDA-dependent cognitive functions, such as learning and memory (Homayoun *et al.*, 2004). In the contrary situation, mGlu5-knockout mice exhibit reductions in NMDA-dependent LTP in certain regions in the hippocampus and, hence, impaired learning (Jia *et al.*, 1998; Lu *et al.*, 1997). A possible underlying mechanism of the modulatory role of mGlu5 receptors in LTP is *via* enhancing the synthesis of endocannabinoids in postsynaptic neurons. The released endocannabinoids activate cannabinoid type 1 (CB1) receptors, mainly present at presynaptic glutamatergic terminals, which inhibit further glutamate release (Olmo, Ferreira-Vieira, & Ribeiro, 2016).

There is compelling evidence that mGlu5 receptors exert many of their physiological effects *via* interaction with other receptors, making it challenging to study the isolated roles of mGlu5 in cognitive and behavioral functions. For instance, corticostriatal LTP requires co-activation of both mGlu1 and mGlu5 receptors (Gubellini *et al.*, 2003). Furthermore, in mice, morphine tolerance was partially reversed by administering mGlu1 and mGlu5 antagonists individually, whereas co-administration of both antagonists completely reversed the tolerance

(Smith *et al.*, 2004). Since mGlu5 receptors are homodimeric (Romano, Yang, & O'Malley, 1996), the interaction between the mGlu1 and mGlu5 receptors are believed to be caused by distinct, yet overlapping, signaling pathways (Thandi, Blank, & Challiss, 2002).

1.1.4. Behavioral Effects of mGlu5 Receptor Transmission

1.1.4.1. Experience-dependent Plasticity and Meta-plasticity

As noted above, mGlu5 receptors play an essential role in regulating NMDA-dependent cognitive functions including learning, memory, and behavioral flexibility (*i.e.*, adaptive changes in response to environmental changes) (Homayoun *et al.*, 2004; Pisani *et al.*, 2001; Stefani & Moghaddam, 2010). For instance, LTP is typically induced in hippocampus *via* activation of NMDA receptors (Abraham & Mason, 1988; Aksoy-Aksel & Manahan-Vaughan, 2015; Davis *et al.*, 1997; Morris *et al.*, 1986), although NMDA-independent forms of LTP induction has also been reported (Derrick, Weinberger, & Martinez, 1991). Activation of mGlu5 receptors, *via* either agonists at the orthrosteric site or positive allosteric modulators (PAMs) at the allosteric site, enhances NMDA-induced LTP (Awad *et al.*, 2000; Ayala *et al.*, 2009; Raymond *et al.*, 2000). Furthermore, mGlu5 receptors regulate NMDA-dependent experience-facilitated long-term depression (LTD), a persistent activity-dependent reduction in synaptic plasticity (Goh & Manahan-Vaughan, 2013; Popkirov & Manahan-Vaughan, 2011). Antagonism of mGlu5 receptors has also shown to suppress both NMDA-dependent (Popkirov & Manahan-Vaughan, 2011) and independent forms of LTD (Faas *et al.*, 2002).

Meta-plasticity, a term first coined in 1996 by Abraham and Bear, who simply defined it as the “plasticity of synaptic plasticity” (Abraham & Bear, 1996), refers to the ability to further modulate synaptic plasticity based on prior activity-dependent changes in neuronal functions.

Meta-plasticity was first observed following the activation of NDMA receptors, which inhibited subsequent NMDA-dependent LTP induction in hippocampus (*i.e.*, raising the threshold for LTP) (Coan, Irving, & Collingridge, 1989; Huang *et al.*, 1992). Contrary to the inhibitory effects of NMDA receptor activation on LTP, studies have shown that activation of mGlu5 receptors mediates both the induction and persistence of NMDA-dependent LTP (*i.e.*, lowering the threshold for LTP) (Bortolotto *et al.*, 1994; Bortolotto *et al.*, 2005). It has been proposed that a mGlu5-mediated "molecular switch" – a form of meta-plasticity – needs to be set for the induction of LTP. Once the "molecular switch" is set *via* the activation of mGlu5 receptors, it stays activated for a prolonged duration, negating the need for further activation of mGlu5 receptors for subsequent LTP induction (Bortolotto *et al.*, 1994; Bortolotto *et al.*, 2005).

1.1.4.2. Stress-induced Glutamate Release

The ability of environmental stressors to increase extracellular glutamate release was first studied using *in vivo* microdialysis in rodents, where acute stress resulted in significant increase in glutamate concentration, mainly in medial prefrontal cortex (mPFC), but also in striatum, hippocampus and NAc (Lupinsky, Moquin, & Gratton, 2010; Moghaddam, 1993). The source of stress-induced glutamate release, whether neuronal or glial, is a question of interest. There are two major classical criteria for neuronal glutamate release: (i) dependence on opening of voltage-gated Na^+ channel, and (ii) Ca^{2+} dependence of release (Musazzi, Racagni, & Popoli, 2011). Blockade of Na^+ conductance with the Na^+ channel blocker tetrodotoxin (TTX) significantly reduces (Moghaddam, 1993) or practically abolishes (Lupinsky, Moquin, & Gratton, 2010) stress-induced glutamate release in PFC, whereas baseline PFC glutamate levels are TTX insensitive (Hashimoto, Oka, & Nishikawa, 1995; Moghaddam, 1993). Furthermore, stress-induced glutamate release was

suppressed following the use of Ca^{2+}-free artificial cerebrospinal fluid (aCSF), but was unaffected in response to a glial cysteine-glutamate exchange blocker (Lupinsky, Moquin, & Gratton, 2010). These findings were also confirmed *via* using rapid microelectrode arrays (Hascup *et al.*, 2010), suggesting that stress-induced glutamate release is largely of neuronal origin.

Glucocorticoids, stress hormones released from the adrenal glands, have been implicated in mediating the glutamate stress response. Acute stress is believed to boost glutamate release from presynaptic terminals in response to a rapid increase in circulating corticosterone (cortisol in humans), a type of glucocorticoid. This in turn enhances the docking of glutamate-containing synaptic vesicles to the presynaptic membrane for subsequent release into synaptic clefts (Musazzi *et al.*, 2010; Popoli *et al.*, 2011). Glucocorticoids can also indirectly influence glutamate release *via* enhancing endocannabinoids production, which in turn stimulate presynaptic CB1 receptors that negatively regulate glutamate release (Hill *et al.*, 2010; Popoli *et al.*, 2011).

The relationship between extracellular glutamate levels and mGlu5 receptor availability is complex. Some studies have shown that acute or chronic mild stress leads to increased hippocampal mGlu5 receptor expression, which is believed to be mediated by glucocorticoid and CB1 receptors (Sun *et al.*, 2017). Other studies, however, identify a reduction in astrocytic mGlu5 receptor expression in the hippocampus in response to chronic stress (Liu *et al.*, 2022). This discrepancy might reflect differences in the duration, intensity, and type of stressor being used. For instance, persistent activation of glucocorticoid receptors caused by chronic exposure to corticosteroids leads to downregulation of mGlu5 receptors (Iyo *et al.*, 2010), which in turn could explain the reduced expression levels of mGlu5 receptors in response to chronic stress. In comparison, the increase in hippocampal mGlu5 receptor expression in response to acute stress might be explained by the downregulation in CB1 receptors (Sun *et al.*, 2017).

1.1.5. Effect of Ethanol on Glutamatergic Neurotransmission

Ethanol (EtOH), the active ingredient in alcoholic beverages, is considered the most widely used psychoactive substance in Canada ("Alcohol and Drug Use in Canada," 2019). Because of its widespread availability and legal status, EtOH use has been associated with a high risk of addiction with devastating health outcomes. Our understanding of EtOH's neuropharmacological effects remains limited, but a few pharmacological targets have been identified. This includes NMDA (Lovinger, White, & Weight, 1989), γ-aminobutyric acid type A ($GABA_A$) (Brickley & Mody, 2012), glycine (Mihic *et al.*, 1997), 5-hydroxytryptamine type 3 (serotonin; $5\text{-}HT_3$) (Lovinger, 1999), dopamine (DA) D_3 (Heidbreder *et al.*, 2007), and nicotinic acetylcholine (nACh) receptors (Narahashi *et al.*, 1999) as well as L-type calcium (Wang *et al.*, 1994) and G-protein activated inwardly rectifying K^+ channels (Kobayashi *et al.*, 1999). The neuropharmacology of EtOH has been previously reviewed by Venegeliene *et al* (Vengeliene *et al.*, 2008).

The glutamatergic system has been widely implicated in the rewarding and reinforcing effects of ethanol (EtOH). This was first demonstrated by reduction in self-administration of EtOH in rodents following microinjection of a competitive NMDA receptor antagonist in NAc (Rassnick, Pulvirenti, & Koob, 1992). This effect is not limited to NMDA receptors since antagonists of mGlu5 receptors have also shown to decrease self-administration of EtOH in rats (Backstrom *et al.*, 2004; Besheer *et al.*, 2008; Schroeder, Overstreet, & Hodge, 2005). It has also been demonstrated that acute EtOH administration could enhance glutamate release in various brain regions, such as the ventral tegmental area (VTA) (Xiao *et al.*, 2009), anterior cingulate cortex (ACC) (Zuo *et al.*, 2007), and prefrontal cortex (PFC) (Fliegel *et al.*, 2013; Selim & Bradberry, 1996). In the NAc, various studies have reported a significant increase in extracellular glutamate concentrations following EtOH administration; however, the results among these studies are

surprisingly inconsistent. For instance, some microdialysis studies did not reveal any significant change in NAc glutamate concentrations in response to neither acute nor chronic exposure to various doses of EtOH (Dahchour, Quertemont, & De Witte, 1996; Kashkin & De Witte, 2004), whereas other studies show a significant increase (Selim & Bradberry, 1996) or decrease (Yan *et al.*, 1998) in NAc glutamate levels in response to acute EtOH exposure. Intriguingly, a meta-analysis study by Fliegel *et al* has shown that the higher the dose of EtOH (1 g/kg *vs*. 2 g/kg *vs*. 3 g/kg), the lower extracellular glutamate is being released in the NAc (Fliegel *et al.*, 2013). By extrapolating the line constructed from glutamate release levels in response to the three doses of EtOH (1, 2 and 3 g/kg) (Fliegel *et al.*, 2013), it is hypothesized that the use of a lower dose of EtOH (0.5 g/kg) will lead to a higher level of extracellular glutamate in NAc. Furthermore, the origin of EtOH-induced glutamate release in the NAc (neuronal *vs*. glial) remains a question of interest. This topic is further discussed in Chapter 3.

1.2. *In Vivo* Imaging of Glutamatergic Neurotransmission

Quantification of neurotransmitter levels *in vivo* is integral to understanding their role in the pathophysiology of neuropsychiatric disorders and medication mechanisms. There is a growing number of techniques to measure glutamatergic neurotransmission *in vivo* in laboratory animals. In striking contrast, there is a paucity of tools to quantify glutamate release in living human brain. Positron emission tomography (PET) is a non-invasive imaging modality that provides a real-time measurement of various physiological functions, such as blood flow, metabolism, as well as receptor occupancy, density, and distribution. Developing a PET radioligand to quantify extracellular glutamate concentrations would be a highly valuable tool to expand our understanding of the glutamatergic system. The literature review below summarizes the current

state of PET radiotracers for glutamatergic system imaging. Part of the following material is from the author's book chapter on preclinical brain PET imaging (Bdair *et al.*, 2023; accepted).

1.2.1. PET and Glutamatergic Neurotransmission

1.2.1.1. Basics of PET Imaging

PET enables detection and mapping of discrete physiological processes implicated in cancers, heart, and brain diseases. PET radiotracers — radioisotopically labelled molecules targeting specific biomarkers — are administered to living subjects *via* intravenous bolus, infusion, or bolus and constant infusion injections, or *via* inhalation. Following beta-plus decay of the radioisotope, a positron (e^+ or β^+) is emitted from the radiotracer and, upon colliding with an electron (e^-), the two particles annihilate to emit two gamma (γ) photons travelling in the opposite directions near the speed of light. These γ photons are then simultaneously captured by the opposite scintillation detectors located in the scanner bore and reconstructed to generate a three-dimensional image of the radiotracer biodistribution over time and, by extension, expression of the targeted biomarker (Krishnamoorthy, Schmall, & Surti, 2017).

[^{18}F]Fluorodeoxyglucose ([^{18}F]FDG) has been a valuable diagnostic PET tool in detecting tumours and their metastases for several decades and is now considered the gold standard radiotracer in diagnosing and staging various cancers. More recently, PET has been rapidly evolving beyond [^{18}F]FDG thanks to the development of the target-specific radiotracers for imaging amyloid load (Garber, 2012), tau protein aggregates (Barthel, 2020) and amino acid decarboxylase (Dhawan *et al.*, 2020) in neurodegenerative diseases as well as neuroendocrine (Hennrich & Kopka, 2019) and prostate tumors (Wurzer *et al.*, 2021), to name a few. Validation of all novel PET tracers involves their preclinical evaluation in various animal species and often

begins with imaging of the small rodents. While mice are perfectly suited for the evaluation of cancer-targeting onco-radiotracers due to the abundance of genetic and xenograft models, the small anatomical size of their brains makes the mice models suboptimal for preliminary studies of the neuro radiotracers. Rats are therefore preferred for brain radiotracer development workflow since they offer a good compromise between brain size, affordability, abundant disease models, and translational potential towards human studies.

For a PET radiotracer to be useful in neuroimaging, certain criteria must first be met (Eckelman & Mathis, 2006; Majo *et al.*, 2013; Waterhouse, 2003): (1) the radiotracer must have a high affinity to its target (in the range of nanomolar IC_{50} or K_i values) along with high selectivity and specificity. For a radiotracer to be considered selective, its affinity to the target needs to be at least 20 times greater than that to other biomarkers in the brain; (2) the molecule must be amenable for facile radiolabelling with either carbon-11 (^{11}C) or fluoride-18 (^{18}F) in high molar activity (A_m). High A_m is essential to avoid significant self-blockade by the non-radioactive (*i.e.*, "cold") counterpart; (3) the ligand must have moderately high lipophilicity (octanol/water distribution (log D) of 1-3.5) and low molecular weight ($\leq$ 450 g/mol) to make it to blood-brain barrier (BBB)-permeable; (4) it must not be a substrate to P-glycoprotein (P-gp) efflux mechanism; (5) it must be metabolically stable or its radiometabolites are either polar (*i.e.*, not brain permeable); (6) the radiotracer's binding potential (BP), the ratio of the density/concentration of the target (B_{max}) to the radiotracer's equilibrium dissociation constant (K_D), must be at least 10 in order to provide a specific signal *in vivo*; and (7) does not exhibit high affinity to peripheral binding sites, such as albumin or other plasma proteins.

1.2.1.2. PET Imaging of Glutamatergic Neurotransmission

Over the past three decades, several PET radiotracers have been developed for *in vivo* imaging of glutamatergic receptors. Herein, I will be reviewing the latest developments in iGlu and mGlu PET radioligands.

1.2.1.2.1. PET Imaging of iGlu Receptors

As noted previously, iGlu receptors are subdivided into three types: NMDA, AMPA and KA receptors. To date, most of PET radioligands for the ionotropic AMPA and KA receptors have failed to demonstrate *in vivo* specific binding, despite exhibiting promising binding properties *in vitro*. For example, ^{11}C- and ^{18}F-labelled *N*-Acetyl-1-aryl-6,7-dimethoxy-1,2,3,4-tetrahydroisoquinoline derivatives, which are highly potent non-competitive AMPA receptor antagonists (Gitto *et al.*, 2003), have been proposed as potential AMPA receptor PET radioligands (Gao *et al.*, 2006). Nonetheless, no *in vivo* evaluation of these radiotracers has been reported to date. Årstad and colleagues reported the radiosynthesis and *in vivo* evaluation of 2-acetyl-1-(4'-chlorophenyl)-6-methoxy-7-[^{11}C]methoxy-1,2,3,4-tetrahydroisoquinoline ([^{11}C]**1**) in rats (Arstad *et al.*, 2006). Preclinical studies with [^{11}C]**1** showed uniform distribution in the CNS with no specific uptake by AMPA-rich brain regions (Arstad *et al.*, 2006). Similarly, *in vitro* autoradiography studies of [^{18}F]LY395153, a PAM of AMPA receptors, revealed high non-specific binding resulting in a largely uninformative uniform distribution across brain regions (Kronenberg *et al.*, 2007). The labelled AMPA receptor antagonist [^{11}C]HMS011 was translated to human studies following its *in vivo* evaluation in rodents and monkeys, and it exhibited moderate brain uptake in laboratory animals with a distribution consistent with the results of autoradiography (Oi *et al.*, 2015). However, [^{11}C]HMS011 exhibited minimal specific binding in human cortex

(Takahata *et al.*, 2017). Furthermore, The AMPA PET candidate ^{18}F-labelled 2-(1-(3-fluorophenyl)-2-oxo-5-(pyrimidin-2-yl)-1,2-dihydropyridin-3-yl) benzonitrile ([^{18}F]**8**) has displayed a decent brain uptake in mice (Yuan *et al.*, 2016). However, no studies examining the *in vivo* specificity and selectivity of this radiotracer have been reported to date. Another AMPA PAM, [^{11}C]AMPA-1905 (Goffin *et al.*, 2018; Miao *et al.*, 2019), was also evaluated in rodents and showed high non-specific binding that could not be blocked by the AMPA receptor antagonist talampanel (Chen *et al.*, 2020). Excitingly, Miyazaki and colleagues have succeeded in developing the first PET radioligand, named [^{11}C]K-2, with demonstrated specificity and selectivity for AMPA receptors in rats and humans (Miyazaki *et al.*, 2020). [^{11}C]K-2 converted rapidly in the brain to its metabolite, [^{11}C]K-2$_{OH}$, with the latter exhibiting a similar binding affinity of the parent compound to cell-surface AMPA receptors, and both lacking affinity to NMDA and KA receptors (Arisawa *et al.*, 2021; Miyazaki *et al.*, 2020). In epileptic patients, [^{11}C]K-2 imaging was shown to provide a direct measure of the elevated excitability of the epileptogenic focus through increased retention of the radiotracer, which offers an advantage of the current imaging tool with [^{18}F]FDG that detects indirect changes (*i.e.*, reduced glucose metabolism) related to the epileptogenic focus (Miyazaki *et al.*, 2020). More recently, several fluorinated analogues of [^{11}C]K-2 have been developed with only one of them, [^{18}F]2, showed *in vivo* affinity to AMPA receptors in the same range of [^{11}C]K-2 (Arisawa *et al.*, 2022). Chemical structures of PET radioligand candidates for AMPA receptors are illustrated in Figure 1.2.

The only PET candidate for KA receptors reported in the literature is a ^{11}C-labelled acromelic acid A analogue; however, its affinity to AMPA receptors is greater than that to KA receptors (Kanazawa *et al.*, 2011). To date, no selective KA receptor-targeting PET radiotracers have been reported, most likely due to the lack of high-affinity ligands for these receptors.

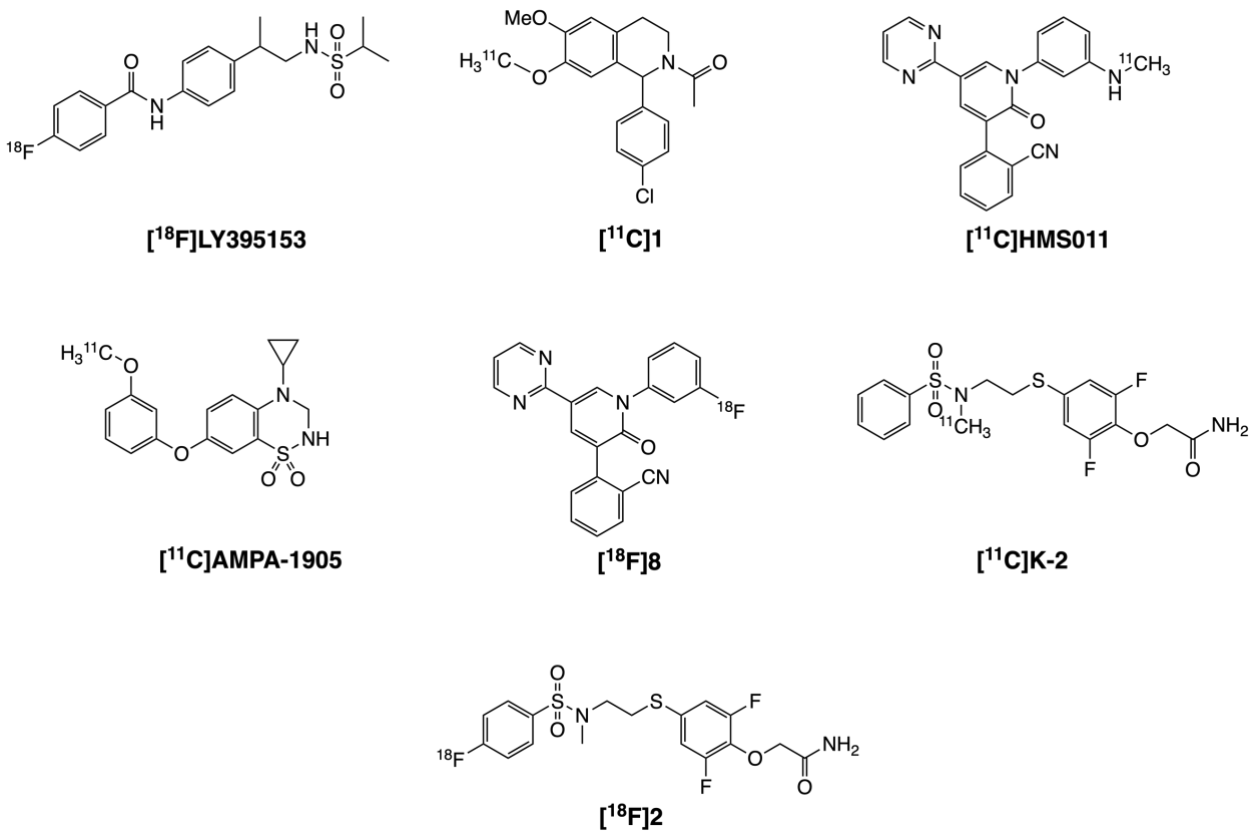

Figure 1.2: Chemical Structures of PET radiotracer candidates for AMPA receptors.

The most success in developing PET radiotracers for iGlu receptor imaging was encountered with NMDA receptors. Structurally, NDMA receptor is a dimer of dimers (*i.e.*, tetraheteromer), composed of two fixed GluN1 subunits along with two GluN2 and/or GluN3 subunits. GluN2 subunits, in turn, are of four types (GluN2A, GluN2B, GluN2C, and GluN2D), whereas GluN3 subunits have two types (GluN3A and GluN3B). NMDA receptor activation requires the binding of glutamate to the GluN2 subunit and a co-agonist, either *L*-glycine or *D*-serine, to the GluN1 subunit to allow Ca^{2+} influx and remove the voltage-dependent channel blockade by Mg^{2+} (for review (Glasgow, Siegler Retchless, & Johnson, 2015)). Although the GluN1 subunit is reserved for *L*-glycine or *D*-serine binding, the diversity in glutamate-binding

GluN2 sites on the NMDA complex impart these receptors various distinct physiological functions (Vieira *et al.*, 2020). The main types of NMDA receptor subunits in the human adult forebrain are GluN2A and GluN2B, which have distinct signalling pathways (Sun *et al.*, 2018).

NMDA radiotracers are classified based on their binding sites on these receptors. There are at least four main sites on NMDA complex for potential targeting by PET radiotracers, including: (1) the receptor ion channel site, which is the binding site of the strong NMDA pore antagonists, MK-801 and phencyclidine (PCP); (2) the *L*-glycine/*D*-serine-binding site on GluN1 subunits; (3) the glutamate-binding sites on GluN2B subunits; and (4) allosteric binding sites on GluN2B subunits. Aside from radioligands targeting GluN2B subunits, there has been little to no success in developing radiotracers for the other sites on NMDA receptors. Accordingly, the main body of research on molecular imaging of NMDA receptor has targeted Glu2B subunits.

One of the first PET radiotracers targeting the MK-801/PCP binding site on the NMDA receptors was ^{18}F-labelled methyl-MK-801 ([^{18}F]FMM) (Blin *et al.*, 1991). Although [^{18}F]FMM showed heterogenous binding throughout baboon brain, blocking studies with PCP and its "cold" counterpart, MK-801, did not reduce the radioligand's regional uptake, indicating non-specific binding that limit its usefulness. The fluorinated derivative of memantine, [^{18}F]AFA, is another pore NMDA antagonist PET radiotracer. This radiotracer exhibited high uptake in brain regions with high NMDA receptor density, such as hippocampus, cerebellum and frontal cortex, which was reduced *via* co-administration of MK-801 in rhesus monkeys (Ametamey *et al.*, 1999). Nevertheless, upon translating it to human studies, [^{18}F]AFA showed homogenous distribution in grey matter and to a lower extent in white matter, which does not reflect the regional concentrations of NMDA receptors, rendering the radiotracer unsuitable (Ametamey *et al.*, 2002). The challenge of non-specific binding is not limited to the latter two PET tracers. Other PET radiotracers for

NMDA ion channel that exhibit homogenous distribution, likely due to non-specific binding, are [^{11}C]GMOM (Waterhouse *et al.*, 2004), [^{11}C]methyl-BIII277CL (Kokic *et al.*, 2002), and [^{18}F]GE-179 (Schoenberger *et al.*, 2018; Vibholm *et al.*, 2020).

Similarly, there are currently no successful PET radiotracers for *L*-glycine/*D*-serine-binding site on GluN1 subunits. [^{11}C]3MPICA is one of the first investigated radioligands for NMDA/*L*-glycine binding site. Preclinical studies with this radiotracer in rodents revealed a low degree of brain uptake with a high blood concentration, which was attributed to high binding affinity to serum albumin (Waterhouse, Sultana, & Laruelle, 2002). Likewise, [^{11}C]L-703,717 and its derivative, [^{11}C]AcL703, both of which target the *L*-glycine/*D*-serine-binding site on GluN1 subunits of NMDA receptors, exhibited high serum album binding with the latter also being a substrate to P-gp efflux pumps that limit their brain uptake (Haradahira *et al.*, 2000; Matsumoto *et al.*, 2007). Structures of PET radiotracer candidates for MK-801/PCP and *L*-glycine binding sites of NMDA receptors are shown in Figure 1.3.

Failure to develop PET radiotracers that bind to NMDA ion channel or GluN1 subunits have motivated a search for GluN2B subunit-targeting radioligands. GluN2B-containing NMDA receptors play a fundamental role in learning and memory (Tang *et al.*, 1999), synaptic plasticity (*i.e.*, LTP) as well as in various neurological and psychiatric disorders (Paoletti, Bellone, & Zhou, 2013). Kramer *et al* reported the radiosynthesis and *in vivo* evaluation of the first successful GluN2B-specific PET radiotracer, known as [^{11}C]Me-NB1 (Kramer *et al.*, 2018). *In vitro* and *in vivo* blocking studies with the GluN2B antagonist eliprodil have shown significant reduction in [^{11}C]Me-NB1 uptake, indicating specific binding (Kramer *et al.*, 2018). Later, upon separating the two enantiomers of [^{11}C]Me-NB1, (*R*) and (*S*), it was demonstrated that (*R*)-[^{11}C]Me-NB1 is the active isomer that exhibits heterogenous binding with high selectivity to GluN2B-rich cortical

regions and low non-specific binding to GluN2B-deficient cerebellar regions (Haider *et al.*, 2019). On the contrary, (*S*)-[^{11}C]Me-NB1 shows homogeneous binding throughout the brain that cannot be blocked with eliprodil (Haider *et al.*, 2019). In addition, blocking studies with drugs targeting the structurally-similar NMDA-modulating sigma (σ)1 receptors revealed that (*R*)-[^{11}C]Me-NB1 binding to GluN2B subunits is independent of the σ1 receptor, whereas (*S*)-[^{11}C]Me-NB1 binding was considerably reduced by σ-1 receptor antagonists (Haider *et al.*, 2019). These findings illustrate the implication of stereoisomerism – molecules with the same molecular formulas and sequence of bonded atoms but differing in three-dimensional orientation of bonded atoms – on selective binding of radiotracers to the target of interest. To date, (*R*)-[^{11}C]Me-NB1 is the only GluN2B-specific PET radiotracer that has advanced to human studies where it showed a heterogenous brain uptake with high test-rest reliability (Rischka *et al.*, 2022). More recently, three other GluN2B-specific PET radiotracer, namely (*R*)-[^{11}C]NR2B-Me, (*R*)-[^{18}F]OF-Me-NB1, and (*S*)-[^{18}F]OF-NB1, have shown promising specificity for GluN2B subunits in non-human primates (NHPs), with the latter being the most promising to be translated into humans (Smart *et al.*, 2022b).

Finally, attempts to develop PET radiotracers for the allosteric sites on GluN2B subunits have been unsuccessful. [^{11}C]N2B-1810 and [^{11}C]N2B-1903 have been developed as negative allosteric modulators (NAM) of GluN2B subunits, but neither showed desirable brain uptake despite demonstrating moderate *in vitro* specific binding (Sun *et al.*, 2021). Structures of PET radiotracer candidates for GluN2B subunit and allosteric binding sites of NMDA receptors are shown in Figure 1.4.

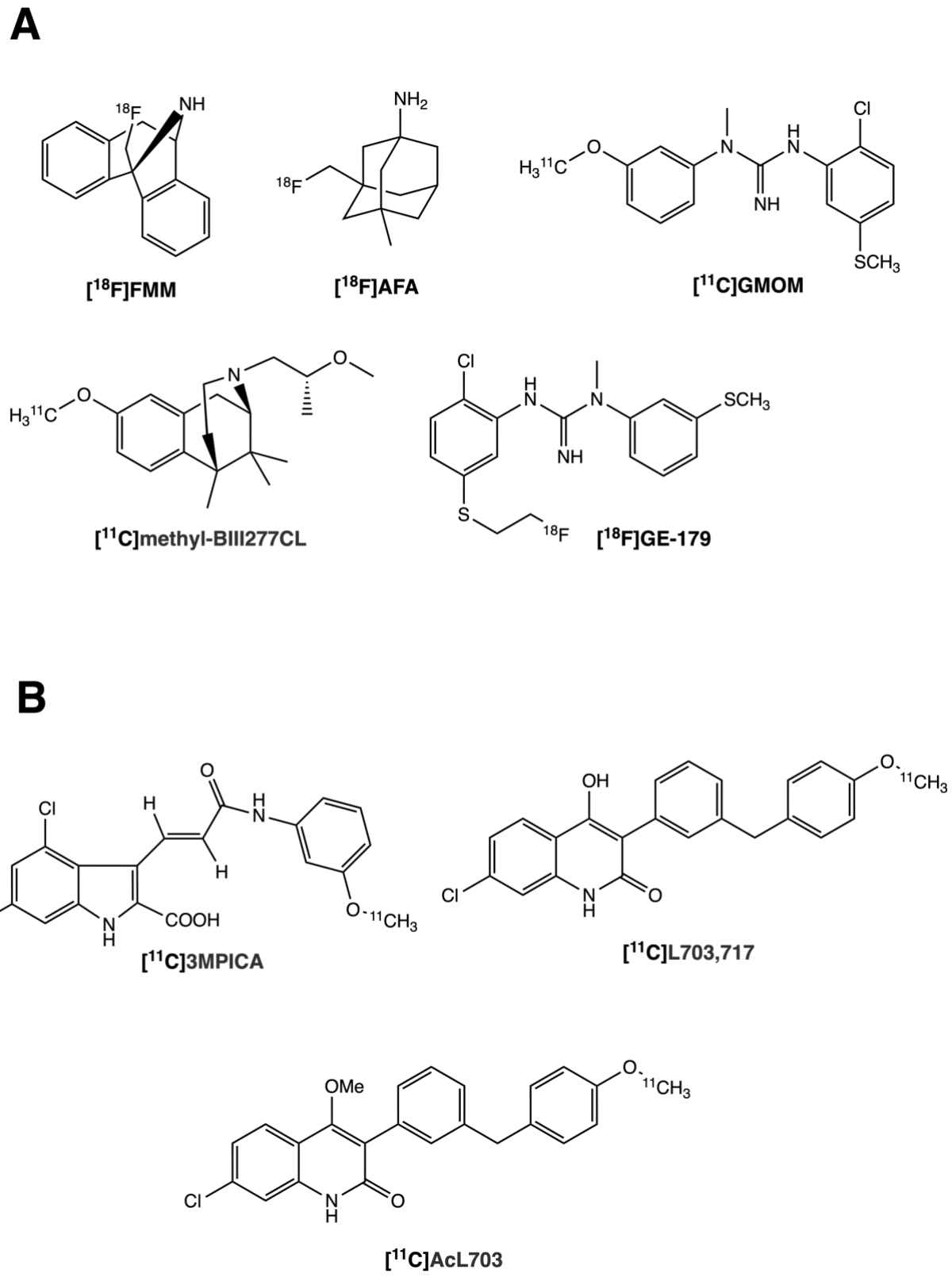

Figure 1.3: Chemical Structures of PET radiotracer candidates for (**A**) MK-801/PCP and (**B**) *L*-glycine binding sites of NMDA receptors.

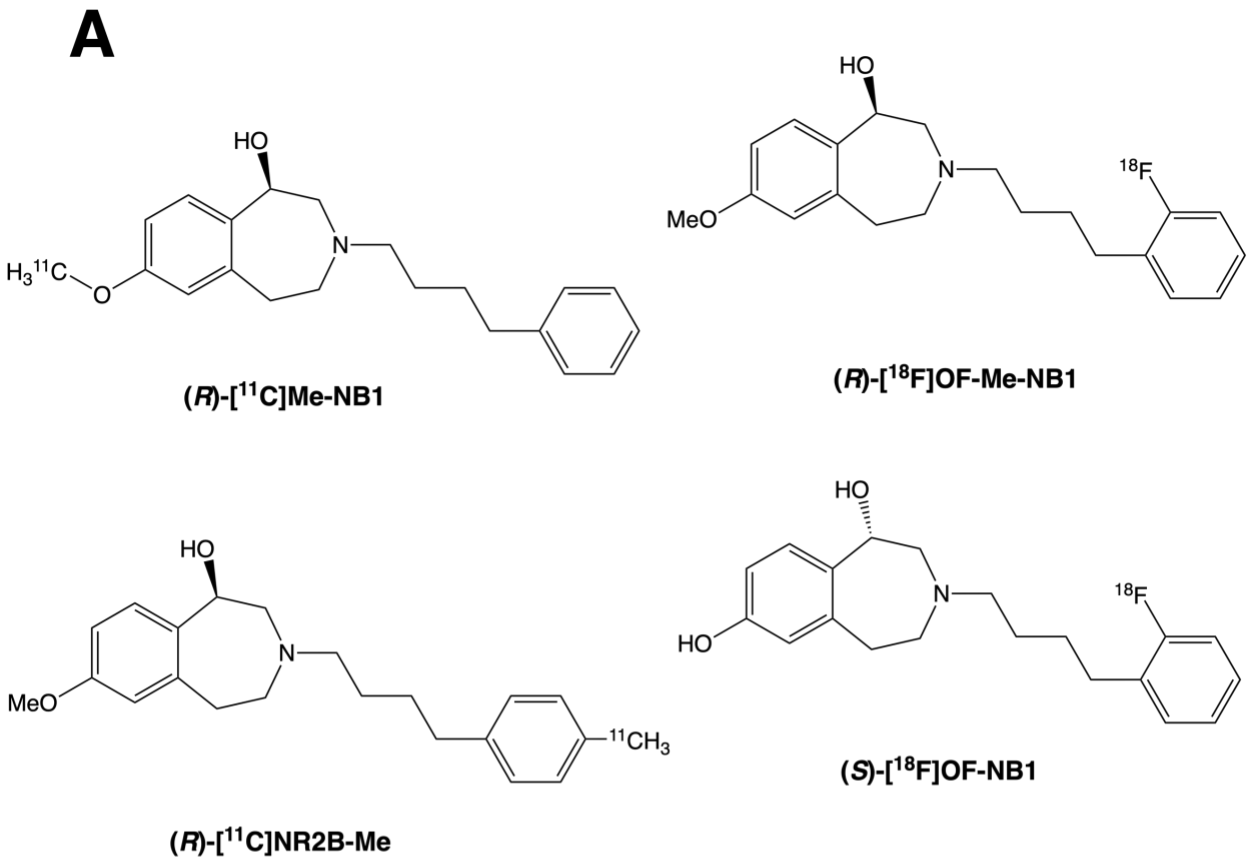

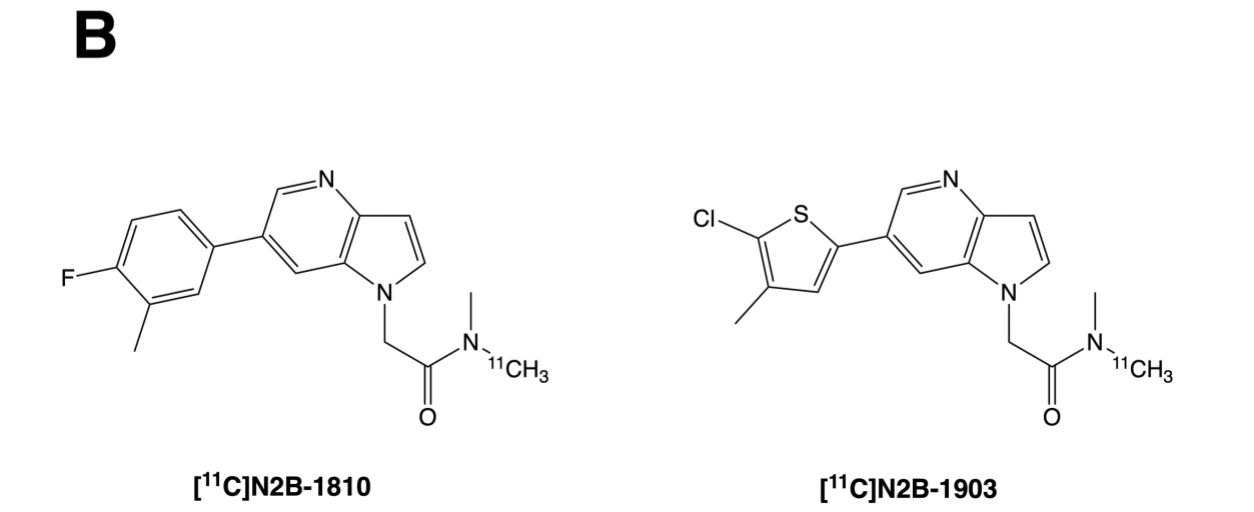

Figure 1.4: Chemical Structures of PET radiotracer candidates for (**A**) GluN2B subunit and (**B**) allosteric binding sites of NMDA receptors.

1.2.1.2.2. PET Imaging of mGlu Receptors

Unlike with iGlu receptors where little success has been encountered in developing PET radioligands for their *in vivo* imaging, several mGlu PET radiotracers are available to study various psychiatric and neurological disorders. As noted previously, mGlu receptors are categorized into three main groups: Group I, II and III.

a. Group I mGlu Receptors

Several PET radiotracers have been explored for Group I mGlu (mGlu1 and mGlu5) receptors, yet very few demonstrated desirable specificity and selectivity for their *in vivo* targets. [^{11}C]JNJ-16567083 is the first reported radiotracer developed for mGlu1 receptor imaging, where it showed a high uptake in the cerebellum, a high mGlu1 expressing region, with demonstrated specificity and selectivity in rodents (Huang *et al.*, 2005). However, upon translating the radiotracer to baboons, [^{11}C]JNJ-16567083 failed to show desirable specific binding in the cerebellum and was not further evaluated (Huang *et al.*, 2012). Another mGlu1 radiotracer candidate [^{11}C]YM-202074 showed high specific binding to the mGlu1-rich cerebellum; however, its low brain uptake along with the extensive presence of its radiometabolites in the brain precluded it from further evaluation (Yanamoto *et al.*, 2010). [^{11}C]MMTP showed high specific binding to cerebellar mGlu1 receptors *in vitro*, with a high *in vivo* uptake in baboon cerebellum (Prabhakaran *et al.*, 2010), but no further evaluation has since been reported. To date, only two ^{11}C-labelled radiotracers targeting mGlu1 have been evaluated in human, including [^{11}C]LY2428703 (Zanotti-Fregonara *et al.*, 2013) and [^{11}C]ITMM (Kenji *et al.*, 2018; Sakata *et al.*, 2017; Toyohara *et al.*, 2013). Despite promising binding characteristics *in vitro* and *in vivo* in rodents, [^{11}C]LY2428703 exhibited low brain uptake in primates and humans that renders it unsuitable for future human

studies (Zanotti-Fregonara *et al.*, 2013). [^{11}C]ITMM, on the other hand, demonstrated slow, yet acceptable, brain uptake and washout in humans (Toyohara et al., 2013), and was later used to study age- and gender-related in mGlu1 receptor expression differences (Sakata *et al.*, 2017), and cerebellar ataxia (Ishibashi *et al.*, 2017). Interestingly, the latter study indicated that mGlu1 imaging with [^{11}C]ITMM provides a more specific evaluation of cerebellar ataxia than the common neuroimaging tool with [^{18}F]FDG (Ishibashi *et al.*, 2017). Building on these promising results, [^{11}C]ITMM was later used to study mGlu1 expression in patients with Alzheimer's disease. No changes in [^{11}C]ITMM BP_{ND} was found between populations with Alzheimer's disease and healthy volunteers (Ishibashi *et al.*, 2019), or during the progression of the disease (Ishibashi *et al.*, 2021).

[^{18}F]MK-1312 was the first reported ^{18}F-labelled radiotracer developed for mGlu1 receptor imaging. Autoradiography and PET studies with [^{18}F]MK-1312 in rhesus monkeys demonstrated promising specific binding in mGlu1-rich brain regions (Hostetler *et al.*, 2011). Subsequently, [^{18}F]FITM was developed for mGlu1 receptor imaging and showed superior binding properties over [^{18}F]MK-1312 in NHPs (Yamasaki *et al.*, 2012), and has been investigated as a diagnostic tool for melanoma (Xie *et al.*, 2014). To overcome the harsh radiosynthesis conditions and slow brain washout of [^{18}F]FITM, its thiazole derivative, [^{18}F]FIMX, has been developed as an alternative with a 3-fold higher affinity for human mGlu1 receptors (Xu *et al.*, 2013). Following the validation of its specificity and selectivity in rhesus monkeys (Xu *et al.*, 2013), [^{18}F]FIMX became the first ^{18}F-labelled mGlu1 radiotracer to be translated to human studies, where it provides superior binding characteristics over the other human-tested mGlu1 radiotracer [^{11}C]ITMM (Zanotti-Fregonara *et al.*, 2016). Accordingly, to date there are two mGlu1-selective PET radiotracers which showed promising potentials for future studies in humans, [^{11}C]ITMM and

[^{18}F]FIMX. Chemical structures of PET radioligand candidates for mGlu1 receptors are illustrated in Figure 1.5.

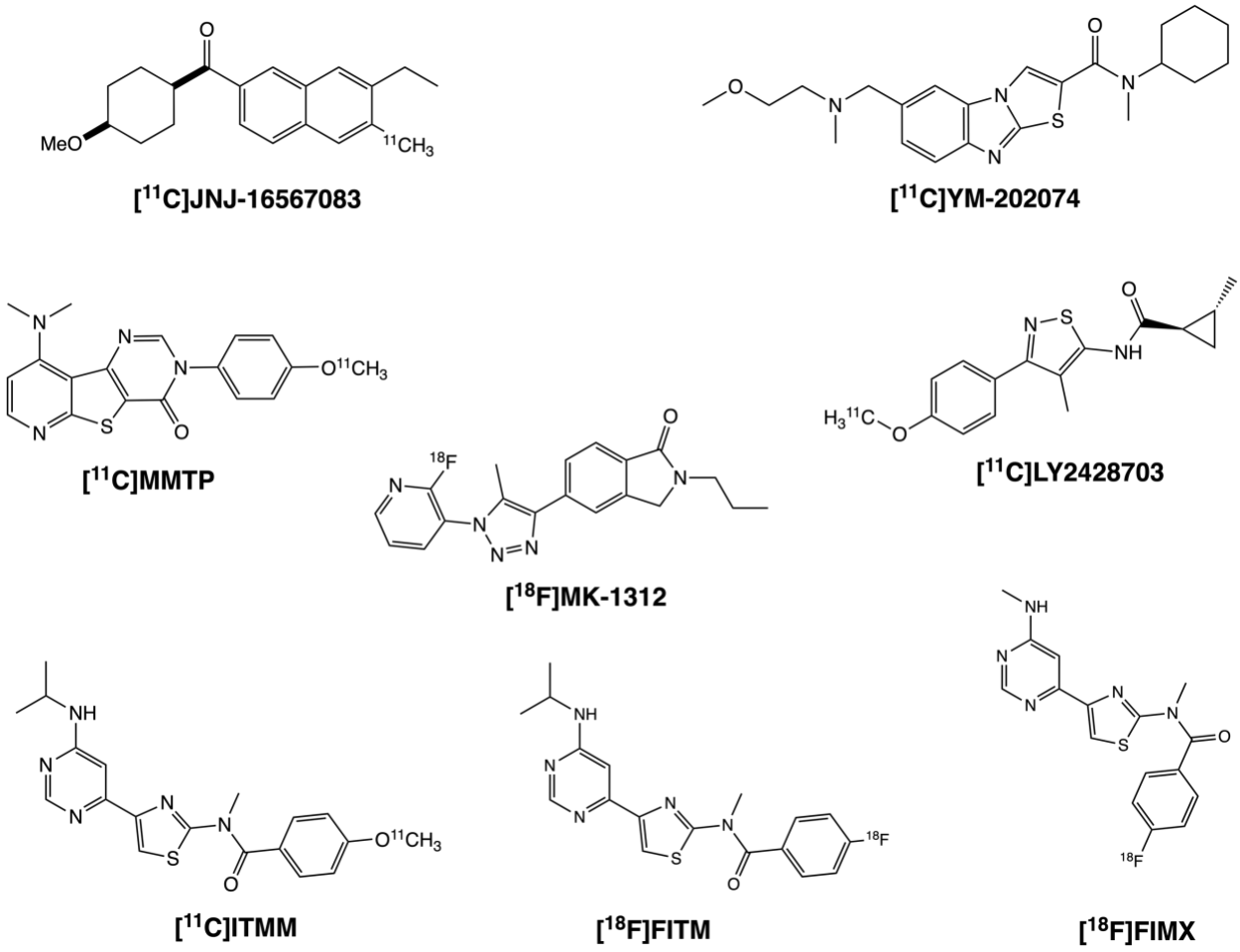

Figure 1.5: Chemical Structures of PET radiotracer candidates for Group I (mGlu1) receptors.

Early PET radiotracer candidates for mGlu5 receptor imaging were derived from 2-methyl-6-(phenylethynyl)pyridine (MPEP), a selective allosteric antagonist of mGlu5 receptors (Gasparini *et al.*, 1999). Neither the ^{11}C-labelled parent compound, [^{11}C]MPEP, nor its ^{11}C-labelled analogues [^{11}C]M-MPEP, [^{11}C]M-PEPy, and [^{11}C]M-FPEP showed desirable specific binding *in vivo* to warrant further development to clinical studies (Kessler, 2004; Severance *et al.*,

2006; Yu *et al.*, 2005). PET radiotracer candidates derived from 3-((2-methyl-4-thiazolyl)-ethynyl)pyridine (MTEP), another selective allosteric antagonist of mGlu5 receptors, did not warrant further translation to humans due to unsuccessful results of preclinical imaging studies. For example, [^{11}C]M-MTEP showed a rapid washout from the brain, suggesting limited retention by mGlu5 receptors (Patel *et al.*, 2005). [^{11}C]M-MTEB and [^{18}F]F-MTEB showed high uptake in the cerebellum of NHPs, a region with low mGlu5 receptor expression, making quantification of brain uptake with the reference tissue method (explained in more details in section 1.2.1.3.3) unattainable (Hamill *et al.*, 2005). The first ^{18}F-labelled mGlu5 PET radiotracer advanced to human studies was [^{18}F]SP203 (Brown *et al.*, 2008). Although it demonstrated high specific binding to mGlu5 receptors in the brain, [^{18}F]SP203 showed *in vivo* defluorination that leads to remarkable bone accumulation in monkeys and, to a lesser extent, in humans (Brown *et al.*, 2008; Simeon *et al.*, 2007). Its ^{11}C-labelled counterpart, [^{11}C]SP203, was developed to avoid accumulation of radioactivity in bone. However, [^{11}C]SP203 poses different challenges of generating lipophilic brain permeable radiometabolites (Lohith *et al.*, 2017; Simeon *et al.*, 2012), which interfere with the quantification of the parent compound. [^{11}C]AZD9272 is an alternative mGlu5 receptor radioligand that differs from MPEP- and MTEP-derived radioligands by the lack of alkyne moiety (Andersson *et al.*, 2013). Although its brain uptake was completely inhibited by fenobam, a NAM of mGlu5 receptors, [^{11}C]AZD9272 binding was only partially (20%) blocked by MTEP in NHPs (Varnas *et al.*, 2018). The discrepancy is [^{11}C]AZD9272 blocking pattern was later attributed to its binding affinity to monoamine oxidase-B (MAO-B) (Varnas *et al.*, 2020), which indicates that this radioligand is not selective to mGlu5 receptors. The ^{18}F-labelled analogue, [^{18}F]AZD9272, has the advantage of a higher image resolution and a longer half-life of ^{18}F, but suffers from the same poor selectivity to the desired target (Nag *et al.*, 2020).

To date, the most successful and widely employed mGlu5-selective PET radiotracers are [^{18}F]FPEB (Hamill *et al.*, 2005) and [^{11}C]ABP688 (Ametamey *et al.*, 2006), both of which are derivatives of MPEP. Animal studies demonstrated specific and selective uptake of [^{18}F]FPEB in mGlu5-rich brain regions (Wang *et al.*, 2007). [^{18}F]FPEB has been used to study various psychiatric and neurological disorders in humans, including major depressive disorder (MDD) (Abdallah *et al.*, 2017), post-traumatic stress disorder (PTSD) (Holmes *et al.*, 2017), alcohol use disorder (Leurquin-Sterk *et al.*, 2016), Parkinson's disease (Kang *et al.*, 2019), and autism (Fatemi *et al.*, 2018). Given that the [^{11}C]ABP688 radiotracer is the main focus of this thesis, its development, validation and applications will be detailed in section 1.2.1.3.

Motivated by encouraging findings of preclinical and clinical imaging studies with [^{11}C]ABP688, researchers have attempted to developed ^{18}F-labelled analogues of ABP688, including [^{18}F]FE-DABP688, [^{18}F]FPECMO, [^{18}F]FDEGPECO, [^{18}F]PSS223 and [^{18}F]PSS232. Nonetheless, none of them were superior to [^{11}C]ABP688 in their ability to quantify mGlu5 receptors. For instance, [^{18}F]FE-DABP688 demonstrated high *in vivo* binding specificity to mGlu5-rich cerebral regions in rodents, comparable to that of [^{11}C]ABP688 (Honer *et al.*, 2007). However, its rapid washout from the forebrain of anesthetized rodents resulted in a relatively short-lived signal (Honer *et al.*, 2007). Although [^{18}F]FPECMO displayed high *in vitro* specific binding to mGlu5-rich brain regions, extensive *in vivo* defluorination and poor permeation of the BBB were observed in small animal studies (Lucatelli *et al.*, 2009). [^{18}F]FDEGPECO showed promising *in vitro* and *in vivo* binding characteristics to mGlu5 receptors (Wanger-Baumann *et al.*, 2011). However, a side-by-side comparison with [^{18}F]FPEB revealed that the target-to-reference ratios of the latter radioligand is more than 4-fold greater than those of [^{18}F]FDEGPECO (Kang *et al.*, 2015). [^{18}F]PSS223, an analogue of [^{18}F]FDEGPECO, displayed high radioactivity accumulation in

rodent skull and jaws due to rapid *in vivo* defluorination, despite demonstrating high specificity and selectivity to mGlu5 receptors (Sephton *et al.*, 2012). [^{18}F]PSS232, another analogue of [^{18}F]FDEGPECO, demonstrated greater metabolic stability over [^{18}F]PSS223 with a high specificity and selectivity to mGlu5 receptors and a desirable test-retest reliability in rodents (Sephton *et al.*, 2015). Two isomers of [^{18}F]PSS232 have been identified to date, including (*E*)-[^{18}F]PSS232 and (*Z*)-[^{18}F]PSS232, with the former exhibiting 15-fold greater affinity to mGlu5 receptors than the latter (Sephton *et al.*, 2013). Encouraged by the findings in laboratory animals, [^{18}F]PSS232 was translated to clinical study, where it displayed an identical brain uptake to that of [^{11}C]ABP688 with high radiotracer binding in mGlu5-rich regions (Warnock *et al.*, 2018). Unlike with [^{11}C]ABP688, [^{18}F]PSS232 binding was shown to be insensitive to drug-induced acute fluctuations in extracellular glutamate release in preclinical and clinical settings (Müller Herde *et al.*, 2018; O'Gorman Tuura *et al.*, 2019). This noted, [^{18}F]PSS232 remains the most promising ^{18}F-labelled analogue of [^{11}C]ABP688 available to date and is expected to find wider application in future clinical studies. Chemical structures of PET radioligand candidates for mGlu5 receptors are illustrated in Figure 1.6.

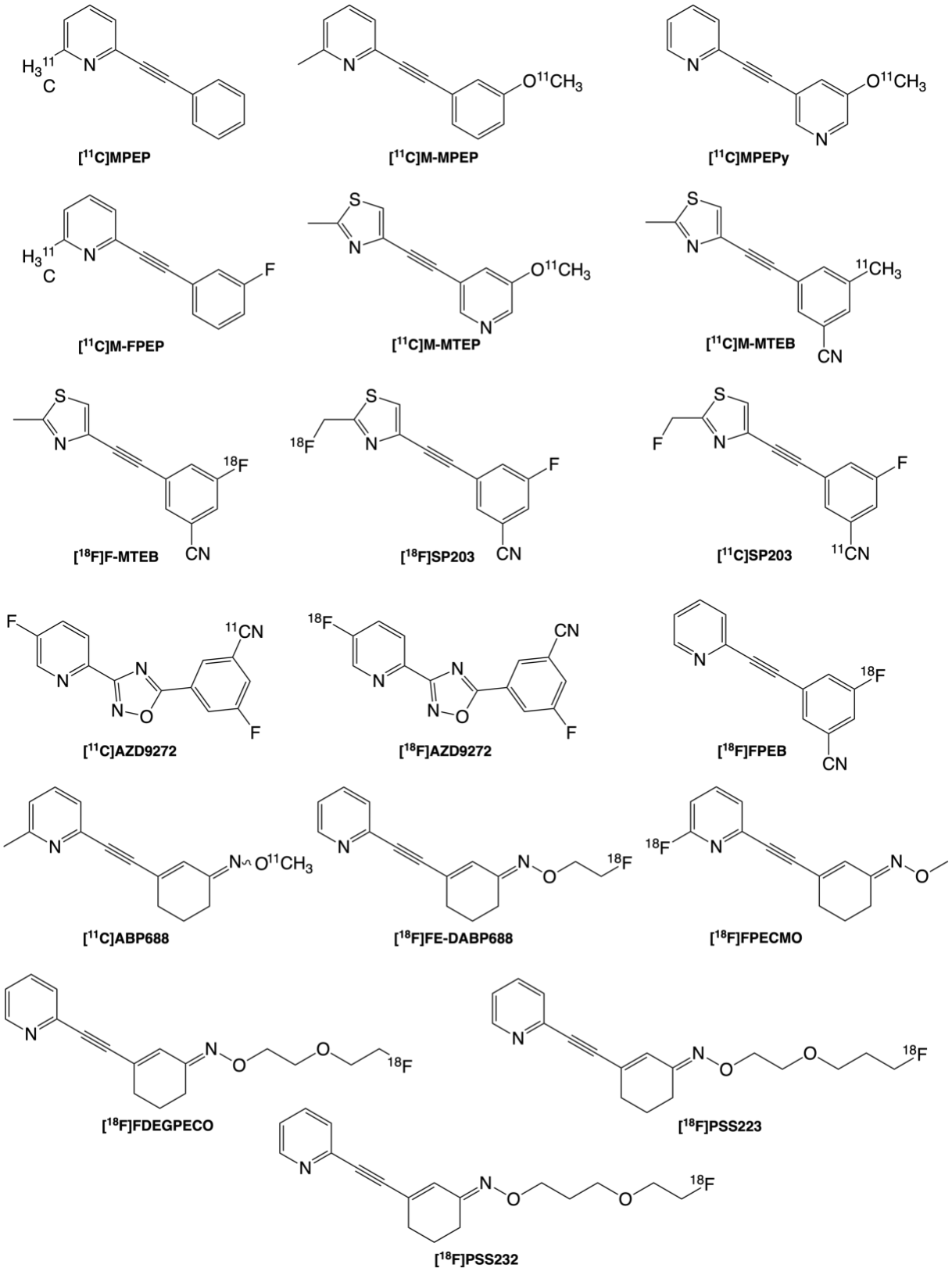

Figure 1.6: Chemical Structures of PET radiotracer candidates for Group I (mGlu5) receptors.

b. Group II mGlu Receptors

As noted earlier, Group II metabotropic glutamate receptors include mGlu2 and mGlu3 receptors. Although several PET radioligands have been developed for mGlu2 receptor imaging, only one radiotracer has warranted translation to clinical studies. The first two PET radiotracers developed for mGlu2 receptor imaging are [^{11}C]CMG and its prodrug, [^{11}C]CMGDE (Wang *et al.*, 2012). Rodent studies with [^{11}C]CMG showed no brain permeability of the radiotracer due to its high hydrophilicity (Log P = –0.52), whereas [^{11}C]CMGDE exhibited limited *in vivo* specific binding (Wang *et al.*, 2012). Another mGlu2 PET radiotracer candidate [^{11}C]CMDC displayed heterogenous *in vitro* binding to mGlu2-rich brain regions; however, *in vivo* studies with this radiotracer revealed low brain permeability with limited specific binding to mGlu2 receptors (Ma *et al.*, 2017). Similarly, both [^{11}C]QCA (Zhang *et al.*, 2017) and [^{11}C]**1** (Kumata *et al.*, 2019) demonstrated *in vitro* specific binding to mGlu2 receptors, but *in vivo* rodent studies showed limited brain uptake of the radiotracer that was attributed to the effect of P-gp efflux pumps. [^{11}C]JNJ42491293, a PAM of mGlu2 receptors, is the only mGlu2-targerting PET radiotracer that has been evaluated in humans (Leurquin-Sterk *et al.*, 2017). Initial promising *in vivo* finding in rodents and monkeys encouraged the research group to translate [^{11}C]JNJ42491293 to clinical studies; however, a high myocardial retention of the radiotracer in humans raised the possibility that the radiotracer displays off-target binding affinity (Leurquin-Sterk *et al.*, 2017). A subsequent PET study with [^{11}C]JNJ42491293 in marmosets failed to demonstrate selectivity to mGlu2 receptors (Kang *et al.*, 2023). [^{11}C]MG2-1812, based on a mGlu2 receptor NAM, demonstrated high *in vitro* and *in vivo* specificity in rodents, with negligible interaction with the efflux pumps in the BBB (Yamasaki *et al.*, 2020), but no further evaluation in higher species has been reported to date. [^{11}C]mG2P001, a recently reported mGlu2 PAM radioligand, has been reported to show

significant uptake by mGlu2-rich brain regions in rodents (Yuan *et al.*, 2020). Blocking studies with a distinct mGlu2 PAM showed 28–37% decrease in radiotracer uptake (Yuan *et al.*, 2020), suggesting limited *in vivo* specificity. Subsequently, the same research group reported a significant increase in radiotracer uptake of [^{11}C]mG2P001 in the brains of rodents and monkeys in self-blocking studies with non-radioactive mG2P001 in rodents and monkeys, which was interestingly attributed to the effect of tissue glutamate concentrations (Yuan *et al.*, 2023). However, the more likely explanation of this effect is the P-gp susceptibility of [^{11}C]mG2P001 which was not investigated. Thereafter, the same research group reported the development of two more PET radioligands: [^{11}C]mG2N001 (Yuan *et al.*, 2022b) and [^{18}F]mG2P026 (Yuan *et al.*, 2022a), which are a mGlu2 receptor NAM and PAM, respectively. Both radiotracer candidates exhibited reasonable *in vivo* binding specificity in rodents and NHPs. The most recent radiotracer developed for mGlu2 imaging is [^{11}C]MK-8056, a mGlu2 receptor NAM, which exhibited a substantial displacement in response to a selective mGlu2 NAM in animal studies, suggesting *in vivo* binding selectivity and specificity to mGlu2 receptors (Perkins *et al.*, 2023). Finally, [^{11}C]MK-8056 exhibited moderate test-retest reliability (16.5%) in rhesus monkeys (Perkins *et al.*, 2023). Chemical structures of PET radioligand candidates for mGlu2 receptors are shown in Figure 1.7.

To the best of our knowledge, there is no selective mGlu3 PET radiotracer reported in the literature.

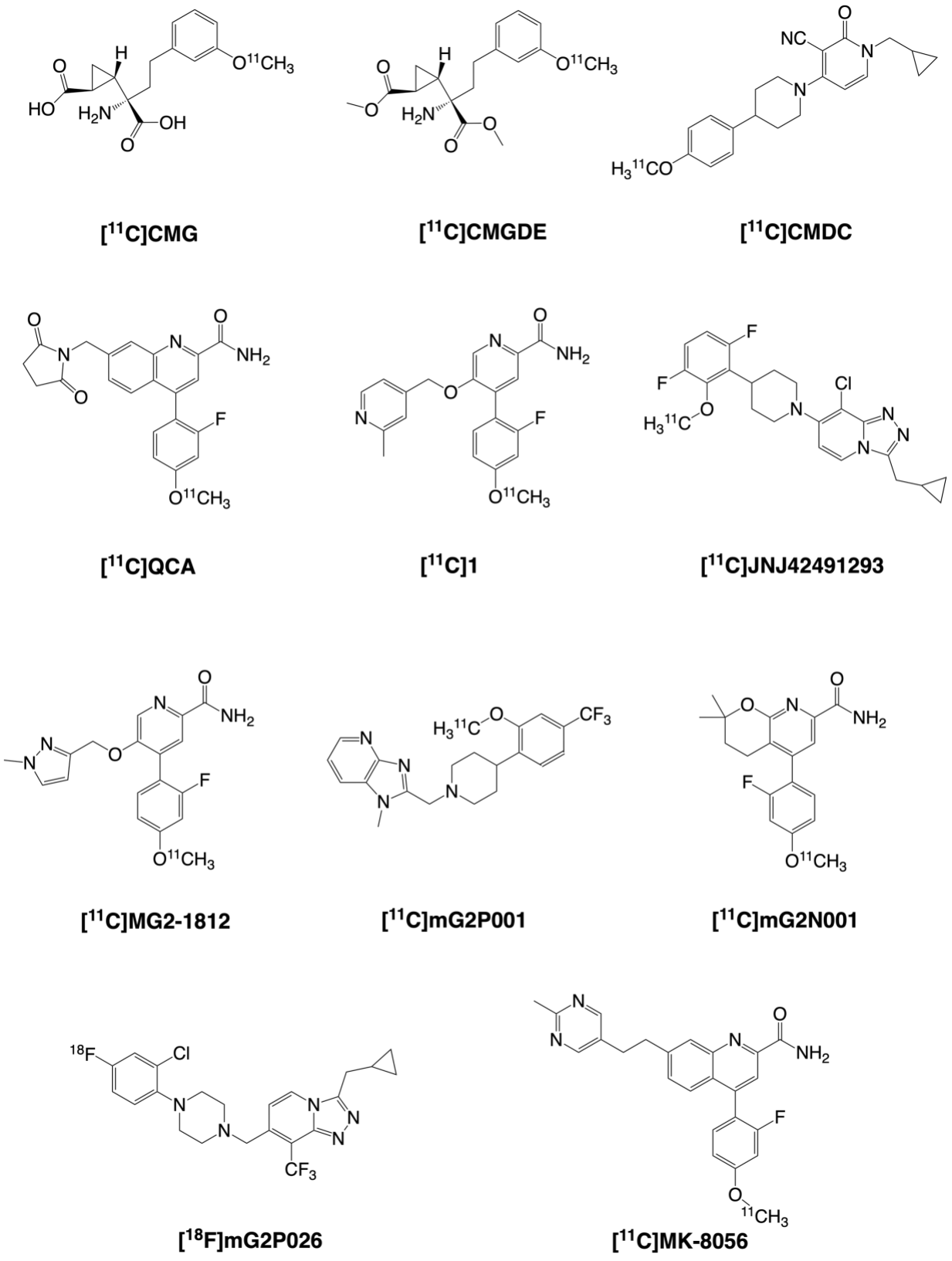

Figure 1.7: Chemical Structures of PET radiotracer candidates for Group II (mGlu2) receptors.

c. Group III mGlu Receptors

Group III mGlu receptors are of four types: mGlu4, mGlu6, mGlu7, and mGlu8. Among this group, only mGlu4 receptors have become a target of PET radiotracer development efforts. This noted, none of the explored radiotracers have been evaluated in humans to date. The mGlu4 PAM [^{11}C]ML128 is the first reported PET radioligand candidate for these receptors. Blocking studies with a selective mGlu4 modulator in rodents revealed a partial displacement (22-28%) of [^{11}C]ML128 from its target, indicating low *in vivo* specificity (Kil *et al.*, 2013). The same research group reported the development and *in vivo* evaluation of the ^{18}F-labelled mGlu4-selective radioligand [^{18}F]KALB001 (Kil *et al.*, 2014). However, similar to [^{11}C]ML128, [^{18}F]KALB001 exhibited unfavorable binding characteristics, including low *in vivo* specificity and rapid washout from the brain (Kil *et al.*, 2014). Likewise, the selective mGlu4 receptor PAM [^{11}C]ADX88178 showed low *in vitro* and *in vivo* specificity following self-blocking studies (Fujinaga *et al.*, 2016). Another mGlu4-selective radioligand [^{11}C]PXT012253 (also called [^{11}C]mG4P012 or [^{11}C]KALB012) displayed a rapid brain uptake in rats followed by a slower washout compared to other mGlu4 PET radioligands (Kil *et al.*, 2016). Blocking studies with a structurally different mGlu4 PAM in NHPs showed a decrease in [^{11}C]PXT012253 binding, but the percentage reduction in radiotracer binding was not reported (Takano *et al.*, 2019). Lastly, the most recent mGlu4-selective PET radiotracer is the ^{18}F-labelled derivative of PXT012253, [^{18}F]mG4P027, that showed low *in vivo* specific binding in response to blocking with the non-radioactive PXT012253 or mG4P027 (Wang *et al.*, 2020). Chemical structures of PET radioligand candidates for mGlu4 receptors are illustrated in Figure 1.8.

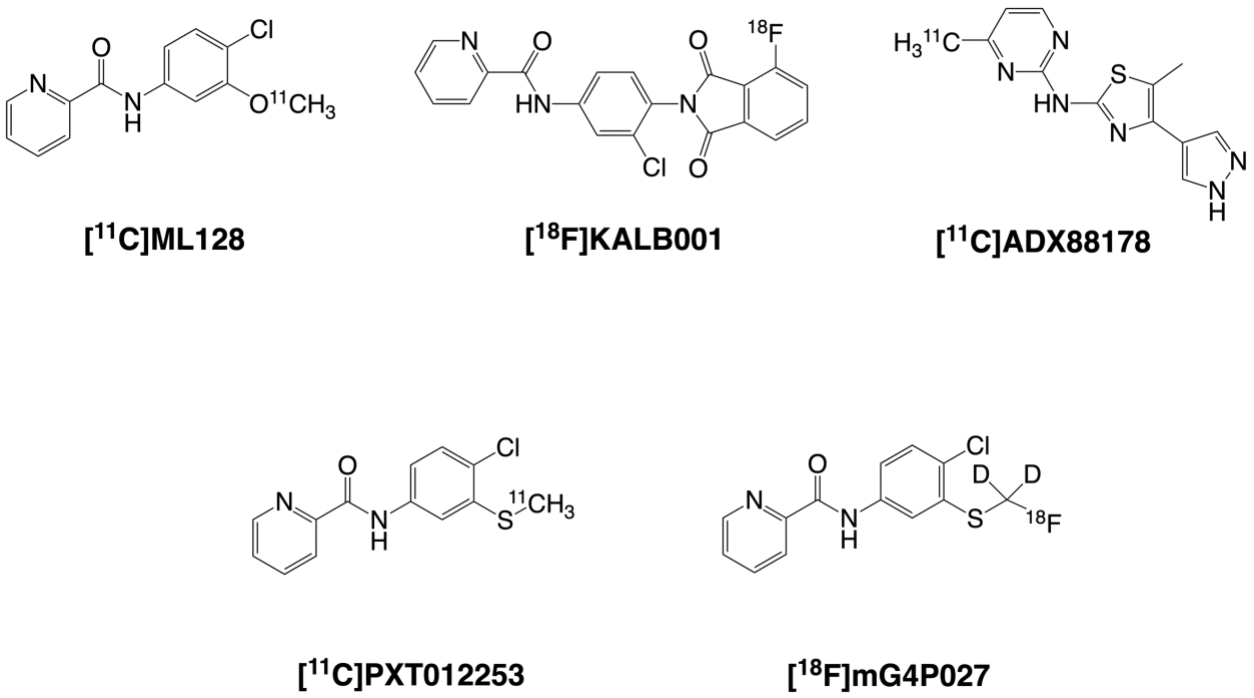

Figure 1.8: Chemical Structures of PET radiotracer candidates for Group III (mGlu4) receptors.

1.2.1.3. Imaging of mGlu5 Receptors with [^{11}C]ABP688

1.2.1.3.1. Development and Radiosynthesis of [^{11}C]ABP688

ABP688 (3-((6-methylpyridin-2-yl)ethynyl) cyclohex-2-en-1-one-*O*-methyl oxime) is a selective allosteric antagonist of mGlu5 receptors with a high *in vitro* binding affinity (K_D = 1.7 - 2 nM) (Ametamey *et al.*, 2006; Hintermann *et al.*, 2007; Wyss *et al.*, 2007). Its high *in vitro* plasma stability along with a preferable lipophilicity profile (Log D = 2.4) allows ABP688 to be freely diffusible through the BBB, which in turn makes it a promising PET candidate for brain imaging (Ametamey *et al.*, 2006; Kessler, 2004). Radiosynthesis of [^{11}C]ABP688 by ^{11}C-methylation of the sodium salt of desmethyl-ABP688 precursor with [^{11}C]methyliodide ([^{11}C]CH_3I) was first reported in 2006 by Ametamey *et al* (Ametamey *et al.*, 2006). Other research groups developed an alternative ^{11}C-methylation method of the same precursor *via* the use of [^{11}C]methyl triflate

([^{11}C]CH_3OTf) (DeLorenzo *et al.*, 2011a; DeLorenzo *et al.*, 2011b; Glorie *et al.*, 2020). Structurally, [^{11}C]ABP688 has two diastereomers, *E* and *Z*, with the former being the active form of the radiotracer with almost 25-fold higher binding affinity to mGlu5 receptors than the latter (Figure 1.9) (Kawamura *et al.*, 2014). Isomerism is the phenomenon where different chemical compounds have the same chemical formula (*i.e.*, same number and kind of atoms) but different chemical structures (*i.e.*, atoms are arranged differently). Stereoisomers are chemical compounds that have the same chemical formula and the sequence of atomic connectivity but differ in their three-dimensional orientations of their atoms in space (Moss, 1996). Diastereoisomers or diastereomers are non-mirror imaged stereoisomers (*i.e.*, non-superimposable) (Muller, 1994). In the case of [^{11}C]ABP688, the presence of asymmetrically substituted C═N double bond leads to diastereoisomerism. Initially, [^{11}C]ABP688 synthesis yielded *E/Z*-isomer with ratios of at least >10:1 (Ametamey *et al.*, 2006), although some methods enhanced the ratio to 70:1 on average (DeLorenzo *et al.*, 2017). The presence of *Z*-isomer in the final formulation has a negative impact on the quantification of [^{11}C]ABP688 binding. Our research group has reported that even modest amounts of the *Z*-isomer can affect estimates of radiotracer binding. More specifically, each 1% of the *Z*-isomer content leads to a 1% and 2% reductions of the mean and minimum BP_{ND} values in striatum, respectively (Smart *et al.*, 2019a). Remarkably, the ratios of *E* to *Z* isomer in the injected doses have rarely been reported in animal and human studies. Accordingly, it is crucial to develop a highly reproducible separation method of the two closely related diastereomers *via* preparative high-performance liquid chromatography (HPLC). Kawamura *et al* have reported for the first time the production of 100% diastereomerically pure (*E*)-[^{11}C]ABP688 using COSMOSIL Cholester column (5 μm, 250 × 10 mm; Nakalai Tesque, Kyoto, Japan) that is designed to separate geometric isomers (Kawamura *et al.*, 2014). However, this column is not widely available and not

commonly used in the preparation of PET radiopharmaceuticals. Accordingly, separation of these two isomers *via* the use of a widely available reversed phase octadecylsilane (C18) HPLC column is highly desirable.

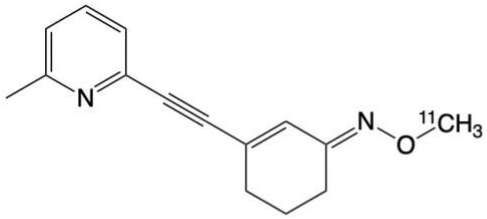

(*E*)-[^{11}C]ABP688

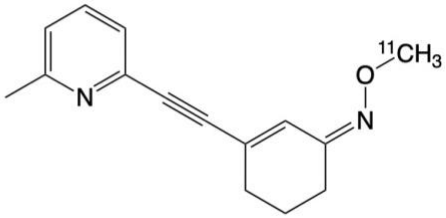

(*Z*)-[^{11}C]ABP688

Figure 1.9: Chemical structures of *E* and *Z* isomers of [^{11}C]ABP688 tracer.

1.2.1.3.2. Imaging Studies with [^{11}C]ABP688

Preclinical PET studies with [^{11}C]ABP688 revealed a high accumulation in mGlu5-rich regions such as cortex, striatum, and hippocampus, with a very little uptake in the cerebellum, a region with negligible mGlu5 expression. Metabolite studies in rodents demonstrated that over 95% of the brain radioactivity represented the parent compound, since the radioactive metabolites are too polar to cross the BBB. Blocking studies with M-MPEP, a mGlu5 receptor antagonist, showed up to 80% reduction in [^{11}C]ABP688 binding in regions with high mGlu5 receptor expression with no change in cerebellar radiotracer uptake, indicating high specific binding (Ametamey *et al.*, 2006; Kessler, 2004; Wyss *et al.*, 2007). A subsequent clinical study with [^{11}C]ABP688 in healthy human

participants confirmed the findings in animal models, where radiotracer uptake was observed in mGlu5-rich regions such as the ACC, medial temporal lobe, amygdala and the dorsal striatum, with limited uptake in mGlu5-deficint regions such as the cerebellum and white matter (Ametamey *et al.*, 2007).

[^{11}C]ABP688 has been used as an investigative tool to study the role of mGlu5 receptors in various neurological and psychiatric disorders, such as epilepsy (DuBois *et al.*, 2016; Lam *et al.*, 2019), dementia (Leuzy *et al.*, 2016), schizophrenia (Akkus *et al.*, 2017), MDD (DeLorenzo *et al.*, 2015b; Deschwanden *et al.*, 2011; Esterlis *et al.*, 2018; Kim *et al.*, 2019), obsessive compulsive disorder (OCD) (Akkus *et al.*, 2014), and substance use disorders (SUDs) (Akkus *et al.*, 2013; Akkus *et al.*, 2018; Akkus *et al.*, 2016; Cox *et al.*, 2020; Hulka *et al.*, 2014; Martinez *et al.*, 2014; Milella *et al.*, 2014; Scala, 2023). In epilepsy patients with focal cortical dysplasia (FCD), a marked reduction in [^{11}C]ABP688 binding was observed in 70% of the patients (DuBois *et al.*, 2016). Similarly, patients with unilateral mesial temporal lobe epilepsy showed a significant reduction in [^{11}C]ABP688 binding in the hippocampus and amygdala, in comparison with healthy volunteers (Lam et al., 2019). Although a significant progressive reduction of [^{11}C]ABP688 binding potential was observed in animal models of OCD-like behavior (Glorie *et al.*, 2022; Glorie *et al.*, 2020), no significant global difference in [^{11}C]ABP688 binding was observed between OCD patients and healthy participants (Akkus *et al.*, 2014). In MDD, studies with [^{11}C]ABP688 have reported inconsistent findings. Several studies have shown a significant decrease in [^{11}C]ABP688 uptake in MDD patients compared to healthy controls (Deschwanden et al., 2011; Esterlis et al., 2018; Kim et al., 2019), but other studies did not find significant difference in radiotracer binding (DeLorenzo et al., 2015). This discrepancy in radiotracer binding might be attributed to the level of social avoidance in MDD population. Indeed, MDD patients with low levels of social avoidance

exhibited lower [^{11}C]ABP688 uptake in the medial part of the right superior frontal cortex than those with high levels of social avoidance and healthy participants (Kim *et al.*, 2022). In SUDs, tobacco smoking has been consistently associated with a significant global reduction (20%) in [^{11}C]ABP688 binding in comparison with non-smokers (Akkus *et al.*, 2013; Hulka *et al.*, 2014). Interestingly, abstinence from smoking appears to revert [^{11}C]ABP688 binding to the levels common in non-smokers over time. For instance, long-term ex-smokers (>18 months) showed higher [^{11}C]ABP688 binding than in recent ex-smokers (average abstinence duration of 6 months), with no significant difference in radiotracer binding between the former group and non-smokers (Akkus *et al.*, 2016). Similar to tobacco smokers, patients with cocaine use disorder exhibited reduced [^{11}C]ABP688 binding (Martinez *et al.*, 2014; Milella *et al.*, 2014), specifically in individuals with more than 75 lifetime cocaine use experiences (Scala, 2023). However, these findings were not observed in another study (Hulka *et al.*, 2014). Findings of [^{11}C]ABP688 studies in patients with alcohol use disorder have been inconsistent. Compared to healthy controls, Akkus and colleagues reported a significant increase in [^{11}C]ABP688 uptake in the temporal lobe in alcohol use disorder with at least 25 days of abstinence (Akkus *et al.*, 2018). However, another study showed both increased and decreased [^{11}C]ABP688 binding in abstinent patients with alcohol use disorder, compared to healthy participants (Joo *et al.*, 2021). The discrepancy in [^{11}C]ABP688 binding is the latter study might be due to the variability in the duration of abstinence of the recruited participants (ranged from 1.5 to 121.5 months). Heavy cannabis use has also been associated with lower [^{11}C]ABP688 BP_{ND} in those also exhibiting high externalizing behavioral traits (Cox *et al.*, 2020). It remains unclear whether this selective effect in the high externalizing participants reflects a differential susceptibility to the mGlu5 change or different patterns of cannabis use. Lower [^{11}C]ABP688 uptake was also observed in patients with behavioral variant

frontotemporal dementia in comparison with cognitively normal participants (Leuzy *et al.*, 2016). More recently, [^{11}C]ABP688 has been used to study drug-induced behavioral sensitization in humans and mice, where it was shown that alterations in mGlu5 receptor availability does not contribute to early neural adaptations in drug-induced behavioral sensitization (Smart *et al.*, 2021).

1.2.1.3.3. Quantification of [^{11}C]ABP688 Binding

The gold standard method to quantify [^{11}C]ABP688 binding is *via* arterial blood sampling (Ametamey *et al.*, 2007). However, considering the technical complexity of this technique along with the psychological burdens to volunteers, the use of non-invasive quantitative methods is preferred. This can be achieved by using the simplified reference tissue method (SRTM) (Lammertsma & Hume, 1996), which allows the calculation of radiotracer binding parameters to a region of interest (ROI) relative to a region devoid of a target of interest, known as a reference region, without the use of arterial input function. The radiotracer binding is often expressed in the form of non-displaceable binding potential (BP_{ND}), which represents the ratio of specific binding in the ROI to the nonspecific (*i.e.*, non-displaceable) binding measured in the reference region (Innis *et al.*, 2007). For [^{11}C]ABP688, the standard reference region is the cerebellar gray matter, since mGlu5 receptor expression is largely absent in the cerebellum of rodents (Elmenhorst *et al.*, 2010; Wyss *et al.*, 2007). Nevertheless, the use of cerebellum as a reference region has been controversial since several studies have reported the expression of these receptors in the cerebellum of humans and baboons (Berthele *et al.*, 1999; DeLorenzo *et al.*, 2011b; Treyer *et al.*, 2007). Notwithstanding these observations, the radiotracer's volume of distribution in human cerebellum is significantly less than in other brain regions (Kagedal *et al.*, 2013). In addition, calculation of [^{11}C]ABP688 BP_{ND} using the cerebellum as the reference region was found to highly

correlate to that measured by the arterial input function (Milella *et al.*, 2011), validating the former as a non-invasive quantitative method of [^{11}C]ABP688 binding in the brain. Furthermore, the method used to reconstruct [^{11}C]ABP688 data could introduce quantification biases propagated into BP_{ND} calculation. Using list-mode reconstruction method of increasing frame length with constant true coincidence counts has been found to minimize potential biases in BP_{ND} calculation (Regio Brambilla *et al.*, 2023).

1.2.1.3.4. Measurement of Endogenous Glutamate Release with [^{11}C]ABP688

Although glutamate is the main excitatory neurotransmitter in mammalian CNS, a non-invasive technique to quantify its extracellular concentrations *in vivo* has not been available. Several PET radiopharmaceuticals have been validated for the measurement of extracellular levels of other neurotransmitters, such as [^{11}C]raclopride and [^{18}F]fallypride for dopamine (Siessmeier *et al.*, 2005), and [^{11}C]CIMBI-36 for serotonin (Erritzoe *et al.*, 2020). There have been several studies that found alternations in [^{11}C]ABP688 binding in response to fluctuations in extracellular glutamate levels, induced by non-pharmacological (Elmenhorst *et al.*, 2016) and pharmacological interventions (DeLorenzo *et al.*, 2015a; Esterlis *et al.*, 2018; Zimmer *et al.*, 2015). In two human studies, [^{11}C]ABP688 brain uptake was found to significantly decrease in response to ketamine administration, a non-competitive NMDA receptor antagonist known to elicit endogenous glutamate release (DeLorenzo *et al.*, 2015a; Esterlis et al., 2018) (Figure 1.10). Moreover, although the glutamate release inducer *N*-acetylcysteine (NAC) did not change [^{11}C]ABP688 binding levels in rodents (Wyckhuys *et al.*, 2013), it did reduce the radiotracer brain uptake in anesthetized NHPs (Miyake *et al.*, 2011; Sandiego *et al.*, 2013). Reducing the extracellular glutamate concentrations *via* the administration of ceftriaxone, an activator of the GLT-1 transporter (EAAT2), in rodents

led to a significant increase in [^{11}C]ABP688 BP_{ND} (Zimmer *et al.*, 2015) (Figure 1.11). Furthermore, [^{11}C]ABP688 BP_{ND} values have been reported to be approximately 10% higher during the sleep phase compared to the awake phase in rodents (Elmenhorst *et al.*, 2016). Although these circadian variations in radiotracer BP_{ND} have been suggested to be due to differences in diurnal mGlu5 receptor expression (DeLorenzo *et al.*, 2017; Elmenhorst *et al.*, 2016), variations in circadian glutamate release (Marquez de Prado *et al.*, 2000) cannot be overlooked as an equally plausible explanation. Indeed, [^{11}C]ABP688 binding in humans also varies between morning and afternoon scans (DeLorenzo *et al.*, 2017; DeLorenzo *et al.*, 2011a). Lastly, [^{11}C]ABP688 brain uptake has been reported to be lower in women than men, which might be attributed to the effect of the interaction between estrogen and mGlu5 receptors (Grove-Strawser, Boulware, & Mermelstein, 2010). Collectively, these findings raise the possibility that changes in extracellular glutamate release rather than mGlu5 receptor density might cause variations in [^{11}C]ABP688 binding and that this radiotracer could provide a non-invasive measure of glutamate release levels in living brains. Still unknown is whether radiotracer binding changes are proportional to changes in extracellular glutamate, thereby allowing the method to become a measure of quantitative changes.

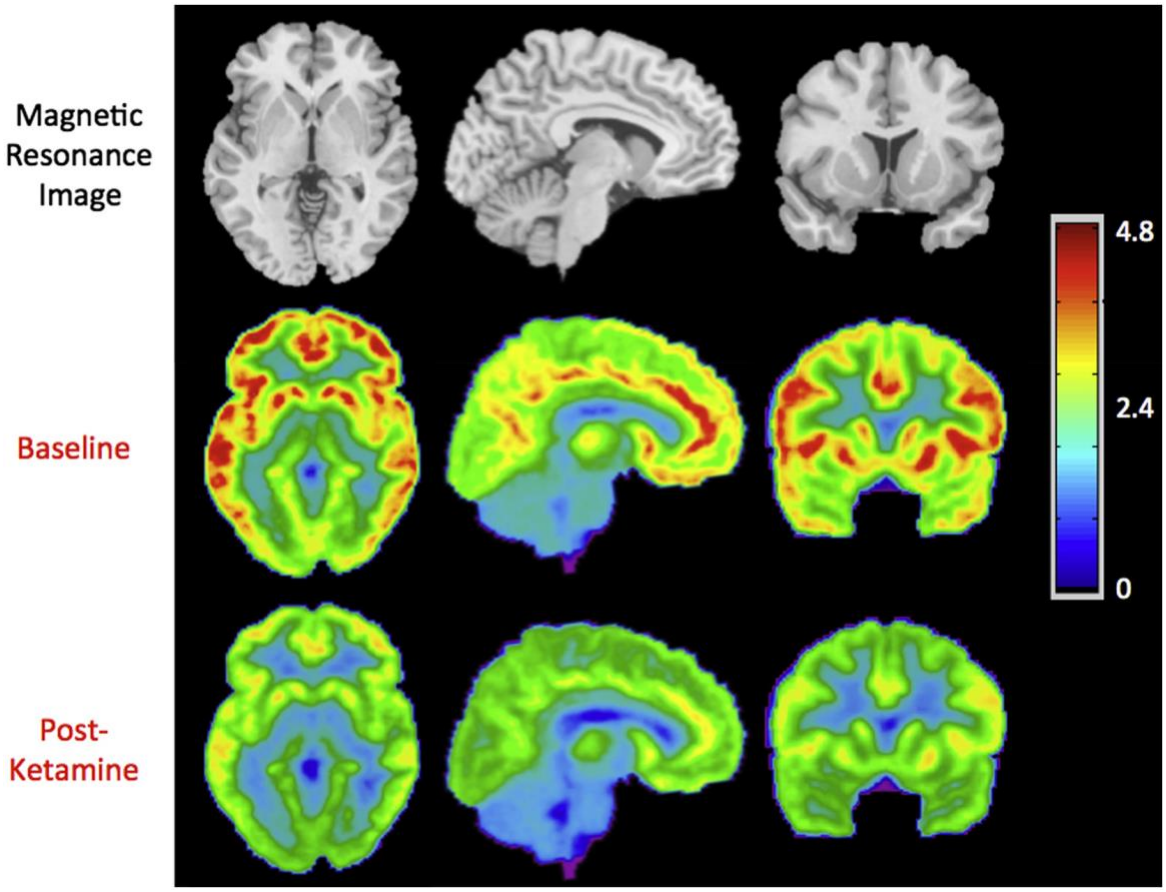

Figure 1.10: Average axial, sagittal, and coronal views of [^{11}C]ABP688 binding before and after ketamine administration. For each subject (n = 10), the volume of distribution (V_T) was calculated at every voxel. The top row shows the magnetic resonance image template, for anatomic reference. The middle and bottom rows show the corresponding views of the mean [^{11}C]ABP688 V_T image. The V_T value associated with each color is indicated by the color bar. Originally published in *DeLorenzo, C., DellaGioia, N., Bloch, M., Sanacora, G., Nabulsi, N., Abdallah, C., Yang, J., Wen, R., Mann, J. J., Krystal, J. H., Parsey, R. V., Carson, R. E., Esterlis, I. (2015). In vivo ketamine-induced changes in [^{11}C]ABP688 binding to metabotropic glutamate receptor subtype 5. Biological Psychiatry, 77(3), 266-275*. Reproduced with permission from Elsevier.

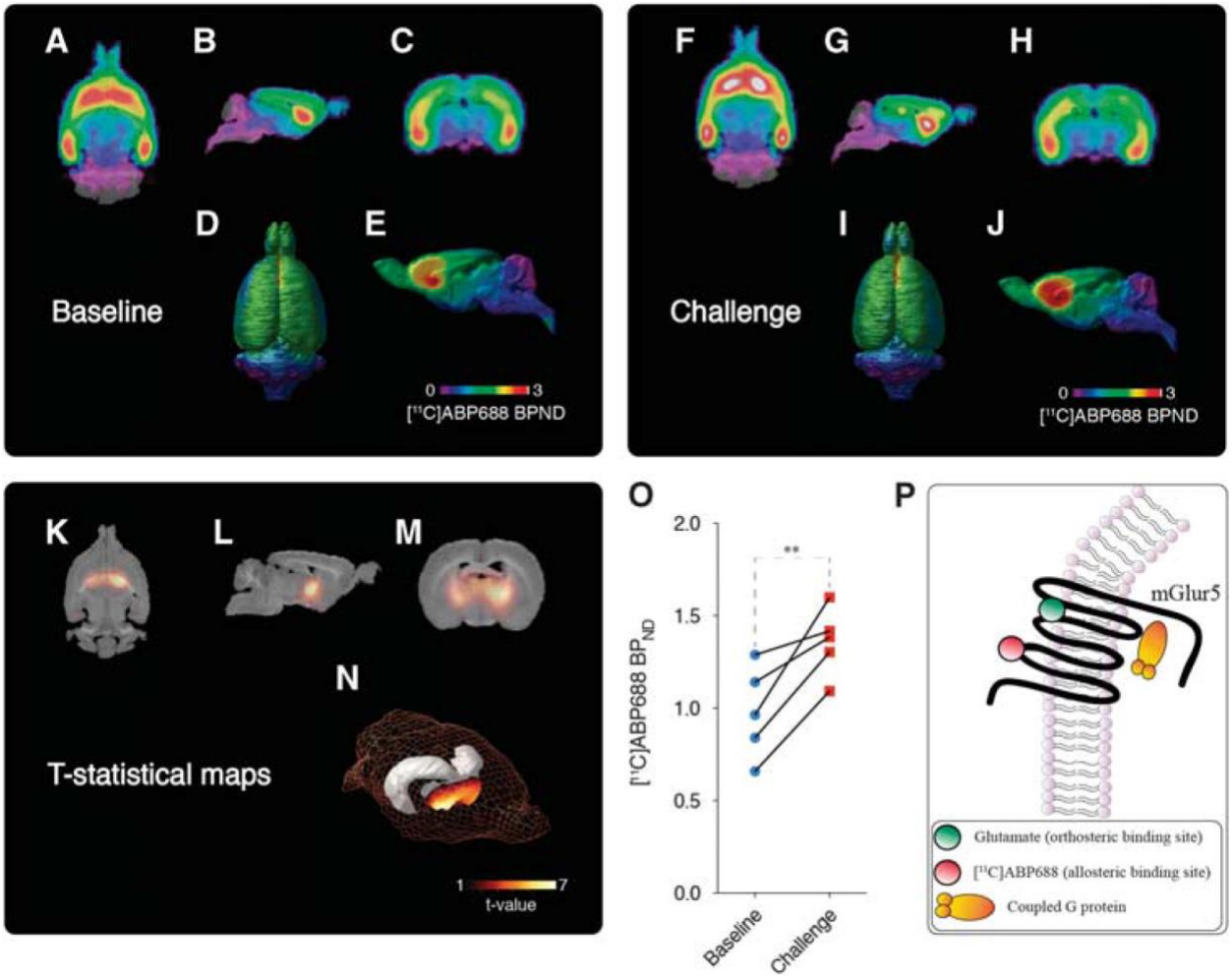

Figure 1.11: Baseline and ceftriaxone (CEF) challenge averaged [^{11}C]ABP688 non-displaceable binding potential (BP_{ND}). Averaged [^{11}C]ABP688 BP_{ND} images obtained during the baseline overlaid on a histologic template are shown in axial (**A**), sagittal (**B**), coronal (**C**), as well as dorsal (**D**) and mid-sagittal surface projections (**E**). Averaged [^{11}C]ABP688 BP_{ND} images obtained after CEF challenge overlaid on a histologic template are shown in axial (**F**), sagittal (**G**), coronal (**H**), as well as dorsal (**I**) and mid-sagittal surface projections (**J**). Statistical parametric images (t-stats contrast (CEF challenge > baseline)) overlaid on a histologic template are shown on axial view (**K**); sagittal view (**L**); coronal view (**M**); and rat brain 3D surface showing (**N**) peak t-stat region (the gray object represents hippocampal position in the 3D surface). Note group differences showing a symmetric cluster in the anterior thalamus, encompassing basal forebrain and posterior striatum with the local maxima at the thalamic VA. [^{11}C]ABP688 BP_{ND} in the local maxima, during baseline and challenge microPET scans (**O**). Schematic representation of [^{11}C]ABP688 BP_{ND} binding in the metabotropic glutamate type 5 (mGlu5) receptor allosteric site (**P**). Images represented as [^{11}C]ABP688 BP_{ND} and *t*-value. Graph represented as Mean ± S.D., $n = 5$. $^{**}p < 0.01$. PET, positron emission tomography. Originally published in *Zimmer, E. R., Parent, M. J., Leuzy, A., Aliaga, A., Aliaga, A., Moquin, L., Schirrmacher, E. S., Soucy, J. P., Skelin, I., Gratton, A., Gauthier, S., Rosa-Neto, P. (2015). Imaging in vivo glutamate fluctuations with [^{11}C]ABP688: a GLT-1 challenge with ceftriaxone. Journal of Cerebral Blood Flow and Metabolism, 35(7), 1169-1174*. Reproduced with permission from SAGE Publications.

1.3. Other Non-invasive Tools to Measure Glutamate Release

1.3.1. Magnetic Resonance Spectroscopy (MRS) and Glutamate

Proton magnetic resonance spectroscopy (^{1}H-MRS) is a powerful non-invasive imaging technique that enables *in vivo* quantification of metabolites, including glutamate and γ-aminobutyric acid (GABA), within the brain. Compared to PET, MRS offers the flexibility of conducting repeated scans in the same session since the latter does not entail exposure to ionizing radiation. Currently, MRS is the only available non-invasive imaging technique that could provide insights of endogenous glutamate levels in human brain. The abundant concentration of glutamate in the brain makes it reliably quantifiable *via* using conventional ^{1}H-MRS acquisition sequences with scanners of magnetic fields of ≥ 3 T (Gussew *et al.*, 2010; Ramadan, Lin, & Stanwell, 2013). This noted, the majority of glutamate in the brain is involved in cellular metabolism, whereas the pool available for neurotransmission, that is later taken up by astrocytes, is considered a major substrate for glutamine (Bak, Schousboe, & Waagepetersen, 2006). To date, there is still a paucity of information regarding the ratio of glutamate involved in cellular metabolism versus neurotransmission. Therefore, MRS studies have focused on measuring the ratio of glutamine to glutamate as a potentially more sensitive index of dynamic changes in synaptic glutamate, which in turn provides a better insight into the neuronal-glial coupling (Yuksel & Ongur, 2010). However, the accuracy of ^{1}H-MRS measurements of glutamine:glutamate ratio remains limited. This is primarily due to similarities in the molecular structure between glutamate and glutamine, which in turn leads to coupled resonance caused by their similar chemical shifts (Ramadan, Lin, & Stanwell, 2013). Therefore, to enhance spectral resolutions of glutamate and glutamine and quantify them separately, stronger magnetic fields (*i.e.*, > 3 T) are required (Gruetter *et al.*, 1998; Tkac *et al.*, 2001), which are not widely accessible in most research centres. Collectively, the spectroscopic

glutamatergic signals are difficult to interpret and are believed to primarily indicate intracellular (neuronal and glial) levels, making the relationship to neurotransmission uncertain (Hasler *et al.*, 2010). In comparison, PET imaging offers the possibility of measuring extracellular levels of neurotransmitter concentrations *via* the use of radiotracers that target synaptic receptors, where released transmitters influence radioligand binding to these receptors.

1.4. Summary and Objectives

In the last two decades, progress has been made in our ability to measure glutamatergic processes in human brain thanks to the recent development of several PET radiotracers, including [^{11}C]ABP688, a highly selective antagonist of mGlu5 receptors. With this radioligand, group differences have been reported between healthy volunteers and people with neuropsychiatric disorders. Despite these encouraging results, the data have exhibited a high degree of variability. Several research groups have proposed that this variability could reflect two features. First, common radiotracer production methods yield two distinct diastereomers: (*E*)- and (*Z*)-[^{11}C]ABP688 isomers, with the former being the active isomer that binds to mGlu5 receptors with higher affinity than the latter. Indeed, even modest amounts of the *Z*-isomer in the injected doses can reduce estimates of radiotracer binding *in vivo*. Solving this technical problem will allow us to reduce a major source of noise in the data. Second, the radiotracer binding to mGlu5 might be sensitive to changes in extracellular glutamate. If the radiotracer binding response is *proportional* to changes in extracellular glutamate, the method will provide us with the first validated tool to non-invasively measure glutamate release in living human brain.

This project breaks down into two independent parts. The first was to develop a new radiosynthesis and purification method that quantitatively separates *(E)*-[^{11}C]ABP688 and *(Z)*-

[^{11}C]ABP688 isomers using a widely available semipreparative C18 HPLC column to obtain 100% of diastereomerically pure *(E)*-[^{11}C]ABP688 isomer. Second, we aimed to demonstrate in rodents that changes in EtOH-induced glutamate concentrations in the ventral striatum are *proportional* to alterations in striatal [^{11}C]ABP688 binding, using simultaneous *in vivo* microdialysis and microPET techniques.

CHAPTER 2: Radiosynthesis of The Diastereomerically Pure (*E*)-[^{11}C]ABP688

Hussein Bdair[1,4] | I-Huang Tsai[2] | Kelly Smart[3] | Chawki Benkelfat[4] | Marco Leyton[4] | Alexey Kostikov[1,2,5]

[1] Montreal Neurological Institute, McGill University, Montreal, Quebec, Canada
[2] McConnell Brain Imaging Centre, Montreal Neurological Institute, McGill University, Montreal, Quebec, Canada
[3] Yale PET Center, Yale University School of Medicine, New Haven, Connecticut, USA
[4] Department of Psychiatry, McGill University, Montreal, Quebec, Canada
[5] Department of Neurology and Neurosurgery, McGill University, Montreal, Quebec, Canada

Correspondence:
Alexey Kostikov, Department of Neurology and Neurosurgery, McGill University, Canada.
Email: alexey.kostikov@mcgill.ca

Keywords:
mGlu5 receptors, PET tracers, radiosynthesis, (*E*)-[^{11}C]ABP688

Disclaimer:
The authors declare that they have no conflict of interest.

Orcid:
Hussein Bdair https://orcid.org/0000-0002-5447-0601
Kelly Smart https://orcid.org/0000-0002-4775-6943
Alexey Kostikov https://orcid.org/0000-0003-1646-761X

2.1. ABSTRACT

We report an efficient protocol for the radiosynthesis of diastereomerically pure (*E*)-[^{11}C]ABP688, a positron emission tomography (PET) tracer for metabotropic glutamate type 5 (mGlu5) receptor imaging. The protocol reliably provides sterile and pyrogen-free formulation of (*E*)-[^{11}C]ABP688 suitable for preclinical and clinical PET imaging with >99% diastereomeric excess (d.e.), >99% overall radiochemical purity (RCP), 14.9 ± 4.3% decay-corrected radiochemical yield (RCY), and 148.86 ± 79.8 GBq/μmol molar activity in 40 minutes from the end of bombardment.

2.2. INTRODUCTION

Metabotropic glutamate type 5 (mGlu5) receptors are widely expressed in the mammalian central nervous system (CNS). Aberrant mGlu5 neurotransmission affects experience-dependent neuroplasticity and is implicated in epilepsy and multiple neurodegenerative and neuropsychiatric disorders (Davis *et al.*, 2017; Esterlis *et al.*, 2018; Kim *et al.*, 2019; Moldrich *et al.*, 2003; Smart *et al.*, 2017). Antagonists and negative allosteric modulators of mGlu5 receptors are being investigated in clinical trials and have shown anxiolytic, antidepressant, and anti-addictive potential (Hughes *et al.*, 2013; Lindemann *et al.*, 2015; Tatarczynska *et al.*, 2001). *In vivo* imaging of mGlu5 receptors in living human brains is therefore of great importance for basic neuroscience research on CNS pathophysiology and in drug development.

The first positron emission tomography (PET) study of mGlu5 receptors in laboratory animals using [^{11}C]ABP688 (3-(6-methyl-pyridin-2-ylethynyl)-cyclohex-2-enone-O-^{11}C-methyloxime, Figure 2.1) was reported by Ametamey *et al* in 2006 (Ametamey *et al.*, 2006), followed by a first-in-human study in 2007 (Ametamey *et al.*, 2007). Despite the emergence of

other imaging agents, most notably [^{18}F]FPEB (Hamill *et al.*, 2005), [^{11}C]ABP688 remained the most widely used PET tracer for mGlu5 receptor imaging in animal and human studies of various psychiatric and neurological disorders (Choi *et al.*, 2014; Kim *et al.*, 2019; Martinez *et al.*, 2014; Smart *et al.*, 2017). However, one drawback of this tracer is the presence of an asymmetrically substituted C═N double bond, which gives rise to two distinct diastereomers, (*E*)-ABP688 and (*Z*)-ABP688 (Figure 2.1). Among them, (*E*)-ABP688 has over 20-fold higher affinity to mGlu5 receptors, and, therefore, the presence of a nearly biologically inactive (*Z*)-isomer decreases the estimates of tracer's *in vivo* binding potential (BP) in rats (Kawamura *et al.*, 2014). Although some radiosynthesis methods can enhance *E*/*Z* ratio to up to 70:1 on average (range: 42:1-98:1) (DeLorenzo *et al.*, 2017), a human study in our PET center has recently observed that the presence of even modest amounts of (*Z*)-[^{11}C]ABP688 in the final product can reduce estimates of non-displaceable binding potential (BP_{ND}), where each 1% increase in (*Z*)-isomer content led to 2% and 1% decreases of the minimum and the mean BP_{ND} values in striatum, respectively (Smart *et al.*, 2019). These results prompted us to improve the tracer radiosynthesis to provide PET researchers with [^{11}C]ABP688 batches of >99% diastereomeric excess (d.e.). Surprisingly, the ratio of the two isomers in injected doses of [^{11}C]ABP688, which depends on the diastereomeric enrichment of desmethyl precursor and ^{11}C-labelling conditions, is rarely reported in studies that use this tracer (Miyake *et al.*, 2011; Sandiego *et al.*, 2013). Because these two factors are difficult to control, separation of the two closely related geometrical isomers by preparative high-performance liquid chromatography (HPLC) would be preferred for reliable production of diastereomerically pure tracer regardless of the quality of precursor and radiosynthesis conditions. To the best of our knowledge, the only report that describes production of 100% pure (*E*)-[^{11}C]ABP68814 uses COSMOSIL Cholester column (5 μm, 250 Å~ 10 mm; Nakalai Tesque,

Kyoto, Japan) that is specialized for separation of geometric isomers. In the present protocol, we aimed to develop alternative conditions for quantitative separation of the two diastereomers formed in the radiosynthesis of [^{11}C]ABP688 by means of a widely used semipreparative Phenomenex Luna C18(2) column that is a versatile reversed-phase HPLC column for preparation of PET radiopharmaceuticals.

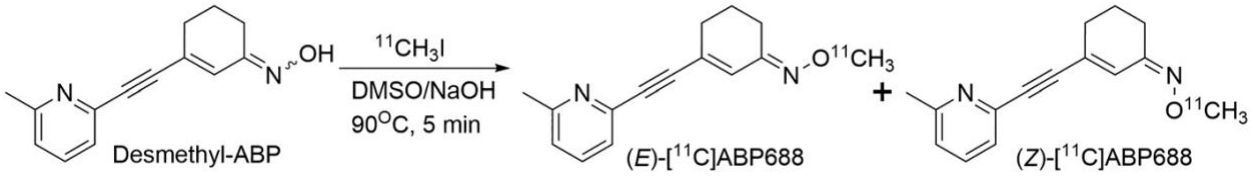

Figure 2.1: Non-stereoselective radiosynthesis of [^{11}C]ABP688.

2.3. PROCEDURE

2.3.1. Production of [^{11}C]Carbon Dioxide

Carbon-11 is obtained in the chemical form of [^{11}C]carbon dioxide ([^{11}C]CO_2) *via* $^{14}N(p,\alpha)^{11}C$ nuclear reaction, by irradiating N_2/O_2 gas mixture (99.5:0.5) (Air Liquide, Canada) with 18-MeV proton beam of 24 to 27 μA for 20 minutes in the gas target (Nitra) of the cyclotron (Cyclone 18/9 IBA, Louvain-La-Neuve, Belgium). The typical amount of [^{11}C]CO_2 produced in the cyclotron target is approximately 37 GBq (1 Ci).

2.3.2. Conversion [^{11}C]Carbon Dioxide to [^{11}C]Methyliodide

The resulting [^{11}C]CO_2 gas is then converted into [^{11}C]methyl iodide ([^{11}C]CH_3I) *via* dry method (catalytic reduction to [^{11}C]methane ([^{11}C]CH_4) followed by radical iodination) using a commercially available Synthra module (Hamburg, Germany). Prior to the target unload, the

module is purged with helium and hydrogen at a flow of 50 mL/min each for 10 minutes, the [^{11}C]CO_2 trap is cooled to −180 °C and the high temperature oven is heated to 740 °C. [^{11}C]Carbon dioxide is then delivered from the cyclotron at a flow of 100 mL/min and trapped at −180 °C in a stainless steel loop trap. The trap is then heated to 50 °C and the [^{11}C]CO_2 is released with a flow of hydrogen gas (40 mL/min) through an oven containing nickel powder (Alfa Aesar, 99.999% purity) and heated to 425 °C, and the resulting [^{11}C]CH_4 is trapped at −140 °C. The trap is heated to 50 °C and then to 125 °C, and the [^{11}C]CH_4 is released with helium using a diaphragm pump in a circular path through an oven containing iodine (Sigma-Aldrich, 99.999% purity) heated to 100 °C followed by the high temperature oven heated to 740 °C and the sodium hydroxide trap. The resulting [^{11}C]CH_3I is trapped on a Porapak Q column at room temperature and then released from the resin with a helium flow (20 mL/min) at 185 °C for the subsequent ^{11}C-methylation reaction.

2.3.3. Radiosynthesis of (*E*)-[^{11}C]ABP688

[^{11}C]ABP688 is synthesized *via* ^{11}C-methylation of desmethyl-ABP688 (ABX, Cat No 3560). Briefly, [^{11}C]CH_3I produced as described above is bubbled at a flow rate of 20 mL/min into a conical 5-mL Wheaton vial containing precursor (5 mg) dissolved in a mixture of dimethyl sulfoxide (0.5 mL) and aqueous sodium hydroxide (5 M, 10 μL). Upon transfer completion, the reaction mixture is heated at 90 °C for 5 minutes, diluted with HPLC eluent (2 mL) and injected onto HPLC system of the automated synthesis unit (Scintomics GRP).

2.3.4. Purification of (*E*)-[^{11}C]ABP688

The product is purified on a semipreparative HPLC column (Phenomenex Luna C18(2) 10 μm, 250 Å~ 10 mm, Cat No 00G-4253-N0) using a mobile phase acetonitrile (CH_3CN): water (50:50) at a flow rate of 5 mL/min. The fraction containing diastereomerically pure (*E*)-[^{11}C]ABP688 (Rt = 18.5 min) is collected, diluted with water (18 mL) and trapped on a solid phase extraction cartridge (Waters, Sep-pak Plus Light C18, Cat No WAT023501), preconditioned with 5-mL ethanol followed by 10-mL sterile water. The cartridge is then washed with sterile water (10 mL), and the radiochemically and diastereomerically pure tracer is eluted with ethanol (0.5 mL) followed by sterile phosphate buffer (9.5 mL) into a sterile vial through a sterile filter. The total radiosynthesis time of (*E*)-[^{11}C]ABP688 from the end of bombardment to the formulation of the final product is 40 minutes.

2.3.5. Quality Control Procedures

The radiochemical identity (RCI), radiochemical purity (RCP), molar activity, diastereomeric ratio and stability of (*E*)-[^{11}C]ABP688 are determined by analytical HPLC system (Agilent 1200) equipped with UV (monitoring at 280 nm) and radioactivity detectors (Gabi, Raytest). Quality control is performed on an analytical HPLC column (MZ Analytical PerfectSil 120 C8 5 μm, 100 Å~ 4.0 mm) using a mobile phase acetonitrile:water (45:55) at a flow rate of 0.7 mL/min. The retention times of (*Z*)- and (*E*)-[^{11}C]ABP688 are 8.5 and 10 minutes, respectively. These conditions were validated for a baseline separation of the two isomers, as under our old previously described radiosynthesis method the d.e. of (*E*)-[^{11}C]ABP688 was 84 ± 3.9% (Smart *et al.*, 2019). The identity of (*Z*)- and (*E*)-ABP688 isomers were validated by analysing ABP688 reference standard (ABX, Cat No 3570) with nuclear magnetic resonance (NMR). The major

product was identified as the *E*-isomer by comparing the ^{1}H NMR spectrum of the reference standard with the data previously reported (Hintermann *et al.,* 2007). The residual solvents are measured using Perkin Elmer Clarus 480 gas chromatograph equipped with a capillary column (Restek MTX-Wax, 30 m Å~ 0.53 mm, ethanol retention time 3.60 min). Formulation pH is measured by pH strips. Bacterial endotoxin levels are measured using Endosafe cartridge reader (Charles River Laboratories) equipped with Limulus Amebocyte Lysate (LAL) cartridges, with threshold set to less than 10 EU/mL. Sterility test is performed on every batch of (*E*)-[^{11}C]ABP688 produced for clinical imaging to detect any bacterial growth in the samples after 14 days of incubation.

2.4. RESULTS AND DISCUSSION

We developed an alternative purification method for production of a diastereomerically pure (*E*)-[^{11}C]ABP688 using a widely available semipreparative HPLC column Phenomenex Luna C18(2). Under optimized conditions, the retention times of (*Z*)- and (*E*)-[^{11}C]ABP688 are 15.5 and 18.5 minutes, respectively, while the unreacted precursor and [^{11}C]CH_3I elute in under 10 min. The sharp elution profile affords a baseline separation of over 1 minute between the two diastereomers (Figure 2.2). (*E*)-[^{11}C]ABP688 is currently used in our PET center in three independent research projects focused on imaging of mGlu5 receptors.

The radiosynthesis method described in this report reliably provides (*E*)-[^{11}C]ABP688 with >99% d.e. and overall radiochemical purity (RCP) and 148.86 ± 79.8 GBq/μmol (Mean ± SD; n = 21) molar activity. The average decay-corrected radiochemical yield (RCY) is 14.9 ± 4.3%, which affords 1380 ± 397 MBq (Mean ± SD; n = 21) of (*E*)-[^{11}C]ABP688 that is suitable to conduct

preclinical and clinical imaging studies. The typical analytical HPLC chromatogram is represented on Figure 3.3.

Ethanol content does not exceed 50 000 ppm (5%), which is a maximum allowed concentration of this solvent for clinical applications. No other organic solvents have been detected. pH is consistently within the 6.5 to 7.0 range. The radiotracer is stable for at least 60 minutes after formulation. All samples were sterile (ie, did not show any bacterial growth after 14 days of incubation) and were pyrogen-free, and therefore the tracer is suitable for use in human or animal subjects and complies with the current Good Manufacturing Practice (cGMP) requirements. The results of three validation radiosynthesis runs are summarized in Table 2.1.

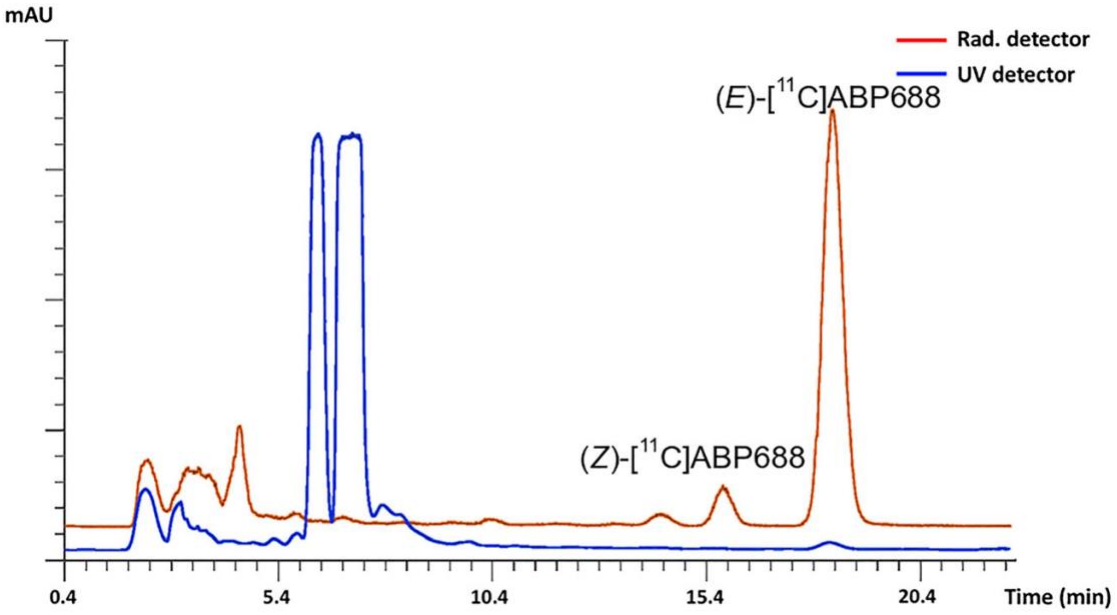

Figure 2.2: Preparative HPLC radioactivity (red) and UV (blue) chromatograms of [^{11}C]ABP688, depicting the baseline resolution of the *Z*- and *E*-isomers (R_t 15.5 and 18.5 min, respectively).

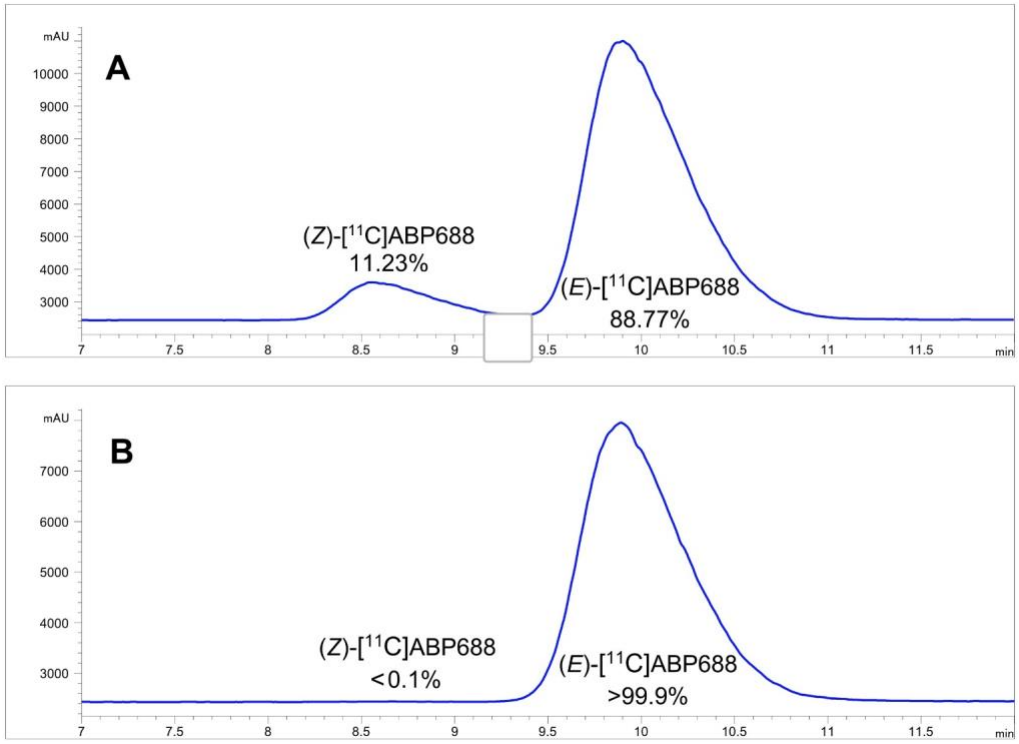

Figure 2.3: Analytical radioactivity HPLC chromatograms of [^{11}C]ABP688, illustrating the differences in end product composition of the previous (**A**) and current (**B**) [^{11}C]ABP688 purification methods.

Table 2.1: Representative results of (*E*)-[^{11}C]ABP688 production runs under optimized conditions.

[^{11}C]CO_2, GBq	38.11	36.70	35.67
(*E*)-[^{11}C]ABP688, GBq	1.52	1.34	1.47
RCY, %[a]	15.9	14.5	16.5
RCP, %	99.07	99.31	99.09
Molar activity, GBq/μmol	186.05	170.91	139.68
Diastereomeric excess	>99%	>99%	>99%
pH (4.5-7.5)	6.5	7.0	6.5
EtOH content, ppm	35,692	38,017	37,759
Acetonitrile, ppm	< LDL[b]	< LDL	< LDL
DMSO, ppm	< LDL	< LDL	< LDL
BET test	<10 EU/mL	<10 EU/mL	<10 EU/mL
Sterility test	No Growth	No Growth	No Growth

a From [^{11}C]CO_2, corrected for decay, total radiosynthesis time is 40 minutes.
b LDL = lower detection limit.

2.5. CONCLUSION

The presented protocol provides an alternative HPLC purification method that produces 100% (*E*)-[^{11}C]ABP688 isomer regardless of the precursor diastereomeric enrichment with high chemical and radiochemical purity, and molar activity, compliant with cGMP regulations. This production protocol allows for consistent and accurate calculations of [^{11}C]ABP688 binding potential, which will positively affect the outcomes of preclinical and clinical PET imaging studies of mGlu5 receptors.

2.6. ACKNOWLEDGEMENTS

The authors would like to acknowledge Messrs. Robert Hopewell and Dean Jolly for technical assistance with production of radiotracers, Mmes. Monica Lacatus-Samoila and Marina Kostikova for help with quality control procedures, Dr. Thomas A. Singleton for analysis of ABP688 reference standard with NMR, and Drs. Jean-Paul Soucy and Gassan Massarweh for access to radioisotopes and the PET radiochemistry facility.

2.7. REFERENCES

Ametamey, S. M., Kessler, L. J., Honer, M., Wyss, M. T., Buck, A., Hintermann, S., . . . Schubiger, P. A. (2006). Radiosynthesis and Preclinical Evaluation of 11C-ABP688 as a Probe for Imaging the Metabotropic Glutamate Receptor Subtype 5. *Journal of Nuclear Medicine, 47*(4), 698-705.

Ametamey, S. M., Treyer, V., Streffer, J., Wyss, M. T., Schmidt, M., Blagoev, M., . . . Buck, A. (2007). Human PET Studies of Metabotropic Glutamate Receptor Subtype 5 with 11C-ABP688. *Journal of Nuclear Medicine, 48*(2), 247.

Choi, H., Kim, Y. K., Oh, S. W., Im, H. J., Hwang, D. W., Kang, H., . . . Lee, D. S. (2014). In vivo imaging of mGluR5 changes during epileptogenesis using [11C]ABP688 PET in pilocarpine-induced epilepsy rat model. *PloS One, 9*(3), e92765.

Davis, M. T., Holmes, S. E., Pietrzak, R. H., & Esterlis, I. (2017). Neurobiology of Chronic Stress-Related Psychiatric Disorders: Evidence from Molecular Imaging Studies. *Chronic Stress (Thousand Oaks), 1*.

DeLorenzo, C., Gallezot, J. D., Gardus, J., Yang, J., Planeta, B., Nabulsi, N., . . . Esterlis, I. (2017). In vivo variation in same-day estimates of metabotropic glutamate receptor subtype 5 binding using [11C]ABP688 and [18F]FPEB. *Journal of Cerebral Blood Flow and Metabolism, 37*(8), 2716-2727.

Esterlis, I., DellaGioia, N., Pietrzak, R. H., Matuskey, D., Nabulsi, N., Abdallah, C. G., . . . DeLorenzo, C. (2018). Ketamine-induced reduction in mGluR5 availability is associated with an antidepressant response: an [11C]ABP688 and PET imaging study in depression. *Molecular Psychiatry, 23*(4), 824-832.

Hamill, T. G., Krause, S., Ryan, C., Bonnefous, C., Govek, S., Seiders, T. J., . . . Burns, H. D. (2005). Synthesis, characterization, and first successful monkey imaging studies of metabotropic glutamate receptor subtype 5 (mGluR5) PET radiotracers. *Synapse, 56*(4), 205-216.

Hintermann, S., Vranesic, I., Allgeier, H., Brulisauer, A., Hoyer, D., Lemaire, M., . . . Auberson, Y. P. (2007). ABP688, a novel selective and high affinity ligand for the labeling of mGlu5 receptors: identification, in vitro pharmacology, pharmacokinetic and biodistribution studies. *Bioorg Med Chem, 15*(2), 903-914.

Hughes, Z. A., Neal, S. J., Smith, D. L., Sukoff Rizzo, S. J., Pulicicchio, C. M., Lotarski, S., . . . Ring, R. H. (2013). Negative allosteric modulation of metabotropic glutamate receptor 5 results in broad spectrum activity relevant to treatment resistant depression. *Neuropharmacology, 66*, 202-214.

Kawamura, K., Yamasaki, T., Kumata, K., Furutsuka, K., Takei, M., Wakizaka, H., . . . Zhang, M. R. (2014). Binding potential of (E)-[11C]ABP688 to metabotropic glutamate receptor subtype 5 is decreased by the inclusion of its 11C-labelled Z-isomer. *Nuclear Medicine and Biology, 41*(1), 17-23.

Kim, J. H., Joo, Y. H., Son, Y. D., Kim, J. H., Kim, Y. K., Kim, H. K., . . . Ido, T. (2019). In vivo metabotropic glutamate receptor 5 availability-associated functional connectivity alterations in drug-naive young adults with major depression. *European Neuropsychopharmacology, 29*(2), 278-290.

Lindemann, L., Porter, R. H., Scharf, S. H., Kuennecke, B., Bruns, A., von Kienlin, M., . . . Jaeschke, G. (2015). Pharmacology of basimglurant (RO4917523, RG7090), a unique metabotropic glutamate receptor 5 negative allosteric modulator in clinical development for depression. *J Pharmacol Exp Ther, 353*(1), 213-233.

Martinez, D., Slifstein, M., Nabulsi, N., Grassetti, A., Urban, N. B., Perez, A., . . . Huang, Y. (2014). Imaging glutamate homeostasis in cocaine addiction with the metabotropic glutamate receptor 5 positron emission tomography radiotracer [11C]ABP688 and magnetic resonance spectroscopy. *Biological Psychiatry, 75*(2), 165-171.

Miyake, N., Skinbjerg, M., Easwaramoorthy, B., Kumar, D., Girgis, R. R., Xu, X., . . . Abi-Dargham, A. (2011). Imaging changes in glutamate transmission in vivo with the metabotropic glutamate receptor 5 tracer [11C]ABP688 and N-acetylcysteine challenge. *Biological Psychiatry, 69*(9), 822-824.

Moldrich, R. X., Chapman, A. G., De Sarro, G., & Meldrum, B. S. (2003). Glutamate metabotropic receptors as targets for drug therapy in epilepsy. *European Journal of Pharmacology, 476*(1-2), 3-16.

Sandiego, C. M., Nabulsi, N., Lin, S. F., Labaree, D., Najafzadeh, S., Huang, Y., . . . Carson, R. E. (2013). Studies of the metabotropic glutamate receptor 5 radioligand [11C]ABP688 with N-acetylcysteine challenge in rhesus monkeys. *Synapse, 67*(8), 489-501.

Smart, K., Cox, S. M. L., Kostikov, A., Shalai, A., Scala, S. G., Tippler, M., . . . Leyton, M. (2019). Effect of (Z)-isomer content on [11C]ABP688 binding potential in humans. *European Journal of Nuclear Medicine and Molecular Imaging, 46*(5), 1175-1178.

Smart, K., Scala, S. G., El Mestikawy, S., Benkelfat, C., & Leyton, M. (2017). Cocaine Addiction and mGluR5. In V. R. Preedy (Ed.), *The Neuroscience of Cocaine* (pp. 269-278). San Diego: Academic Press.

Tatarczynska, E., Klodzinska, A., Chojnacka-Wojcik, E., Palucha, A., Gasparini, F., Kuhn, R., & Pilc, A. (2001). Potential anxiolytic- and antidepressant-like effects of MPEP, a potent, selective and systemically active mGlu5 receptor antagonist. *British Journal of Pharmacology, 132*(7), 1423-1430.

BRIDGING STATEMENT

As discussed in Chapter 1, the presence of even modest amounts the *Z*-isomer of [^{11}C]ABP688 in the injected formulation affects the quantification of radiotracer binding (Smart *et al.*, 2019a). The research presented in Chapter 2 addressed this challenge by developing a radiosynthesis purification method that allows us to produce >99% (*E*)-[^{11}C]ABP688 isomer in the final formulation. This method in turn minimizes the variability in the calculations of radiotracer BP_{ND} values, a major source of noise in the data.

Notably, several preclinical and clinical studies have observed alterations in [^{11}C]ABP688 binding in response to glutamate release inducing or suppressing interventions. For instance, two human studies have shown a reduction in [^{11}C]ABP688 binding in response to ketamine, a glutamate release inducer (DeLorenzo *et al.*, 2015; Esterlis *et al.*, 2018). In laboratory animals, reduction of extracellular glutamate concentrations *via* the use of ceftriaxone, an activator of GLP-1 transporter, has led to a significant rise in [^{11}C]ABP688 brain uptake (Zimmer *et al.*, 2015). Similarly, it has been shown that [^{11}C]ABP688 binding varies throughout the day (Elmenhorst *et al.*, 2016), which could reflect circadian fluctuations in extracellular glutamate concentrations (Marquez de Prado *et al.*, 2000). These findings raise the possibility that [^{11}C]ABP688 binding is sensitive to changes in extracellular glutamate levels. Still unknown, however, is whether alterations in [^{11}C]ABP688 binding are proportionate to changes in extracellular glutamate concentrations. If proven, [^{11}C]ABP688 has the potential to be utilized as a non-invasive measure of glutamate release.

Chapter 3 consists of a research article, titled "Testing PET-[^{11}C]ABP688 as a Tool to Quantify Glutamate Release *In Vivo*", that was submitted to *Imaging Neuroscience*, 2023. In this

study, we applied a validated technique utilized to examine the potential of a radiotracer to quantify extracellular neurotransmitter levels. This includes the simultaneous use of PET imaging along with *in vivo* microdialysis – an invasive technique that quantifies, in real-time, extracellular neurotransmitter levels in living brain. In our study, low-dose EtOH (20%, 0.5 g/kg, i.p.) was used as an inducer of glutamate release in anesthetized rats. With such a low dose of EtOH, our research group was able to show a doubling of ventral striatal glutamate concentrations in awake animals. Accordingly, the work presented in Chapter 3 investigated whether changes in EtOH-induced glutamate levels are proportional to changes in [^{11}C]ABP688 BP_{ND}.

CHAPTER 3: Testing PET-[^{11}C]ABP688 as a Tool to Quantify Glutamate Release *In Vivo*

Hussein Bdair[1,2], Marie Sato-Fitoussi[1], Stéphane Planche[1], Luc Moquin[3], Min Su Kang[4], Arturo Aliaga[2,4], Atsuko Nagano-Saito[1], Kelly Smart[1], Sylvia ML Cox[1], Jamie Near[3], Argel Aguilar-Valles[5], Gassan Massarweh[2], Pedro Rosa-Neto[1,2,4], Chawki Benkelfat[1], Jean-Paul Soucy[2], Alexey Kostikov[2,6], Alain Gratton[3], Marco Leyton[1,2]*

1- Department of Psychiatry, McGill University, Montreal, QC, H3A 1A1, Canada.
2- Department of Neurology and Neurosurgery, Montreal Neurological Institute-Hospital, Montreal, QC, H3A 2B4, Canada.
3- Department of Psychiatry, Douglas Mental Health University Institute, McGill University, Montreal, QC, H4H 1R3, Canada.
4- Translational Neuroimaging Laboratory, McGill University Research Centre for Studies in Aging, Alzheimer's Disease Research Unit, Douglas Research Institute, Montreal, Quebec H4H 1R3, Canada
5- Department of Neurosciences, Health Sciences building, Carleton University, Ottawa, ON, K1S 5B6, Canada.
6- Department of Chemistry, McGill University, Montreal, QC, H3A 0B8, Canada.

*Corresponding author: Marco Leyton
Department of Psychiatry
McGill University
1033 Pine Ave West
Montreal, QC, Canada, H3A 1A1
Tel: 1-514-398-5804
Email: marco.leyton@mcgill.ca

Keywords

metabotropic glutamate type 5 (mGlu5) receptors, positron emission tomography, magnetic resonance spectroscopy, *in vivo* microdialysis, ethanol, transmitter release

3.1. ABSTRACT

The excitatory neurotransmitter glutamate plays a critical role in experience-dependent neuroplasticity including addiction-related processes. To date, however, it is not possible to measure glutamate release in humans. Positron emission tomography (PET) with [^{11}C]ABP688, a selective allosteric antagonist of metabotropic type 5 glutamate (mGlu5) receptors, could offer a strategy to quantify glutamate release *in vivo*. To test this proposition, we conducted a series of studies in rats using microdialysis and [^{11}C]ABP688 microPET imaging, and in humans using PET and magnetic resonance spectroscopy (MRS). Significant calcium-dependent glutamate release was identified in the ventral striatum of awake rats (190.5 ± 34.7%, $p < 0.05$; $n = 7$) following administration of a low dose of ethanol (EtOH; 20%, 0.5g/kg), a pharmacological challenge readily translatable to human research. Simultaneous microdialysis and microPET studies in anesthetized rats yielded concurrent increases in glutamate release (126.9 ± 5.3%, $p < 0.001$; $n = 11$) and decreases in striatal [^{11}C]ABP688 binding (6.8 ± 9.6%, $p < 0.05$). These latter two effects, however, were not significantly correlated ($r = 0.25$, $p = 0.46$). In humans, a laboratory stressor yielded significant changes in self-reported mood ($ps < 0.041$), sympathetic system activations ($ps < 0.042$), and the MRS index of striatal glutamate reuptake following excitatory neurotransmission, Glx/Cr levels ($p = 0.048$). These effects, however, were not accompanied by significant changes in [^{11}C]ABP688 BP_{ND} ($ps > 0.21$, $n = 9$) or correlated with each other ($ps > 0.074$). Together, these studies document EtOH-induced glutamate release from neurons, EtOH-induced decreases in [^{11}C]ABP688 binding, and stress-induced changes in glutamate turnover, yet fail to provide evidence that the PET [^{11}C]ABP688 method can be exploited to quantify moderate changes in glutamate levels. The results underscore the need for highly controlled testing conditions during PET measures of mGlu5 receptors.

3.2. INTRODUCTION

Glutamate is the primary excitatory neurotransmitter in mammalian brain where it plays a central role in the effects of drugs and alcohol, drug withdrawal, and experience-dependent neuroplasticity (Dahchour & De Witte, 2003; Fliegel *et al.*, 2013; Saal *et al.*, 2003; Stuber *et al.*, 2008; Vigneault *et al.*, 2015). Based on these observations, medications targeting glutamate neurotransmission are in development for various neuropsychiatric disorders, including schizophrenia, depression, addictions, and fragile X syndrome (Dolen & Bear, 2008; Goff & Coyle, 2001; Hashimoto, Sawa, & Iyo, 2007; Kalivas, 2009; Levenga *et al.*, 2011). Despite these advances, a lack of tools has hampered our ability to measure glutamate features that might be specific to humans and human brain-based diseases.

To date, several aspects of glutamate neurotransmission in living human brain, including changes in glutamate levels, have only been assessed indirectly. Functional imaging techniques such as blood oxygen level dependent-functional magnetic resonance imaging (BOLD-fMRI) and [^{18}F]fluorodeoxyglucose/positron emission tomography ([^{18}F]FDG/PET) can identify brain regional changes in activity, but their signals are not transmitter-specific (Knutson & Gibbs, 2007; Shafiei *et al.*, 2019). Proton magnetic resonance spectroscopy (^{1}H-MRS) can measure stress and pain-induced changes in glutamate turnover rate in a pre-specified region of interest (ROI) (Bryant *et al.*, 2013; Gutzeit *et al.*, 2013), but these spectroscopic signals are difficult to interpret and are believed to primarily indicate intracellular (neuronal and glial) levels, making the relation to neurotransmission uncertain (Ramadan, Lin, & Stanwell, 2013).

A proposed alternative approach is to use positron emission tomography (PET) with [^{11}C]ABP688 [3-((6-methylpyridin-2-yl)ethynyl) cyclohex-2-en-1-one-*O*-[^{11}C]methyloxime], a tracer that binds with high selectivity to the allosteric site of metabotropic type 5 glutamate (mGlu5)

receptors (Ametamey *et al.*, 2006; Scala *et al.*, 2021). PET/[^{11}C]ABP688 studies have identified alterations in mGlu5 receptor availability in populations with various psychiatric and neurodegenerative disorders, including major depressive disorder, substance use disorders, epilepsy, and frontotemporal dementia (Choi *et al.*, 2014; Cox *et al.*, 2020; Kim *et al.*, 2019; Leuzy *et al.*, 2016; Martinez *et al.*, 2014; Milella *et al.*, 2014; Smart *et al.*, 2017).

Preliminary evidence also indicates that, in both laboratory animals and humans, [^{11}C]ABP688 binding is affected by interventions that increase (DeLorenzo *et al.*, 2015; Esterlis *et al.*, 2018) and decrease (Zimmer *et al.*, 2015) extracellular glutamate concentrations. One possibility is that the changes in tracer binding are caused by glutamate release-inducing conformational changes that alter affinity at the allosteric binding site. Alternatively, since the reductions can remain for up to 24 hrs, a glutamate surge-induced receptor internalization is also possible. Indeed, this mechanism is thought to account for long-lasting decreases in the binding of D_2 receptor radioligands, such as [^{11}C]raclopride and [^{123}I]IBZM, following dopamine release (Laruelle, 2012; Laruelle *et al.*, 1997). Finally, [^{11}C]ABP688 binding values can vary by up to 70% when repeated PET scans are conducted on the same day. These changes might reflect circadian rhythm related influences on both mGlu5 receptor expression (DeLorenzo *et al.*, 2017; Elmenhorst *et al.*, 2016) and glutamate release (Marquez de Prado *et al.*, 2000) or, alternatively, diminished stress-induced glutamate release during the second scan (DeLorenzo *et al.*, 2017; Lupinsky, Moquin, & Gratton, 2010, 2017). In either scenario, these findings together raise the possibility that changes in extracellular glutamate concentrations affect mGlu5 tracer binding systematically thereby providing a non-invasive measure of glutamate release.

The gold standard for validating a PET measure of altered extracellular neurotransmitter levels is demonstrating that changes in PET tracer binding are *proportional* to changes in

extracellular transmitter concentration using *in vivo* microdialysis (Breier *et al.*, 1997; Laruelle, 2012; Laruelle *et al.*, 1997). To apply these techniques to PET-[^{11}C]ABP688, a glutamate-release enhancer is required. Several animal studies have tentatively demonstrated that moderately high doses of aqueous ethanol (EtOH) at a 20% concentration can promote neuronal dose-dependent glutamate release in the ventral striatum in rodents (Fliegel *et al.*, 2013). If confirmed at a dose more suitable for human ingestion, EtOH would be an easily accessible and administered glutamate trigger, fostering the translation of preclinical findings to clinical research.

Based on these observations, we first tested whether a low dose (0.5 g/kg) of 20% EtOH would lead to a glutamatergic response in the ventral striatum, as assessed with *in vivo* microdialysis. Second, we measured the correlation between changes in EtOH-induced glutamate concentrations in the ventral striatum and alterations in striatal [^{11}C]ABP688 non-displaceable binding potential (BP_{ND}) values using simultaneous *in vivo* microdialysis and microPET. Finally, we examined, in healthy humans, the effect of acute stress on [^{11}C]ABP688 BP_{ND} values, as measured with PET in mGlu5 receptor dense regions (Shigemoto *et al.*, 1993). This latter work was combined with MRS measures of the effect of acute stress on glutamate and glutamine levels in regions with reported stress-induced alterations in glutamate–glutamine balance (Auer *et al.*, 2000; Sheth *et al.*, 2019; Ullmann *et al.*, 2020). The associations between [^{11}C]ABP688 BP_{ND} values and brain tissue glutamate and glutamine levels were then assessed. A PET ligand sensitive to proportionate changes in endogenous glutamate release in humans would be a valuable new tool.

3.3. METHODS

3.3.1. [^{11}C]ABP688 Radiochemistry

Higher than 99% diastereomerically pure *E*-isomer, (*E*)-[^{11}C]ABP688 was produced as previously described by our group (Bdair *et al.*, 2019).

3.3.2. Animal Study

All experimental designs were approved by McGill University Animal Care Committee (UACC; Animal Use Protocol # MNI-7914), in compliance with the guidelines of the Canadian Council on Animal Care (CCAC).

3.3.2.1. Subjects

Male Lewis rats at age 60-65 postnatal days (PND) were purchased from Charles River (Saint Constant, QC, Canada) and housed at the Douglas Research Centre Animal Facility or the Center of Neurological Disease Models (CNDM) / McGill University, under 12-h/12-h light/dark cycle (lights open at 7:00 am) in a stress- and noise-free environment. Water and a protein-rich laboratory chow diet were provided *ad libitum* in their cages. A maximum of two rats were housed in a single standard cage, supplied with a standard environmental enrichment. After arrival, the rats were left to acclimate for at least seven days before use. Lewis strain was selected because it exhibits stronger characteristic neurochemical and behavioural aspects of drug-seeking behaviour (Cadoni, 2016).

3.3.2.2. Cannulation

Anesthesia was induced in rats inside an induction chamber using 4–5% isoflurane in medical air admixture at a flow rate of 2 L/min. The anesthesia was maintained with 2–2.5 isoflurane at the same flow, and rats were then placed on a stereotaxic bed with a pre-warmed pad. The eyes were treated with artificial tears to prevent ocular dryness, the scalp was shaved, and its skin was injected with 0.1 mL of 5 mg/mL bupivacaine intradermally to desensitise the scalp. An incision was made to the scalp using a sharp medical blade and skull was cleaned with hydrogen peroxide (H_2O_2). The target location of the cannula in the left ventral striatum (anteroposterior; AP: +1.20 mm, mediolateral; ML: –1.40 mm) was determined following Paxinos coordinates (Paxinos & Watson, 2005). With a handheld drill, apertures for the cannula and three anchor screws were made and the screws were the threaded in the cranium. A 22-gauge quartz guide cannula was inserted 6.00 mm along the dorsoventral (DV) axis and fixed to the cranium using superglue followed by acrylic dental cement. The guide cannula was then capped with a stainless-steel obturator that extends 2.50 mm beyond the end of the cannula to prevent infection and cerebral spinal fluid (CSF) leakage. Post-operatively, the rats were then injected subcutaneously with 20 g/kg of 0.9% NaCl (for one day), and with 2.5 mg/kg carprofen (for 3 consecutive days) to compensate for the lost blood and provide post-operative analgesia, respectively. A topical antibiotic (Polysporin®) was applied to the wound and the animals were left for at least a week for recovery, housed one per cage, before testing.

3.3.2.3. *In Vivo* Microdialysis

3.3.2.3.1. Standalone Microdialysis

In vivo microdialysis was initially conducted as a standalone technique in awake, freely moving rats (n = 7). Following a 20-min habituation period, the microdialysis probe was inserted into the guide cannula and connected from the other end to a Hamilton syringe filled with artificial cerebral spinal fluid (aCSF) and secured to a computer-controlled microinfusion pump (CMA). The aCSF (26 mM $NaHCO_3$, 1.2 mM NaH_2PO_4, 1.3 mM $MgCl_2$, 2.3 mM $CaCl_2$, 3.0 mM KCl, 126 mM NaCl, 0.2 mM L-ascorbic acid) was pumped to the probe at a flow rate of 1 µL/min for a minimum of 1 hr to stabilise neurotransmitter levels. Samples were then collected at 20-min intervals, mixed with 1 µL of 0.25 M perchloric acid and stored in -80˚C refrigerator for subsequent HPLC analyses. Following the collection of three baseline dialysate fractions, the animals received an intraperitoneal (i.p.) injection of 0.5 g/kg saline and five dialysate fractions were collected, followed by i.p. injection of 0.5 g/kg 20% EtOH with the collection of eleven dialysate fractions (Figure 3.1A).

Furthermore, to study the calcium dependency of the hypothesised EtOH-induced glutamate release, the experiment was repeated with the use of a Ca^{2+}-free aCSF instead (n = 4). In the latter, $CaCl_2$ was replaced with an equimolar concentration of $MgCl_2$ (final concentration: 3.6 mM). The paradigm was similar to the EtOH challenge microdialysis described above. However, after collecting four baseline samples, the perfusate was switched from aCSF to Ca^{2+}-free aCSF using a liquid switch (CMA), following which four fractions were collected. After the animal received an i.p. injection of 0.5 g/kg 20% EtOH, eleven fractions were collected (Figure 3.1B).

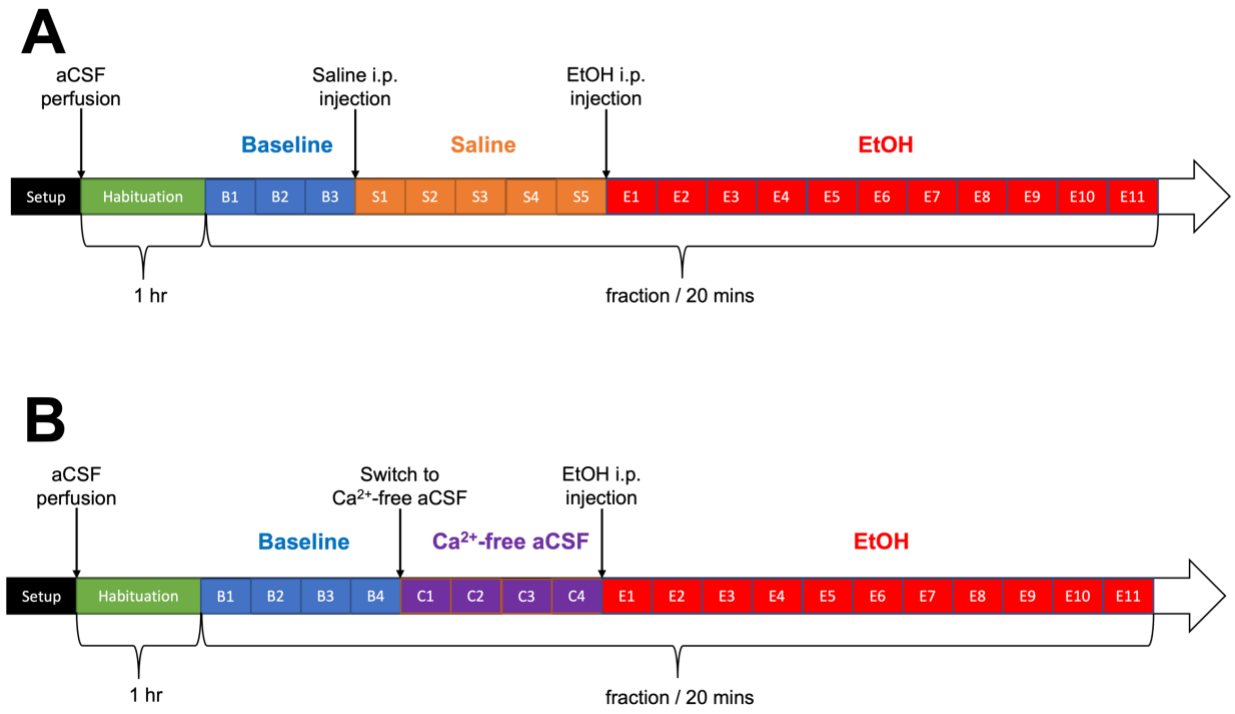

Figure 3.1: Diagrams of the microdialysis study using either (**A**) artificial cerebrospinal fluid (aCSF; n = 7) or (**B**) calcium-deprived aCSF (*n* = 4), in awake animals.

3.3.2.3.2. Simultaneous Microdialysis and MicroPET

In vivo microdialysis was conducted simultaneously with microPET scanning in anesthetized animals (*n* = 11). Herein, animals were induced in a chamber with 4–5% isoflurane in medical air admixture and then maintained with 1.5–2.5% isoflurane at 0.8 L/min flow rate through a nose cone. The rats were placed in prone position on the prewarmed bed of the microPET scanner (CTI, Concorde Microsystems, LLC). Each rat underwent two microdialysis/microPET scans on separate days of < 7 days apart, where the animal received i.p. injection of 0.5 g/kg of either saline or 20% EtOH.

As in the standalone microdialysis study, aCSF was pumped at a flow rate of 1 µL/min and dialysate fractions were collected every 20 min. Subsequent to the collection of four baseline

dialysate fractions, rats received an i.p. injection of the pharmacological intervention (i.e., saline or 20% EtOH). The collection of first post-saline or -EtOH dialysate sample started at the moment of injection. The radiotracer was injected intravenously 5 min post-saline or -EtOH injection. The *simultaneous* microdialysis and microPET study design is depicted in Figure 3.2.

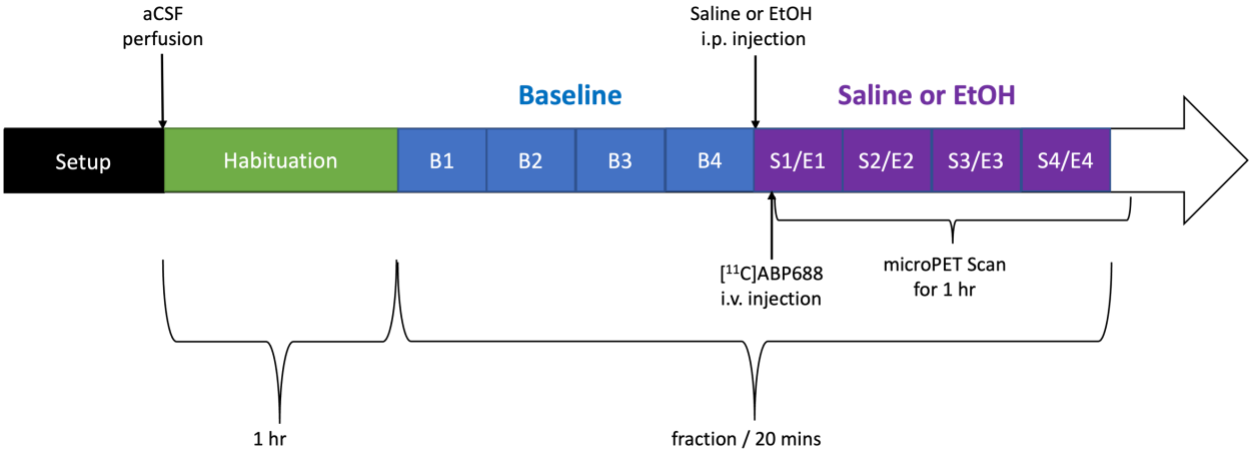

Figure 3.2: Diagram of the simultaneous microdialysis plus microPET study.

3.3.2.4. Analysis of Dialysate Samples

Measurements of dialysate glutamate concentrations were determined with an HPLC precolumn derivatization with ultimate 3000 RS fluorescence detection (ex: 322 nm; emission: 455 nm) and further described by Lupinsky *et al* (Lupinsky, Moquin, & Gratton, 2010). The HPLC system consisted of a Dionex pump (ultimate 3000) and a Dionex RS autosampler (ultimate 3000) bundled with a Waters Xterra MS C18 3.0 × 50 mm 5 µm analytical column. The mobile phase is 3.5% CH_3CN, 20% methanol (CH_3OH), and 100 mmol/L sodium phosphate dibasic (Na_2HPO_4) adjusted to pH 6.7 with 85% phosphoric acid (H_3PO_4). The flow rate was set at 0.5 mL/min. Working standards (100 ng/mL) and derivatization reagents were prepared fresh daily and loaded with samples into a refrigerated (10°C) Dionex RS autosampler (ultimate 3000). Before injection onto the analytical column, each fraction was sequentially mixed with 20 µL of o-phthaldehyde

(0.0143 mol/L) diluted with 0.1 mol/L sodium tetraborate and 20 µL of 3-mercaptopropionic acid (0.071 mol/l) diluted with H_2O and allowed to react for 10 minutes. After each injection, the injection loop was flushed with 20% CH_3OH to prevent contamination of subsequent samples. Under these conditions, the retention time for glutamate was approximately 1 min with a total run time of 30 min/sample.

3.3.2.5. Animal PET Scanning

All rats (n = 11) underwent two microPET scans, baseline and challenge, conducted between 11:00 and 13:00 (to mitigate potential effects of circadian glutamate variations). The microPET procedure was conducted in the anesthetized rats using microPET R4 scanner (CTI, Concorde Microsystems, LLC; spatial resolution of approximately 1.85 mm (Knoess *et al.*, 2003)). After collecting a minimum of 4 baseline dialysate samples, 0.5 g/kg of either saline (baseline) or 20% EtOH (challenge) was injected intraperitoneally, and the rats were placed in the scanner's centre field of view (FOV). Five minutes after EtOH or saline injection, a 0.5–1.0 mL bolus injection of (*E*)-[^{11}C]ABP688 at an average dose of 21.83 MBq (range: 19.94–24.98 MBq) was administered intravenously in the lateral tail vein through a pre-inserted catheter, followed by a 60-min dynamic emission acquisition. A total of 27 frames were acquired (9 × 30 s, 6 × 1 min, 5 × 2 min, 7 × 5 min), followed by a 9-min transmission scan using a rotating ^{57}Co source.

3.3.2.6. Animal MRI Scanning

Magnetic resonance imaging (MRI) structural images for co-registration purposes were obtained using a 7T Bruker Pharmascan pre-clinical MRI system, with a Bruker volume resonator radiofrequency (RF) coil designed for rat brain imaging. Two-dimensional T2-weighted MRI

images were obtained with multi-slice TurboRARE acquisition, in-plane resolution of 0.2 × 0.2 mm^2, and slice thickness of 0.5 mm. The sequence included a TR of 6000 ms, TEeff of 30 ms, RARE factor of 4, 42 slices covering the whole rat brain, 20 signal averages and total acquisition time of 42 min. The in-plane FOV was 2.50 cm × 3.50 cm.

3.3.2.7. Image Processing and Analyses

Images were reconstructed using *Maximum a Posteriori* (MAP) algorithm with scatter correction, then processed and analysed using MINC toolkit software (http://bic-mni.github.io). Co-registration of PET and MRI images was performed with MINC toolkit using both eyes, olfactory bulbs, temporal poles, and base of the skull as registration landmarks. Atlas-based auto-segmentation of various ROIs was performed with ITK-SNAP (v. 3.6.0; http://www.itksnap.org/pmwiki/pmwiki.php) (Yushkevich *et al.*, 2006), based on brain region delineations reported in Waxholm Space atlas of the Sprague Dawley rat brain (Papp *et al.*, 2014), where the MRI images were linearly co-registered to the atlas. Mean BP_{ND} of ROIs was calculated relative to the non-specific binding in cerebellum, using the simple reference tissue model (SRTM) (Gunn *et al.*, 1997), as previously reported (Elmenhorst *et al.*, 2010). Percent change in [^{11}C]ABP688 BP_{ND} was calculated as following: (($BP_{ND\ BASELINE} - BP_{ND\ CHALLENGE}$)/ $BP_{ND\ BASELINE}$) × 100.

3.3.3. Human Study

3.3.3.1. Participants

Healthy, right-handed volunteers (5 males and 4 females) aged 25.1 ± 6.0 (Mean ± SD) years old were recruited from the general population using online advertisements on the McGill

University website and through classified advertisements. Exclusion criteria included: (1) current or past DSM-5 disorders, including current or past substance use except for occasional cannabis use (< once per month), social tobacco use (< once per week) and occasional drinking (≤ seven drinks per week); (2) family history of DSM-5 Axis I disorder; (3) current or past chronic medication use, excluding birth control; (4) significant physical illness in the past 12 months; (5) any history of head injury/loss of consciousness; (6) any counterindications to MRI or PET including claustrophobia, and the presence of a medical condition that makes pain stimuli dangerous (e.g., cardiac disease, hypertension, pulmonary disease, seizure disorder, osteopenia, and anxiety syndromes). The study protocol was approved by the Research Ethics Board of the Montreal Neurological Institute and the Faculty of Medicine and was carried out in accordance with the Declaration of Helsinki. Next, physical health was evaluated by a routine examination, a standard blood work and electrocardiogram. A urine toxicology test for illicit drugs of abuse (Triage, Biosite Diagnostics, San Diego, CA, responsive to amphetamines, methamphetamines, barbiturates, benzodiazepines, cocaine, 2-ethylene-1,5-dimethyl-3,3-diphenylpyrrolidine (EDDP), opiates, Δ^9-tetrahydrocannabinol (Δ^9-THC) and tricyclic antidepressants) and a urine pregnancy test for women was performed on the screening day and prior to each PET session.

3.3.3.2. Stress Administration

All participants underwent two scanning sessions consisting of a 1-hour PET scan followed by a 45 min MRI scan with MRS. The two scanning days were conducted in a counter-balanced, within-subjects cross-over design, at least 3 days apart, with each PET and MR scan conducted at the same time of the day to mitigate potential effects of circadian glutamate variations (Figure 3.3).

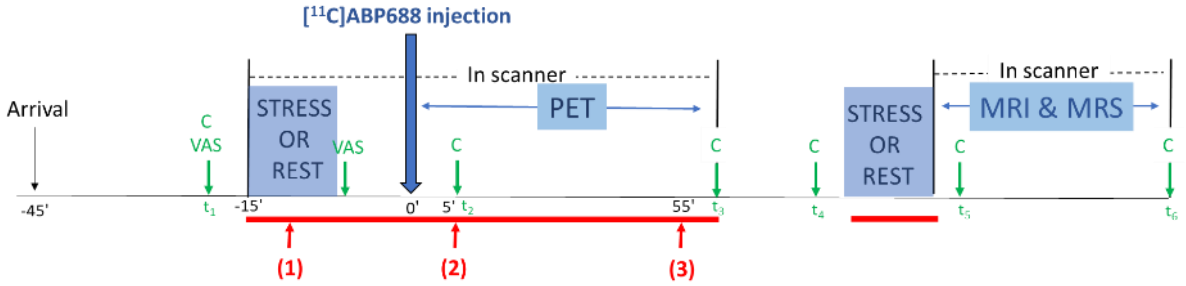

Figure 3.3: Timing of test sessions. X-axis denotes time relative to injection at time 0. Participants underwent a stress or rest task 15 min before injection of the PET tracer and starting the MR scan. Mood and physiological data were collected throughout. The red bars represent periods when electrodermal activity was tracked. VAS = visual analog scale; C = cortisol measurement.

The acute stress stimulus consisted of unpredictable electrical stimulation of the wrist administered immediately below the individual's pain threshold, defined as the lowest intensity at which a sensation of mild pain is felt. Participants observed 20s countdowns followed by a blank screen during which electric stimulation occurred 67% of the time, pseudo-randomized. After a 10s rest, the paradigm was repeated. In six min, participants experienced 12 × 30s blocks, for a total of eight electrical stimulations out of 12 trials. Participants were instructed prior to the stress task that they would receive intermittent electrical stimulation at the level of their threshold. Participants were not given a distinguishing cue to identify whether a stimulation would be followed by a given countdown nor were they informed of the contingency rate. Participants provided verbal ratings of discomfort on the pain scale and visual analog scale (VAS; Figure 3.4) every time the stimulus was presented permitting adjustments to the intensity.

The pain threshold was determined outside of the PET scanner environment as follows. Electric stimulation was initiated with a duration of 200ms and voltage of 20V and was increased in increments of 2V until the lowest voltage at which subjects experienced moderate discomfort was reached. This was defined as a score of 3 on the 5-point pain scale and at least 20 on the VAS. The threshold was re-established on the stress session, immediately prior to the stress task. The

pain threshold determined earlier was used as a starting point to minimize the number of shocks administered before the task. The intensity of shock corresponding to the threshold was then used as the target intensity for the stimulation during the stress task.

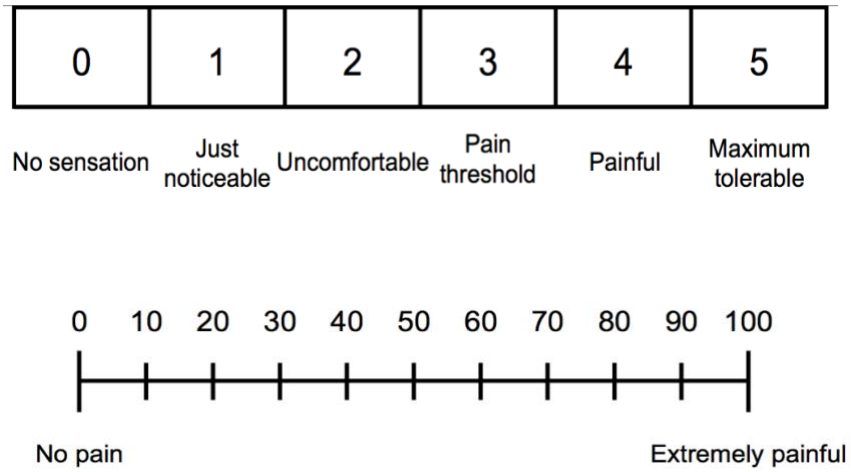

Figure 3.4: Pain scale (top) and pain visual analog scale (bottom).

3.3.3.3. Objective Indices of Stress Response

To assess the effectiveness of the stimuli, variation of the electrical conductance in response to skin secretion was tracked continuously throughout stress/rest tasks and PET scanning sessions. First, phasic deflections in the skin conductance responses (SCRs) were analyzed (Pitman & Orr, 1986). The SCR amplitudes during the stress task were calculated by subtracting the mean skin conductance level 2s before expectation of a shock, from the peak value obtained immediately after administration of the shocks. To avoid habituation (Davis, 1934), phasic increases occurring over the first 5 trials of shocks were taken into account. The same calculation was applied over the first 3 periods of blank screens in which shock was expected but not triggered. During the same time interval at rest, amplitudes of non-specific SCRs (occurring in the absence of stimuli) were calculated. Lastly, tonic skin conductance was compared: three-time intervals were averaged,

including (1) stress task or rest, (2) the first 5 to 10 minutes of PET, and (3) the last 5 minutes of PET (Figure 3.3). The time interval (2) corresponds to the peak of the hypothalamus-pituitary-adrenal (HPA) axis response in response to stress, which is expected to begin 20 minutes after the initiation of the stimulus (t2).

The HPA axis response to stress was assessed by measuring cortisol concentrations from saliva samples collected using oral swabs (Salimetrics, LLC). In total, six saliva samples were collected over 120 minutes: at baseline (t_1 and t_4), at two time points after initiation of the task (t_2 and t_5: 20 min after initiation of the task), and at the end of each scan (t_3 and t_6). Area under the curve with respect to ground (AUC_G), and with respect to increase from cortisol value at t_1 (AUC_I) were calculated as described (Pruessner *et al.*, 2003). AUC_G is the total area under the curve, whereas AUC_I is calculated with reference to the first value (cortisol value at t_1). Samples were stored at −20 °C until biochemical analysis took place.

3.3.3.4. Behavioral Assessment

Subjective ratings of mood, anxiety, and alertness were measured using the state-trait anxiety inventory (STAI)-State (Spielberger, 1983), and visual analog scale of alertness. Each scale was collected two times each session, before and immediately after the first stress task (Figure 3.3).

3.3.3.5. Human PET Scanning

All PET scans were performed using a High-Resolution Research Tomograph (HRRT; Siemens/CTI, Knoxville, TN, USA) at the Montreal Neurological Institute. Scans consisted of a 60-min dynamic acquisition collected in list-mode format, followed by a 6-min ^{137}Cs rotating point

source transmission scan for attenuation correction. The acquisition was binned into frames, which durations consisted of the following sequence: 3 × 10 s, 5 × 30 s, 4 × 60 s, 4 × 120 s, 5 × 300 s, 2 × 60s. The scan initiated concurrently with the beginning of the venous injection of an average dose of 385.54 MBq (range: 333–407 MBq) of (*E*)-[^{11}C]ABP688 through an intravenous catheter installed at the participant's right arm vein (antecubital region).

3.3.3.6. Human MRI and MRS Scanning

For PET/MR co-registration and spectroscopy voxel placement, all subjects also underwent high-resolution T1-weighted MRI scan after each PET session. Scans were acquired in a 3T Siemens TRIO Magneton scanner (Siemens Medical Solutions, Erlangen, Germany) using an ADNI-3D MPRAGE protocol. Images were acquired in 3D repetition time (TR) = 2300 ms, echo time (TE) = 3.42 ms, flip angle = 9°, field of view = 256 mm, and FOV = 256 × 256; 1 mm resolution isotropic resolution.

During the same session, MR spectroscopy scanning was conducted in two volumes of interests from which measures of combined glutamate (Glu) and glutamine (Gln), referred to as Glx, and Glu alone were obtained. Spectroscopic voxels were prescribed from anatomic images: a 20 × 15 × 10 mm^3 voxel was placed bilaterally over the anterior cingulate cortex (ACC), immediately anterior to the rostrum of the corpus callosum, and perpendicular to the infra-callosal line. The striatum voxel was 25 × 12 × 12 mm^3 in size, encompassing the right dorsal caudate-putamen. The water suppressed proton spectra were acquired using a 90˚–180˚–180˚ (PRESS) sequence (TR =3000 ms, TE = 40 ms), giving a total of 196 acquisitions. A water-unsuppressed reference scan to enable correction for eddy current-induced phase shifts was obtained immediately after the water-suppressed scan using the same TR, TE, voxel position and shim

settings with 16 acquisitions.

3.3.3.7. Image Processing and Analyses

CIVET pipeline (https://www.bic.mni.mcgill.ca/ServicesSoftware/CIVET) was used to preprocess the native MRI image. The resampled images were then classified into white matter (WM), grey matter (GM), CSF and segmented in the main brain structures and automatically labelled, using the ANIMAL probabilistic atlas-based algorithm (Collins *et al.*, 1999). Then, the PET images were co-registered with the subject's own MRI transformed into the Montreal Neurological Institute (MNI) template brain using transformed parameters obtained from the registration of MRI to MNI152 space. Mean BP_{ND} of ROI was estimated using SRTM (Gunn *et al.*, 1997), with the cerebellar grey matter as reference region. Subcortical limbic regions amygdala and hippocampus were yielded by the segmentation generated by the ANIMAL image registration algorithm. A standard mask was used to functionally segment the striatum into ventral (VST), associative (AST), and sensorimotor (SMST) subregions, as proposed by Mawlawi et al (Mawlawi *et al.*, 2001). Remaining cortical ROIs were manually drawn on a template MRI in stereotaxic space using the software DISPLAY (http://www.bic.mni.mcgill.ca/software/Display/Display.html) and was based on the approach defined by Abi-Dargham et al (Abi-Dargham *et al.*, 2000). Percent change in [^{11}C]ABP688 BP_{ND} was calculated as following: $((BP_{ND\ STRESS} - BP_{ND\ REST})/ BP_{ND\ REST}) \times 100$.

3.3.4. Statistical Analyses

Analyses were performed using SPSS software. (Version 29). Differences were considered statistically significant at $p < 0.05$. Shapiro–Wilk tests established normal distribution of all data.

For standalone microdialysis study, the effects of EtOH administration were tested using a one-way repeated measures analysis of variance (rmANOVA) with time as the within-group factor containing 17 levels (pooled baseline and each subsequent fraction; five saline samples and eleven EtOH samples). Average values were extracted for each condition (baseline: B1-3; saline: S1-5; EtOH: E1-6) and compared using a one-way rmANOVA with condition as the within-group factor containing three levels. Both ANOVAs contained tests for violations of sphericity; Huynh-Feldt corrections were applied when necessary. Bonferroni-corrected paired t-tests were then used to compare the three experimental conditions.

In the simultaneous microdialysis and microPET study, a two-way within-subject rmANOVA test was performed to study the effect of treatment (saline *vs*. EtOH) over time (5 levels; pooled baseline and four subsequent posttreatment fraction) on extracellular glutamate levels in the ventral striatum, as assessed with microdialysis. Regarding PET images, a one sample (*i.e.*, paired) t-test was conducted to determine the percent difference in [^{11}C]ABP688 BP_{ND} in the ventral striatum. Pearson's *r* test was then used to examine the correlation between the percent difference between extracellular glutamate concentrations (saline *vs*. EtOH) and [^{11}C]ABP688 displacement. Percent change of individual dialysate fraction (averaged across all animals) was calculated relative to pooled baseline fractions. Peak percent of baseline is defined as the dialysate fraction with the highest extracellular glutamate concentration compared to pooled baseline fractions.

For the human study, the effect of stress on subjective anxiety and physiological measurements (cortisol and IL1- β) were identified using two-way rmANOVAs or mixed- model analyses when data were missing, with sessions (rest *vs*. stress) and timepoints as within-subject factors. Simple-main effects analyses followed when indicated. Planned pair-wise t-tests were

carried out to identify differences in the magnitude of SCR and non-stimuli SCR relative to the non-specific SCRs. Summary BP_{ND} values were computed as the unweighted mean of all examined regions in order to assess the effects of tracer and scan characteristics (mass of tracer injected per kilogram body weight and time of injection). Relationships between BP_{ND} and scans characteristics were assessed using Pearson's *r*. To test the main hypothesis of differences in BP_{ND} between conditions, separate Condition x Region x Hemisphere repeated measures ANOVAs were performed for (i) striatal regions (VST, AST, SMST), (ii) prefrontal regions (medial (mPFC), dorsolateral (dlPFC) prefrontal cortices, orbitofrontal cortex (OFC), and ACC), and (iii) limbic regions (amygdala and hippocampus). These were followed by planned, uncorrected two-tailed dependent measures t-tests to assess each contrast in the selected ROIs between conditions. For each ROI, percent change from scan 1 to scan 2 (($BP_{ND\ STRESS} - BP_{ND\ REST}$)/ $BP_{ND\ REST} \times 100\%$) was calculated for each participant. Parametric maps of BP_{ND} were compared in voxel-wise paired *t*-tests from scan 1 to scan 2 in each participant using RMINC with a significance threshold of $p < 0.05$, corrected for false discovery rate. To determine the significance of detected metabolites concentration differences due to shock administration, a Condition (rest, stress) by Region (ACC, striatum) two-way rmANOVA was applied to the MRS data. Finally, potential associations of mGlu5 receptor availability with behavioral and physiological variables were examined using Pearson's *r*. Given the large number of correlations performed, the unadjusted alpha level was divided by the number of studied ROIs, which resulted in a significance threshold of $p = 0.05/9 = 0.0056$. In a secondary voxel-wise analysis, further exploratory correlations using mGlu5 binding across the whole brain were assessed with parameters which revealed to be significantly correlated with ROI-wise BP_{ND}.

3.4. RESULTS

3.4.1. Radiochemistry

The diastereomeric excess (d.e.) and radiochemical purity (RCP) of *(E)*-[^{11}C]ABP688 were both >99%. Mean molar activity (A_m) at time of injection was 83.24 GBq/µmol (range: 28.46–268.28 GBq/µmol, $n = 22$) in the animal study and 91.71 GBq/µmol (range: 23.1–163.6 GBq/µmol; $n = 18$) in the human study.

3.4.2. *In Vivo* Microdialysis

As depicted in Figure 3.5A, there were main effects of time ($F(4.891,29.346) = 2.901$, $p = 0.035$) and condition ($F(1.240,7.439) = 10.621$, $p = 0.010$) in awake rats. This reflected significant increases in extracellular glutamate concentrations following EtOH administration (E1 – E5) as compared to samples collected following the saline injection (S1 – S5: $t(6) = 3.322$, $p = 0.048$) and the pre-injection samples (B1 – B3: $t(6) = 3.372$, $p = 0.045$). As expected, no differences were seen between the baseline and saline conditions ($p > 0.50$). Compared to the average saline response, the largest effect occurred during the third dialysate sample collected between 40-60 min after EtOH injection (E3) ($t(6) = 2.458$, uncorrected $p = 0.049$). During this E3 fraction, extracellular glutamate concentrations reached 190.5 ± 34.7% of average baseline and 212.05 ± 47.52% of average saline. This effect of EtOH was abolished when using the Ca^{2+}-free aCSF (Figure 3.5B).

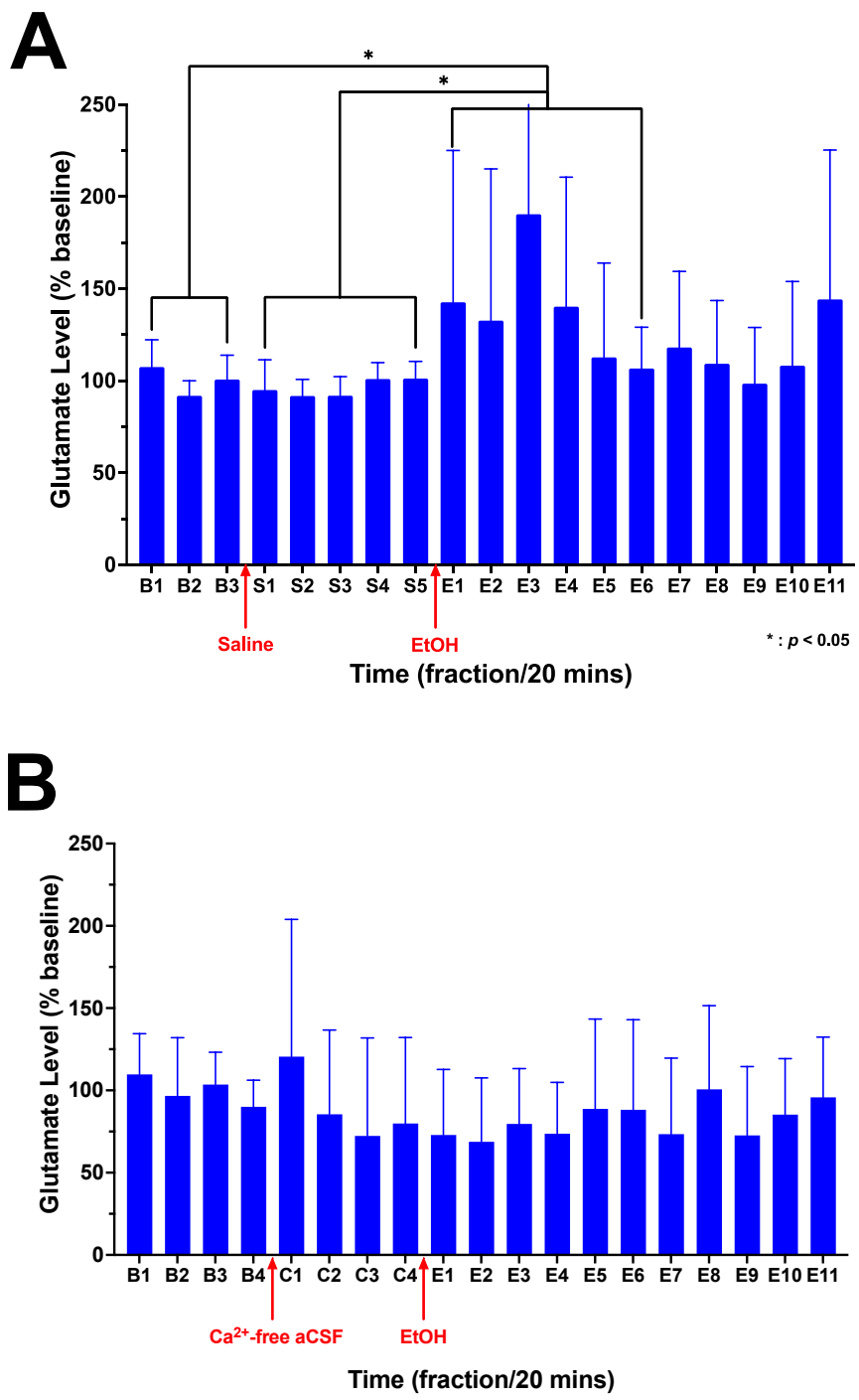

Figure 3.5: Percent change from baseline of extracellular glutamate concentrations in the ventral striatum as measured by microdialysis in *awake* animals, following (**A**) i.p. injection of 0.5 g/kg saline and 0.5 g/kg 20% EtOH (n = 7), or (**B**) infusion of Ca^{2+}-free aCSF and i.p. injection of 0.5 g/kg 20% EtOH (n = 4). Values are Mean ± SD. * $p < 0.05$

During the simultaneous microdialysis and microPET study in anesthetized rats, a two-way rmANOVA yielded a significant treatment (saline *vs*. EtOH) by time interaction ($F(2.505,25.046) = 3.353$, $p = 0.042$; $n = 11$). Post-hoc pairwise comparisons revealed a significant difference between the first two post-treatment dialysate fractions from the pooled baseline ($ps < 0.05$, uncorrected), and there was a significant difference between the effects of EtOH and saline in the first fraction (S1 *vs*. E1: ($t(10) = –5.066$, $p < 0.001$) reflecting concentrations that were 126.9 ± 5.3% of baseline (Figure 3.6).

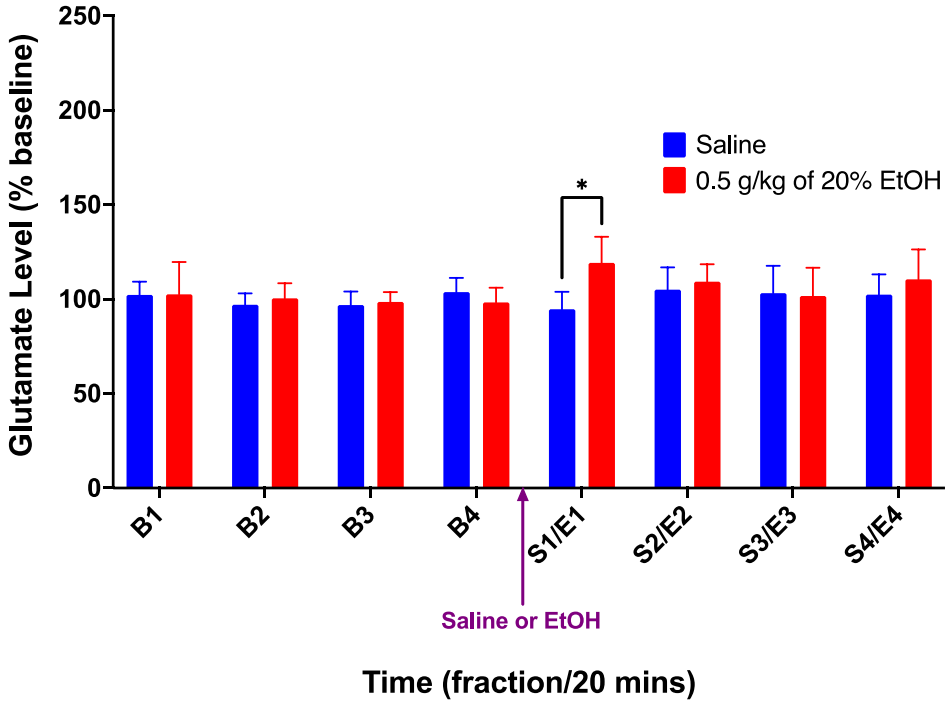

Figure 3.6: Percent change from baseline (B1-4) of extracellular glutamate concentrations in the ventral striatum as measured by microdialysis, following i.p. injection of 0.5 g/kg of either saline or 20% EtOH in *anesthetized* animals ($n = 11$). Values are Mean ± SD. * $p < 0.05$

3.4.3. Animal PET Scanning

The two PET scans did not significantly differ ($ps > 0.05$) in the injected *(E)*-[^{11}C]ABP688 dose (baseline: mean 22.24 MBq, range 20.72–24.98 MBq; challenge: mean 21.43 MBq, range

19.94–24.98 MBq), A_m (baseline: mean 55.79 GBq/µmol, range 28.46–131.15 GBq/µmol; challenge: mean 107.95 GBq/µmol, range 37.72–269.28 GBq/µmol), injected volume (baseline: mean 0.62 mL, range 0.5–1.0 mL; challenge: mean 0.58 mL, range 0.5–0.75 mL), injected mass (baseline: mean 1.3 pmol/g, range 0.5–2.3 pmol/g; challenge: mean 0.9 pmol/g, range 0.3–2.0 pmol/g), start time (baseline: mean 12:22, range 11:09–13:15; challenge: mean 12:24, range 11:13–13:29) or weight of the animals (baseline: mean 306.8 g, range 276–384 g; challenge: mean 311.3 g, range 266–349 g). The average age of the animals was 83.5 ± 7.7 (Mean ± SD) at the time of the baseline scan, and 87.8 ± 7.1 days (Mean ± SD) at the time of the challenge scan.

There was a significant percent reduction in striatal [^{11}C]ABP688 BP_{ND} in response to EtOH administration compared to saline, corresponding to a percent change of 6.8 ± 9.6% (baseline BP_{ND}: 4.78 ± 0.55 (Mean ± SD), range 4.18–5.83; challenge BP_{ND}: 4.45 ± 0.69 (Mean ± SD), range 3.23–5.85; $t(10) = 2.424$, $p = 0.036$) (Figure 3.7). The ratio of percent glutamate increase during E1 (compared to S1) to percent [^{11}C]ABP688 BP_{ND} reduction was 4:1. Percent changes in extracellular glutamate concentrations in the ventral striatum were not significantly correlated with percent changes in striatal [^{11}C]ABP688 BP_{ND} ($r = 0.25$, $p = 0.46$).

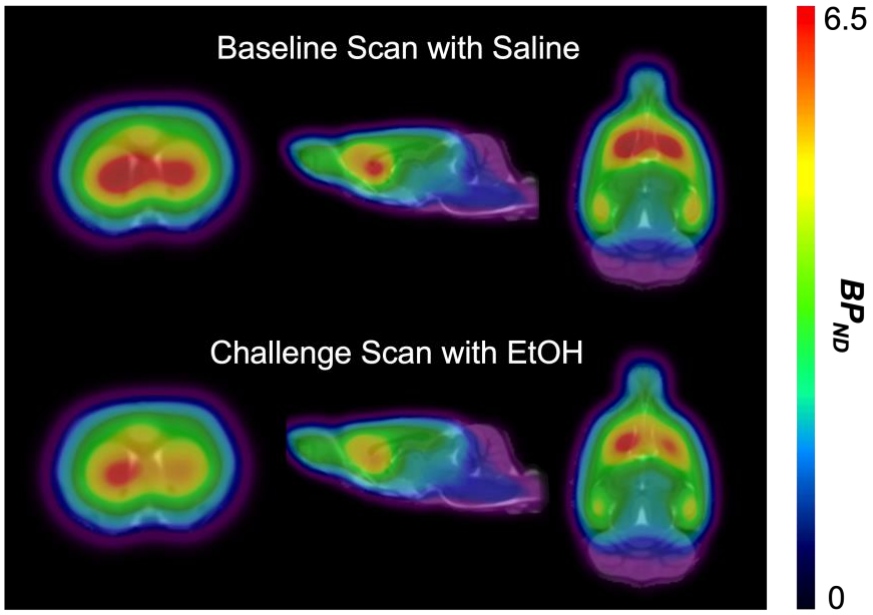

Figure 3.7: Average PET images in rodents (n = 11, coronal: left, sagittal: middle, axial: right) showing [^{11}C]ABP688 BP_{ND} following i.p. injection of 0.5 g/kg of either saline (top) or 20% EtOH (bottom).

3.4.4. Human Study

3.4.4.1. Physiological Stress Responses

Skin conductance responses were significantly higher following exposure to the stressor ($t(7) = 4.65$, $p = 0.0023$). Numerically greater increases also occurred when shocks were expected, but not given, but this response was more variable and at the trend level only ($t(7) = 2$, $p = 0.09$) (Figure 3.8). Twenty minutes following initiation of the task, skin conductance levels remained elevated ($t(7) = 3$, $p = 0.04$) before normalizing after an hour ($t(7) = 0.047$, $p = 0.96$).

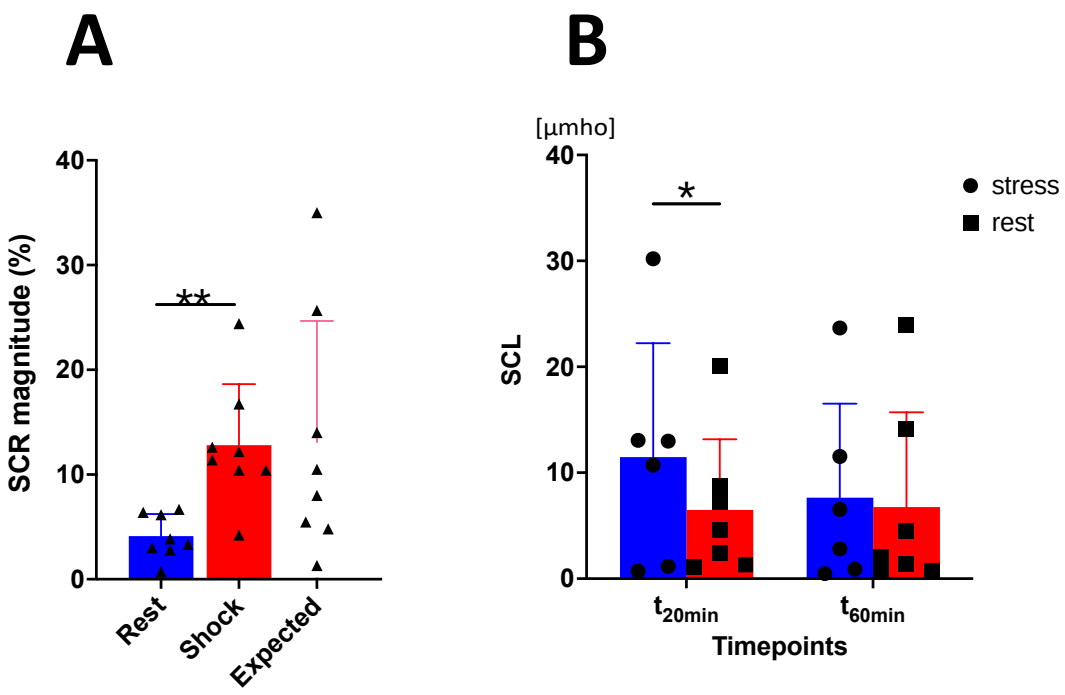

Figure 3.8: (**A**) The Skin Conductance Response was significantly higher during shock exposure than rest. The peak that occurs when shocks were expected but not given also showed trend-level effects reflecting higher peaks than at rest. (**B**) 20 min after the initiation of shocks SCL remained higher than at rest, but this effect did not persist after an hour. Values are Mean ± SD. * $p < 0.05$; ** $p < 0.01$

AUC_I between stress and rest were significantly different ($t(7) = 2$, $p = 0.041$), reflecting increased *vs*. decreased cortisol levels during the stress ($AUC_{I\ STRESS} = 6.97$) *vs*. rest session ($AUC_{I\ REST} = -6.83$). The stress-induced percent increases in cortisol and skin conductance levels were significantly correlated ($r = 0.838$, $p = 0.009$).

3.4.4.2. Self-Report Responses

Significant Condition × Timepoint interactions were obtained for the "alert" ($F(1,7) = 9.471$, $p = 0.018$) and "anxious" VAS measures ($F(1,7) = 6.25$, $p = 0.041$), but not "afraid" ($F(1,7) = 3.3$, $p = 0.11$). Further inspection of the data confirmed that in the stress condition, alertness and anxiety

ratings were higher post-stress (t2) relative to pre-stress (t1) (alert: t(7) = 3.784, p = 0.0137; anxious: t(7) = 3.005, p = 0.0396, respectively; Figure 3.9).

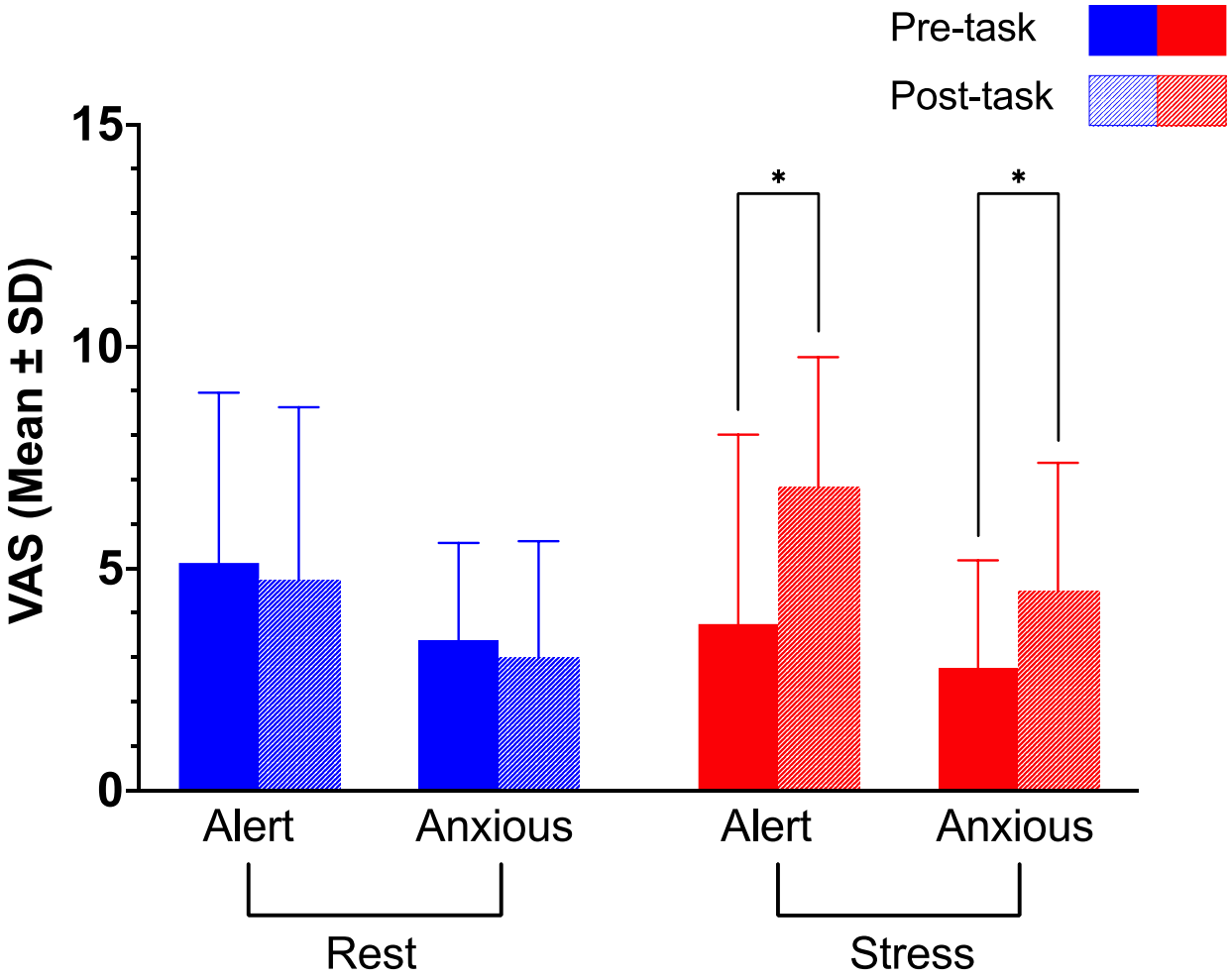

Figure 3.9: Anxiety and alertness rating was significantly higher after administration of the stress task relative to before administration and relative to baseline. Solid bars represent pre-task. White -hashed bars represent post-task (t = –20 min pre-injection, t = +20 min post-injection, respectively). Red indicates rest session; blue indicates stress session. Values are Mean ± SD. * p < 0.05

3.4.4.3. PET/MRS

The two PET test sessions did not differ in injected tracer dose (rest: mean 378.88 MBq, range 355.2-392.2 MBq; stress: mean 388.87 MBq, range 333-407 MBq; t(8) = -1.16, p = 0.28),

A_m (rest: mean 89.32 GBq/µmol, range 23.1-128 GBq/µmol; stress mean 94.1 GBq/µmol, range 24-163.6 GBq/µmol; t(8) = 1.204, p = 0.26), or start time (rest: mean 12:30, range 11:07-15:03; stress: mean 12:37, range 11:03-14:08; t(8) = -0.28, p = 0.79). Global BP_{ND} values were not related to the mass of [^{11}C]ABP688 injected (r = 0.22, p = 0.37) or time of injection (r = 0.27, p = 0.79).

Three-way Condition x Subregion x Hemisphere repeated measures ANOVAs did not identify a significant main or interaction effects (Fs<0.97, *ps*>0.41). Controlling for test session order (stress session in the first scan *vs*. second scan) did not affect the results. Likewise, replacing the "Condition" factor by the "Day" factor (first scan *vs*. second scan) did not change the results. Percent change in BP_{ND} was calculated and averaged across all ROIs within a subject, which ranged from -17.5% to 18.6%. A global tendency of increase was found across regions between conditions, but this did not reach statistical significance in post-hoc pairwise comparisons (*ps* > 0.3, uncorrected). Voxel-wise parametric analyses were consistent with these findings, with no clusters of significant voxels emerging.

Analysis of the combined Glutamate + Glutamine (Glx) levels did not yield a significant main effect of Session (F(1,7) = 1.09, p = 0.33) but a trend level Region x Session interaction was seen (F(1,7) = 0.16, p = 0.08). Post-hoc exploratory tests yielded evidence of significant stress-induced increases in Glx concentrations in the striatum (13% increase, p = 0.048) but not in the ACC (2% increase, p = 0.5; Figure 3.10).

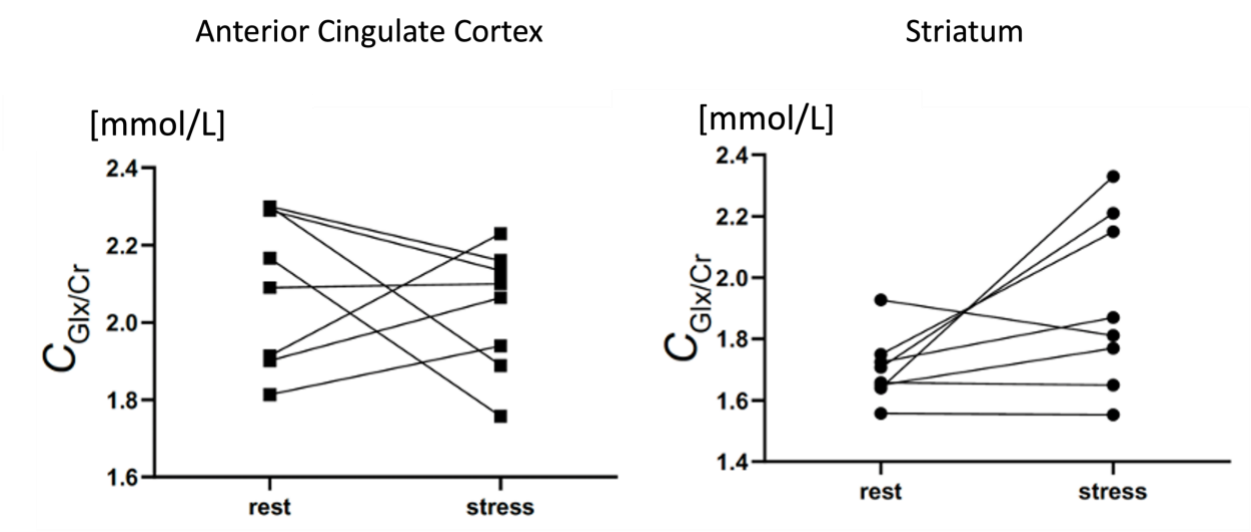

Figure 3.10: Changes from rest scan to stress scan in combined glutamate and glutamine concentrations (mmol/L) for each participant in the anterior cingulate cortex (squares) and striatum (circles).

3.4.4.4. Correlations

In humans, there were no significant associations between stress-induced changes in BP_{ND} values and stress-induced changes in Glx/Glu ratios or between BP_{ND} values and Glx/Glu ratios at rest. However, BP_{ND} values on the stress session ($BP_{ND\ STRESS}$) in limbic, sensorimotor and associative striatum, OFC and left amygdala were all negatively correlated with stress-induced changes in Glx/Glu levels in the ACC ($rs > -0.71$, $ps < 0.044$, uncorrected). $BP_{ND\ STRESS}$ values were also associated with Glx/Glu levels in the ACC at stress in the ACC and both associative and sensorimotor striatum ($rs > -0.43$, $ps < -0.71$, $ps < 0.048$, uncorrected), and to a lesser extent in the hippocampus ($r = -0.7$, $p = 0.054$, uncorrected). Stress-induced changes in the cortisol AUC_G were also correlated with $BP_{ND\ STRESS}$ values in the striatum, OFC, amygdala and hippocampus ($rs < -0.72$, $ps < 0.045$, uncorrected). Correlations that survived at $p = 0.0056$ are shown in Figure 3.11.

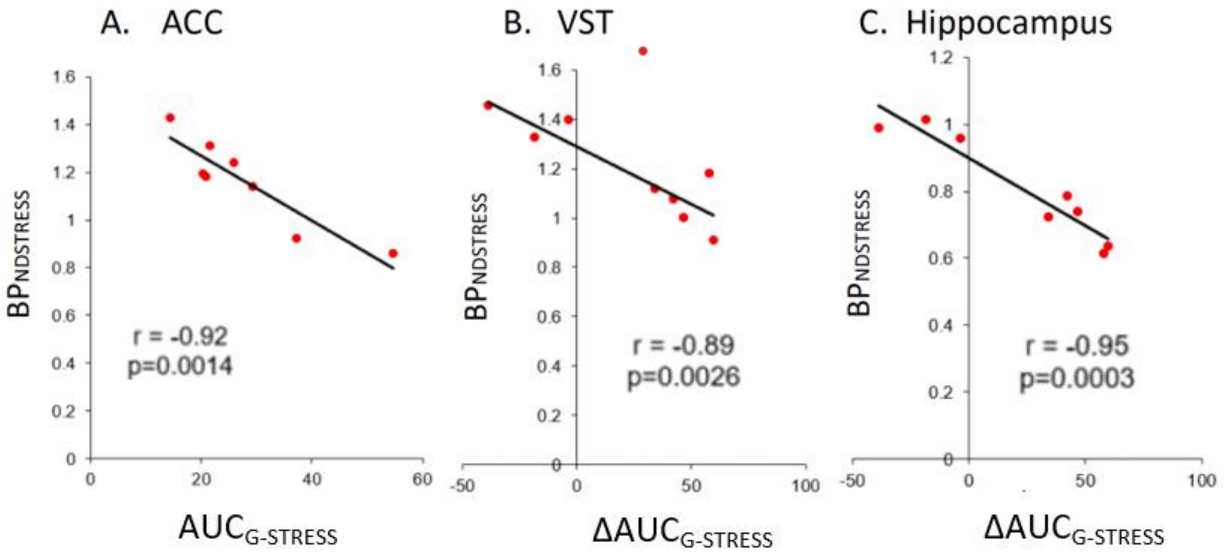

Figure 3.11: Association between mGlu5 receptor availability on the stress session and cortisol $AUC_{G\text{-}STRESS}$ response (A) and changes in cortisol AUC_G (B-C). **A**: Anterior Cingulate Cortex (ACC). **B**: Right ventral (limbic) striatum (VST). Regions that demonstrated significance at $p \leq 0.0056$ are shown.

3.5. DISCUSSION

The present series of experiments yielded four novel findings. First, as predicted, administration of 0.5 g/kg of 20% EtOH led to a doubling of extracellular glutamate concentrations within the ventral striatum. This contrasts with smaller glutamate effects produced by higher EtOH doses, as predicted by Fliegel *et al* (Fliegel *et al.*, 2013). By extrapolating the trend line constructed from the ventral striatal glutamatergic responses to higher EtOH doses (1, 2 and 3 g/kg) (Fliegel *et al.*, 2013), they hypothesized that a lower dose (*i.e.*, 0.5 g/kg) would lead to a glutamatergic response of about 200%. Second, this glutamatergic effect of EtOH relies on Ca^{2+}-dependent exocytotic release, implicating a neuronal source of the transmitter. Third, the low-dose EtOH challenge induced significant decreases in striatal [^{11}C]ABP688 BP_{ND} values in rodents. Fourth, changes in BP_{ND} values did not systematically covary with the changes in dialysate glutamate concentrations or MRS measured indices of glutamate turnover in humans.

The mechanism by which low-dose EtOH induces a glutamatergic response is not fully understood. One possibility is that EtOH acts as a negative modulator of the ionotropic glutamatergic receptors, *N*-methyl-D-aspartate (NMDA). Drawing such a conclusion is plausible since ketamine, a non-competitive NMDA receptor antagonist, was found to elicit a similar dose-dependent glutamatergic effect to that proposed with EtOH (Moghaddam *et al.*, 1997). Furthermore, there is evidence that NMDA receptor antagonism is linked to the activation of the glutamatergic α-amino-3-hydroxy-5-methyl-4-isoxazolepropionic acid (AMPA) receptors (Maeng *et al.*, 2008) *via* predominately decreased activity of inhibitory γ-aminobutyric acid (GABA) interneurons (Homayoun & Moghaddam, 2007).

Contrary to what was observed in awake animals, the glutamatergic responses in anesthetized rats peaked at approximately 127% of saline during the E1 fraction instead of continuing to grow through to the E3 fraction. This curtailed response likely reflects an effect of the anesthetic, isoflurane. Isoflurane is believed to abate excitatory glutamatergic transmission *via* decreasing synaptic glutamate release (Larsen *et al.*, 1998) and increasing uptake by isolated nerve terminals (Larsen *et al.*, 1997) and astrocytes (Miyazaki *et al.*, 1997). The glutamate-suppressing effect of isoflurane could also explain why ketamine administration causes a significant reduction in [^{11}C]ABP688 binding in humans (DeLorenzo *et al.*, 2015; Esterlis *et al.*, 2018), but not in anesthetized rodents (Kosten *et al.*, 2018). Nevertheless, despite the relatively limited increase in EtOH-induced glutamate release in anesthetized rodents, we observed a significant EtOH-induced reduction in striatal [^{11}C]ABP688 BP_{ND}. This adds to the evidence that striatal [^{11}C]ABP688 binding responds to changes in glutamate concentrations with a microdialysis to PET ratio of 4:1. This change compares quite favorably to the 44:1 and 64:1 ratios seen for [^{11}C]raclopride and dopamine release responses induced by 0.2 and 0.4 mg/kg of *d*-amphetamine, respectively (Breier

et al., 1997). Despite this, the percent change in striatal [^{11}C]ABP688 BP_{ND} did not correlate with changes in extracellular glutamate concentrations (r = 0.25, p = 0.46). This might be attributed to the small increase in EtOH-induced glutamate release (~27%), which in turn could have a limited effect on [^{11}C]ABP688 displacement from mGlu5 receptors. Indeed, the percent change in EtOH-induced decreases in [^{11}C]ABP688 BP_{ND} is in the range of test-retest variability for the striatum previously reported in rodents (Elmenhorst *et al.*, 2012) (6.8% *vs*. 4.8%). In comparison, *d*-amphetamine (0.2 and 0.4 mg/kg) induces larger effects on both [^{11}C]raclopride binding (10.5% and 21.3%) and dopamine release (459% and 1365%), respectively (Breier *et al.*, 1997).

Since [^{11}C]ABP688 and glutamate do not share the same binding site, our microdialysis/microPET findings suggest that glutamate binding to the active orthosteric site causes indirect displacement of the radiotracer from the allosteric site. This might reflect either altered affinity of the allosteric site to [^{11}C]ABP688 or internalization of mGlu5 receptors, precluding the radiotracer from binding to the allosteric site.

A limitation of our study is that the microdialysis measurements represent changes in ventral striatum glutamate concentrations, whereas the PET signal represents the full striatum. This noted, Fliegel *et al* (Fliegel *et al.*, 2013) hypothesized that a low dose of EtOH (*i.e.*, 0.5 g/kg) would increase glutamate release throughout the entire striatum (*i.e.*, ventral striatum and caudate-putamen). Future studies could also address whether the EtOH-induced glutamate response from neurons reflects impulse-dependent activity; this could be tested by measuring the effect of tetrodotoxin (TTX), a Na^+ channel blocker that inhibits the firing of action potentials (Lupinsky, Moquin, & Gratton, 2010). Another limitation to our animal studies is that only male rats were tested. Future studies will be needed to examine [^{11}C]ABP688 sensitivity to glutamate release in female animals.

In our study in humans, a series of electric shocks was sufficient to increase striatal Glx:Glu ratios, putatively reflecting elevated glutamine metabolism (Yuksel & Ongur, 2010) following stress-induced glutamate release, enhanced glial glutamate reuptake and subsequent conversion to glutamine. However, these effects were not large. Potentially related to this, exposure to the laboratory stressor did not lead to significant changes in [^{11}C]ABP688 BP_{ND} values. This might reflect marked individual differences in the responses rather than statistical noise. Indeed, exploratory analyses identified negative correlations between stress-induced increases in salivary cortisol and BP_{ND} values in the amygdala, ACC, OFC, and limbic striatum on the stress session. Since, however, correlations were not seen with stress-induced changes in BP_{ND} values, the above associations should be interpreted cautiously. Furthermore, since the human study's sample size was small, the effect of sex on [^{11}C]ABP688 BP_{ND} could not be examined.

Although our study reduced time of the time-related scan variability as much as possible, both across sessions and between individual participants, one participant underwent a control scan much later than the stress scan due to a tracer production failure. This same person exhibited higher binding at rest compared to other participants, which could be attributed to circadian rhythm effects, causing diurnal variations in [^{11}C]ABP688 binding as previously reported in both laboratory animal and human studies (DeLorenzo *et al.*, 2011; Elmenhorst *et al.*, 2016).

Finally, we found associations between [^{11}C]ABP688 BP_{ND} values on the stress session with ACC Glx:Glu values at stress, as well as with stress-induced changes in ACC Glx:Glu values. However, these correlations did not survive correction for multiple comparisons, somewhat limiting the generalizability of the findings. Supporting this caution, laboratory stress-induced changes in mGlu5 receptor availability and MRS measures of glutamate have been measured in cocaine-dependent and healthy subjects (Milella *et al.*, 2014) and correlations between the two

modalities were not found. In comparison, a second study identified a correlation between MRS measured glutamate turnover in the ACC and [^{18}F]FPEB binding, another PET tracer that binds to the same site as [^{11}C]ABP688, in patients with major depression (Abdallah *et al.,* 2017). However, these results likely reflected long term effects of elevated glutamate levels on receptor availability, an interpretation supported by post-mortem tissue evidence that patients with a history of depression have reduced mGlu5 protein expression (Deschwanden *et al.*, 2011).

3.6. CONCLUSION

The present study has demonstrated that a low dose (0.5g/kg) of 20% EtOH causes a significant calcium-dependent increase in ventral striatum glutamate release in awake animals. Although the EtOH-induced glutamatergic response was less pronounced in anesthetized rats, this smaller increase in glutamate release was accompanied by a significant reduction in striatal [^{11}C]ABP688 BP_{ND} with a ratio of 4:1. Nevertheless, a significant correlation was not observed between changes in ventral striatum glutamate release and striatal [^{11}C]ABP688 binding. Lastly, no correlation was observed between stress-induced changes in Glx/Glu and [^{11}C]ABP688 BP_{ND} in humans. Together, these findings suggest that [^{11}C]ABP688 binding could be affected by moderate fluctuations in extracellular glutamate release but does not provide a proportional measure. Future PET studies of mGlu5 receptor availability should use highly controlled testing conditions to avoid these effects.

3.7. ACKNOWLEDGEMENT

We extend our thanks to the PET Radiochemistry team at Montreal Neurological Institute for providing us access to the tracer, and to the human and small animal PET scanners. We would

also like to thank Dr. David Rudko and Marius Tuznik for their assistance with the animal MR imaging. The study benefited from the financial support of Health Canada, through the Canada Brain Research Fund, an innovative partnership between the Government of Canada (through Health Canada) and Brain Canada, and the Montreal Neurological Institute.

3.8. REFERENCES

Abdallah, C. G., Hannestad, J., Mason, G. F., Holmes, S. E., DellaGioia, N., Sanacora, G., . . . Esterlis, I. (2017). Metabotropic Glutamate Receptor 5 and Glutamate Involvement in Major Depressive Disorder: A Multimodal Imaging Study. *Biol Psychiatry Cogn Neurosci Neuroimaging, 2*(5), 449-456.

Abi-Dargham, A., Martinez, D., Mawlawi, O., Simpson, N., Hwang, D. R., Slifstein, M., . . . Laruelle, M. (2000). Measurement of striatal and extrastriatal dopamine D1 receptor binding potential with [11C]NNC 112 in humans: validation and reproducibility. *Journal of Cerebral Blood Flow and Metabolism, 20*(2), 225-243.

Ametamey, S. M., Kessler, L. J., Honer, M., Wyss, M. T., Buck, A., Hintermann, S., . . . Schubiger, P. A. (2006). Radiosynthesis and Preclinical Evaluation of 11C-ABP688 as a Probe for Imaging the Metabotropic Glutamate Receptor Subtype 5. *Journal of Nuclear Medicine, 47*(4), 698-705.

Auer, D. P., Putz, B., Kraft, E., Lipinski, B., Schill, J., & Holsboer, F. (2000). Reduced glutamate in the anterior cingulate cortex in depression: an in vivo proton magnetic resonance spectroscopy study. *Biological Psychiatry, 47*(4), 305-313.

Bdair, H., Tsai, I. H., Smart, K., Benkelfat, C., Leyton, M., & Kostikov, A. (2019). Radiosynthesis of the diastereomerically pure (E)-[11 C]ABP688. *J Labelled Comp Radiopharm, 62*(12), 860-864.

Breier, A., Su, T.-P., Saunders, R., Carson, R. E., Kolachana, B. S., de Bartolomeis, A., . . . Pickar, D. (1997). Schizophrenia is associated with elevated amphetamine-induced synaptic dopamine concentrations: Evidence from a novel positron emission tomography method. *PNAS, 94*(6), 2569-2574.

Bryant, R. A., Felmingham, K. L., Das, P., & Malhi, G. S. (2013). The effect of perceiving control on glutamatergic function and tolerating stress. *Molecular Psychiatry, 19*, 533.

Cadoni, C. (2016). Fischer 344 and Lewis rat strains as a model of genetic vulnerability to drug addiction. *Frontiers in Neuroscience, 10*(13), 13.

Choi, H., Kim, Y. K., Oh, S. W., Im, H. J., Hwang, D. W., Kang, H., . . . Lee, D. S. (2014). In vivo imaging of mGluR5 changes during epileptogenesis using [11C]ABP688 PET in pilocarpine-induced epilepsy rat model. *PloS One, 9*(3), e92765.

Collins, D. L., Zijdenbos, A. P., Baaré, W. F., & Evans, A. C. (1999). *ANIMAL+ INSECT: improved cortical structure segmentation.* Paper presented at the Information Processing in Medical Imaging: 16th International Conference, IPMI'99 Visegrád, Hungary, June 28–July 2, 1999 Proceedings 16.

Cox, S. M. L., Tippler, M., Jaworska, N., Smart, K., Castellanos-Ryan, N., Durand, F., . . . Leyton, M. (2020). mGlu5 receptor availability in youth at risk for addictions: effects of vulnerability traits and cannabis use. *Neuropsychopharmacology, 45*(11), 1817-1825.

Dahchour, A., & De Witte, P. (2003). Excitatory and inhibitory amino acid changes during repeated episodes of ethanol withdrawal: an in vivo microdialysis study. *European Journal of Pharmacology, 459*(2-3), 171-178.

Davis, R. C. (1934). Modification of the galvanic reflex by daily repetition of a stimulus. *Journal of Experimental Psychology, 17*(4), 504-535.

DeLorenzo, C., DellaGioia, N., Bloch, M., Sanacora, G., Nabulsi, N., Abdallah, C., . . . Esterlis, I. (2015). In vivo ketamine-induced changes in [11C]ABP688 binding to metabotropic glutamate receptor subtype 5. *Biological Psychiatry, 77*(3), 266-275.

DeLorenzo, C., Gallezot, J. D., Gardus, J., Yang, J., Planeta, B., Nabulsi, N., . . . Esterlis, I. (2017). In vivo variation in same-day estimates of metabotropic glutamate receptor subtype 5 binding using [11C]ABP688 and [18F]FPEB. *Journal of Cerebral Blood Flow and Metabolism, 37*(8), 2716-2727.

DeLorenzo, C., Kumar, J. S., Mann, J. J., & Parsey, R. V. (2011). In vivo variation in metabotropic glutamate receptor subtype 5 binding using positron emission tomography and [11C]ABP688. *Journal of Cerebral Blood Flow and Metabolism, 31*(11), 2169-2180.

Deschwanden, A., Karolewicz, B., Feyissa, A. M., Treyer, V., Ametamey, S. M., Johayem, A., . . . Hasler, G. (2011). Reduced metabotropic glutamate receptor 5 density in major depression determined by [11C]ABP688 PET and postmortem study. *American Journal of Psychiatry, 168*(7), 727-734.

Dolen, G., & Bear, M. F. (2008). Role for metabotropic glutamate receptor 5 (mGluR5) in the pathogenesis of fragile X syndrome. *Journal of Physiology, 586*(6), 1503-1508.

Elmenhorst, D., Aliaga, A., Bauer, A., & Rosa-Neto, P. (2012). Test-retest stability of cerebral mGluR5 quantification using [11C]ABP688 and positron emission tomography in rats. *Synapse, 66*(6), 552-560.

Elmenhorst, D., Mertens, K., Kroll, T., Oskamp, A., Ermert, J., Elmenhorst, E. M., . . . Bauer, A. (2016). Circadian variation of metabotropic glutamate receptor 5 availability in the rat brain. *Journal of Sleep Research, 25*(6), 754-761.

Elmenhorst, D., Minuzzi, L., Aliaga, A., Rowley, J., Massarweh, G., Diksic, M., . . . Rosa-Neto, P. (2010). In vivo and in vitro validation of reference tissue models for the mGluR5 ligand [11C]ABP688. *Journal of Cerebral Blood Flow and Metabolism, 30*(8), 1538-1549.

Esterlis, I., DellaGioia, N., Pietrzak, R. H., Matuskey, D., Nabulsi, N., Abdallah, C. G., . . . DeLorenzo, C. (2018). Ketamine-induced reduction in mGluR5 availability is associated with an antidepressant response: an [11C]ABP688 and PET imaging study in depression. *Molecular Psychiatry, 23*(4), 824-832.

Fliegel, S., Brand, I., Spanagel, R., & Noori, H. R. (2013). Ethanol-induced alterations of amino acids measured by in vivo microdialysis in rats: a meta-analysis. *In Silico Pharmacol, 1*(1), 7.

Goff, D. C., & Coyle, J. T. (2001). The emerging role of glutamate in the pathophysiology and treatment of schizophrenia. *American Journal of Psychiatry, 158*(9), 1367-1377.

Gunn, R. N., Lammertsma, A. A., Hume, S. P., & Cunningham, V. J. (1997). Parametric imaging of ligand-receptor binding in PET using a simplified reference region model. *Neuroimage, 6*(4), 279-287.

Gutzeit, A., Meier, D., Froehlich, J. M., Hergan, K., Kos, S., C, V. W., . . . Brugger, M. (2013). Differential NMR spectroscopy reactions of anterior/posterior and right/left insular subdivisions due to acute dental pain. *European Radiology, 23*(2), 450-460.

Hashimoto, K., Sawa, A., & Iyo, M. (2007). Increased levels of glutamate in brains from patients with mood disorders. *Biological Psychiatry, 62*(11), 1310-1316.

Homayoun, H., & Moghaddam, B. (2007). NMDA receptor hypofunction produces opposite effects on prefrontal cortex interneurons and pyramidal neurons. *Journal of Neuroscience, 27*(43), 11496-11500.

Kalivas, P. W. (2009). The glutamate homeostasis hypothesis of addiction. *Nature Reviews: Neuroscience, 10*(8), 561-572.

Kim, J. H., Joo, Y. H., Son, Y. D., Kim, J. H., Kim, Y. K., Kim, H. K., . . . Ido, T. (2019). In vivo metabotropic glutamate receptor 5 availability-associated functional connectivity alterations in drug-naive young adults with major depression. *European Neuropsychopharmacology, 29*(2), 278-290.

Knoess, C., Siegel, S., Smith, A., Newport, D., Richerzhagen, N., Winkeler, A., . . . Heiss, W. D. (2003). Performance evaluation of the microPET R4 PET scanner for rodents. *European Journal of Nuclear Medicine and Molecular Imaging, 30*(5), 737-747.

Knutson, B., & Gibbs, S. E. (2007). Linking nucleus accumbens dopamine and blood oxygenation. *Psychopharmacology, 191*(3), 813-822.

Kosten, L., Verhaeghe, J., Wyffels, L., Stroobants, S., & Staelens, S. (2018). Acute Ketamine Infusion in Rat Does Not Affect In Vivo [11C]ABP688 Binding to Metabotropic Glutamate Receptor Subtype 5. *Molecular Imaging, 17*, 1536012118788636.

Larsen, M., Hegstad, E., Berg-Johnsen, J., & Langmoen, I. A. (1997). Isoflurane increases the uptake of glutamate in synaptosomes from rat cerebral cortex. *British Journal of Anaesthesia, 78*(1), 55-59.

Larsen, M., Valo, E., Berg-Johnsen, J., & Langmoen, I. (1998). Isoflurane reduces synaptic glutamate release without changing cytosolic free calcium in isolated nerve terminals. *European Journal of Anaesthesiology, 15*(2), 224-229.

Laruelle, M. (2012). Measuring Dopamine Synaptic Transmission with Molecular Imaging and Pharmacological Challenges: The State of the Art. In G. Gründer (Ed.), *Molecular Imaging in the Clinical Neurosciences* (pp. 163-203). Totowa, NJ: Humana Press.

Laruelle, M., Iyer, R. N., al-Tikriti, M. S., Zea-Ponce, Y., Malison, R., Zoghbi, S. S., . . . Bradberry, C. W. (1997). Microdialysis and SPECT measurements of amphetamine-induced dopamine release in nonhuman primates. *Synapse, 25*(1), 1-14.

Leuzy, A., Zimmer, E. R., Dubois, J., Pruessner, J., Cooperman, C., Soucy, J. P., . . . Rosa-Neto, P. (2016). In vivo characterization of metabotropic glutamate receptor type 5 abnormalities in behavioral variant FTD. *Brain Struct Funct, 221*(3), 1387-1402.

Levenga, J., Hayashi, S., de Vrij, F. M., Koekkoek, S. K., van der Linde, H. C., Nieuwenhuizen, I., . . . Oostra, B. A. (2011). AFQ056, a new mGluR5 antagonist for treatment of fragile X syndrome. *Neurobiology of Disease, 42*(3), 311-317.

Lupinsky, D., Moquin, L., & Gratton, A. (2010). Interhemispheric regulation of the medial prefrontal cortical glutamate stress response in rats. *Journal of Neuroscience, 30*(22), 7624-7633.

Lupinsky, D., Moquin, L., & Gratton, A. (2017). Interhemispheric regulation of the rat medial prefrontal cortical glutamate stress response: role of local GABA- and dopamine-sensitive mechanisms. *Psychopharmacology, 234*(3), 353-363.

Maeng, S., Zarate, C. A., Jr., Du, J., Schloesser, R. J., McCammon, J., Chen, G., & Manji, H. K. (2008). Cellular mechanisms underlying the antidepressant effects of ketamine: role of alpha-amino-3-hydroxy-5-methylisoxazole-4-propionic acid receptors. *Biological Psychiatry, 63*(4), 349-352.

Marquez de Prado, B., Castaneda, T. R., Galindo, A., del Arco, A., Segovia, G., Reiter, R. J., & Mora, F. (2000). Melatonin disrupts circadian rhythms of glutamate and GABA in the neostriatum of the awake rat: a microdialysis study. *Journal of Pineal Research, 29*(4), 209-216.

Martinez, D., Slifstein, M., Nabulsi, N., Grassetti, A., Urban, N. B., Perez, A., . . . Huang, Y. (2014). Imaging glutamate homeostasis in cocaine addiction with the metabotropic glutamate receptor 5 positron emission tomography radiotracer [11C]ABP688 and magnetic resonance spectroscopy. *Biological Psychiatry, 75*(2), 165-171.

Mawlawi, O., Martinez, D., Slifstein, M., Broft, A., Chatterjee, R., Hwang, D. R., . . . Laruelle, M. (2001). Imaging human mesolimbic dopamine transmission with positron emission tomography: I. Accuracy and precision of D(2) receptor parameter measurements in ventral striatum. *Journal of Cerebral Blood Flow and Metabolism, 21*(9), 1034-1057.

Milella, M. S., Marengo, L., Larcher, K., Fotros, A., Dagher, A., Rosa-Neto, P., . . . Leyton, M. (2014). Limbic system mGluR5 availability in cocaine dependent subjects: a high-resolution PET [11C]ABP688 study. *Neuroimage, 98*, 195-202.

Miyazaki, H., Nakamura, Y., Arai, T., & Kataoka, K. (1997). Increase of glutamate uptake in astrocytes: a possible mechanism of action of volatile anesthetics. *Anesthesiology, 86*(6), 1359-1366; discussion 1358A.

Moghaddam, B., Adams, B., Verma, A., & Daly, D. (1997). Activation of glutamatergic neurotransmission by ketamine: a novel step in the pathway from NMDA receptor blockade to dopaminergic and cognitive disruptions associated with the prefrontal cortex. *Journal of Neuroscience, 17*(8), 2921-2927.

Papp, E. A., Leergaard, T. B., Calabrese, E., Johnson, G. A., & Bjaalie, J. G. (2014). Waxholm Space atlas of the Sprague Dawley rat brain. *Neuroimage, 97*, 374-386.

Paxinos, G., & Watson, C. (2005). The Rat Brain in Stereotaxic Coordinates. 5th Edn. Sidney. In: NSW: Academic Press.

Pitman, R. K., & Orr, S. P. (1986). Test of the conditioning model of neurosis: differential aversive conditioning of angry and neutral facial expressions in anxiety disorder patients. *Journal of Abnormal Psychology, 95*(3), 208-213.

Pruessner, J. C., Kirschbaum, C., Meinlschmid, G., & Hellhammer, D. H. (2003). Two formulas for computation of the area under the curve represent measures of total hormone concentration versus time-dependent change. *Psychoneuroendocrinology, 28*(7), 916-931.

Ramadan, S., Lin, A., & Stanwell, P. (2013). Glutamate and glutamine: a review of in vivo MRS in the human brain. *NMR in Biomedicine, 26*(12), 1630-1646.

Saal, D., Dong, Y., Bonci, A., & Malenka, R. C. (2003). Drugs of abuse and stress trigger a common synaptic adaptation in dopamine neurons. *Neuron, 37*(4), 577-582.

Scala, S. G., Smart, K., Cox, S. M. L., Benkelfat, C., & Leyton, M. (2021). PET Imaging of Type 5 Metabotropic Glutamate Receptors. In M. F. Olive, B. T. Burrows, & J. M. Leyrer-Jackson (Eds.), *Metabotropic Glutamate Receptor Technologies* (pp. 39-56). New York, NY: Springer US.

Shafiei, G., Zeighami, Y., Clark, C. A., Coull, J. T., Nagano-Saito, A., Leyton, M., . . . Misic, B. (2019). Dopamine signaling modulates the stability and integration of intrinsic brain networks. *Cerebral Cortex, 29*(1), 397-409.

Sheth, C., Prescot, A. P., Legarreta, M., Renshaw, P. F., McGlade, E., & Yurgelun-Todd, D. (2019). Reduced gamma-amino butyric acid (GABA) and glutamine in the anterior cingulate cortex (ACC) of veterans exposed to trauma. *Journal of Affective Disorders, 248*, 166-174.

Shigemoto, R., Nomura, S., Ohishi, H., Sugihara, H., Nakanishi, S., & Mizuno, N. (1993). Immunohistochemical localization of a metabotropic glutamate receptor, mGluR5, in the rat brain. *Neuroscience Letters, 163*(1), 53-57.

Smart, K., Scala, S. G., El Mestikawy, S., Benkelfat, C., & Leyton, M. (2017). Cocaine addiction and mGluR5. In V. R. Preedy (Ed.), *The Neuroscience of Cocaine* (pp. 269-278). San Diego: Academic Press.

Spielberger, C. D. G., R.L. (1983). Manual for the State-Trait Anxiety Inventory (Form Y) ("Self-Evaluation Questionnaire). *Consulting Psychologists Press*.

Stuber, G. D., Hopf, F. W., Hahn, J., Cho, S. L., Guillory, A., & Bonci, A. (2008). Voluntary ethanol intake enhances excitatory synaptic strength in the ventral tegmental area. *Alcoholism, Clinical and Experimental Research, 32*(10), 1714-1720.

Ullmann, E., Chrousos, G., Perry, S. W., Wong, M.-L., Licinio, J., Bornstein, S. R., . . . Yehuda, R. (2020). Offensive Behavior, Striatal Glutamate Metabolites, and Limbic–Hypothalamic–Pituitary–Adrenal Responses to Stress in Chronic Anxiety. *International Journal of Molecular Sciences, 21*(20). doi:10.3390/ijms21207440

Vigneault, E., Poirel, O., Riad, M., Prud'homme, J., Dumas, S., Turecki, G., . . . El Mestikawy, S. (2015). Distribution of vesicular glutamate transporters in the human brain. *Frontiers in Neuroanatomy, 9*, 23.

Yuksel, C., & Ongur, D. (2010). Magnetic resonance spectroscopy studies of glutamate-related abnormalities in mood disorders. *Biological Psychiatry, 68*(9), 785-794.

Yushkevich, P. A., Piven, J., Hazlett, H. C., Smith, R. G., Ho, S., Gee, J. C., & Gerig, G. (2006). User-guided 3D active contour segmentation of anatomical structures: significantly improved efficiency and reliability. *Neuroimage, 31*(3), 1116-1128.

Zimmer, E. R., Parent, M. J., Leuzy, A., Aliaga, A., Aliaga, A., Moquin, L., . . . Rosa-Neto, P. (2015). Imaging in vivo glutamate fluctuations with [11C]ABP688: a GLT-1 challenge with ceftriaxone. *Journal of Cerebral Blood Flow and Metabolism, 35*(7), 1169-1174.

CHAPTER 4: General Discussion

4.1. Summary of Findings

The present research sought to investigate sources of variability in [^{11}C]ABP688 BP_{ND} reported in the literature, and offer solutions to address this variability. Two major sources have been identified. First, the presence of the inactive form of the radiotracer, *Z*-isomer, in the final formulation has been shown to reduce estimate of *in vivo* [^{11}C]ABP688 binding. Second, pharmacological and nonpharmacological interventions known to cause fluctuations in extracellular glutamate levels have led to alterations in [^{11}C]ABP688 binding. By addressing the first challenge through eliminating (*Z*)-[^{11}C]ABP688 isomer from the injected dose, we could then better investigate the potential sensitivity of [^{11}C]ABP688 radiotracer to changes in glutamate concentrations.

In this work, we optimized the radiosynthesis of [^{11}C]ABP688, enabling us to isolate the active form of the radiotracer, (*E*)-[^{11}C]ABP688 isomer, from the inactive *Z*-isomer. This was achieved with retention times on the semipreparative HPLC column of 18.5 min and 15.5 min, respectively. The unreacted precursor and [^{11}C]CH_3I were eluted under 10 min. Obtaining 100% diastereomerically pure (*E*)-[^{11}C]ABP688 isomer was achieved through the use of the widely available, versatile reverse-phase Phenomenex Luna C18(2) column, along with manipulating mobile phase composition, concentration, and its pumping flow rate.

With the diastereomerically pure (*E*)-[^{11}C]ABP688 isomer in hand, we investigated whether the radiotracer binding is sensitive to fluctuations in extracellular glutamate release *via* conducting simultaneous microdialysis and PET imaging experiments in anesthetized rodents. EtOH administration (20%, 0.5 g/kg, i.p.) significantly increased extracellular glutamate concentrations in ventral striatum (~27%). Notably, EtOH-induced glutamate release caused a

significant reduction in striatal [^{11}C]ABP688 BP_{ND}, but these changes were not significantly correlated with changes in glutamate release.

4.1.1. [^{11}C]ABP688 Radiosynthesis Findings

As mentioned in Chapter 1, the presence of an asymmetrically substituted C=N double bond in [^{11}C]ABP688 chemical structure leads to diastereomerism. Accordingly, [^{11}C]ABP688 exists as two isomers, (*E*)-[^{11}C]ABP688 and (*Z*)-[^{11}C]ABP688, with the former being the active form of the radiotracer that exhibits almost 25-fold higher binding affinity to mGlu5 receptors than the latter (Kawamura *et al.*, 2014). Our research group has demonstrated that the presence of the *Z*-isomer in the final formulation of radiotracer is a major contributor to the variability in [^{11}C]ABP688 binding in humans (Smart *et al.*, 2019a). Prior to our study described in Chapter 2, only one research study reported the separation of (*E*)-[^{11}C]ABP688 and (*Z*)-[^{11}C]ABP688 diastereomers (Kawamura *et al.*, 2014). Kawamura and colleagues were able to segregate the two diastereomers *via* using COSMOSIL Cholester semipreparative HPLC column that is designed to separate geometric isomers (Kawamura *et al.*, 2014). However, this column is not widely available, and is thus not routinely used in the preparation of PET radiopharmaceuticals. In Chapter 2, we proposed the use of Phenomenex Luna C18(2), a commonly used versatile reversed-phased HPLC column in the preparations of PET radioligands. Building on the previous production method of [^{11}C]ABP688 in our PET centre at the Montreal Neurological Institute, we modified the HPLC eluent composition (H_2O: CH_3CN), ratio (50:50), as well as the pumping flow rate (5 mL/min). These modifications have reliably provided *E*-isomer with >99% radiochemical purity. The molar activity of [^{11}C]ABP688 in the present study (148.86 ± 79.8 GBq/μmol) is comparable to what has been reported in other studies that used [^{11}C]CH_3I- (Ametamey *et al.*, 2006; Kawamura *et al.*, 2014)

or [^{11}C]CH_3OTf-based (DeLorenzo *et al.*, 2011) radiolabelling method. The retention time of (*E*)-[^{11}C]ABP688 in our study was relatively longer than that reported by Kawamura *et al* (Kawamura *et al.*, 2014) (18.5 min *vs*. 10.4 min). Subsequent to the publication of our research highlighting an optimized radiosynthesis method of [^{11}C]ABP688 (Bdair *et al.*, 2019), Glorie *et al* reported the isolation of (*E*)-[^{11}C]ABP688 using a similar C18 column (Waters XBridge C18, 5 μm, 4.6 × 150 mm) with a different mobile phase (50 mM sodium acetate:EtOH; 55:45) (Glorie *et al.*, 2020). However, the retention times of the *E* and *Z* isomers were not reported in their study. Another study has also reported the separation of (*Z*)-[^{11}C]ABP688 and (*E*)-[^{11}C]ABP688 isomers using an unspecified C18 HPLC column and a mobile phase of CH_3CN:100 mM NH_4HCO_2 (50:50) (Lee, 2020). This was achieved with a relatively shorter retention time (10.8 min) than that reported in our study (18.5 min) (Lee, 2020). Together, these studies were able to replicate our findings in radiosynthesis of diastereomerically pure (*E*)-[^{11}C]ABP688.

In the literature concerning [^{11}C]ABP688, the ratio of *E* to *Z* isomers in the final formulation have rarely been documented, and many animal and human studies failed to report corrections for the *Z*-isomer content while calculating the radiotracer BP_{ND} (Akkus *et al.*, 2017; DuBois *et al.*, 2016; Elmenhorst *et al.*, 2016; Zimmer *et al.*, 2015). Furthermore, correcting for the content of the *Z*-isomer during the calculation of [^{11}C]ABP688 BP_{ND} is challenging, since the amount of the *Z*-isomer in the injected dose could vary from one production batch to another, and from one laboratory to another. For instance, some research groups have showed the *E*:*Z* isomeric ratio to be as low as >10:1 (Ametamey *et al.*, 2006; Scala, 2023), whereas others reported a much greater ratio of 70:1 (DeLorenzo *et al.*, 2017). Accordingly, comparisons of [^{11}C]ABP688 findings from different studies and/or research groups could be challenging, or otherwise unachievable, particularly if the content of the *Z*-isomer is not reported or significantly varies between studies.

Thus, elimination of the *Z*-isomer from the final formulation would reduce the variability in [^{11}C]ABP688 BP_{ND} estimates in previous reports. With >99% diastereomerically pure *(E)*-[^{11}C]ABP688 we were able to reliably investigate whether changes in [^{11}C]ABP688 binding are caused by fluctuations in glutamatergic responses, and whether these changes are proportionally correlated with each other.

4.1.2. *In Vivo* Microdialysis Findings

In Chapter 3, we investigated the influence of low-dose EtOH (20%, 0.5g/kg, i.p.) on glutamatergic responses in NAc (*i.e.*, ventral striatum) using *in vivo* microdialysis technique in anesthetized rodents. As expected, saline did not elicit any significant changes in ventral striatal glutamate concentrations. In comparison, a significant increase in extracellular glutamate release from the baseline (~27%) was observed in the ventral striatum in response to EtOH. The increase in glutamate release was detected only during first 20 min post-EtOH injection (*i.e.*, E1 fraction), followed by reduction to baseline levels in subsequent dialysate fractions (Figure 3.6). These results were in contrast to our group's findings in awake animals, where EtOH triggered a greater glutamate response (max. release: 190% *vs*. 127%) in the ventral striatum (Planche, 2018). Furthermore, the rise in glutamate release from the baseline lasted much longer in awake animals compared to anesthetized ones (100 min *vs*. 20 min) (Planche, 2018). This indicates that EtOH-induced glutamate release in anesthetized animals is impeded.

The relatively low EtOH-induced glutamate release in anesthetized rats could be attributed to the glutamate-suppressing effect of the inhaled anesthetic isoflurane. There is evidence that isoflurane diminishes glutamatergic transmission *via* reducing synaptic glutamate release (Larsen

et al., 1998) and increasing uptake by isolated nerve terminals (Larsen *et al.*, 1997) and astrocytes (Miyazaki *et al.*, 1997).

The mechanisms by which low-dose EtOH induces glutamate release in ventral striatum are not fully understood. One potential mechanism whereby EtOH promotes glutamate release is *via* acting as a negative modulator of NMDA receptors. This mechanism is plausible given that a blockade of NMDA receptors with a competitive (AP5) and a non-competitive (MK-801) NMDA antagonists leads to a significant increase in extracellular glutamate concentrations in the striatum (Bustos *et al.*, 1992; Liu & Moghaddam, 1995). Furthermore, the non-competitive NMDA antagonist ketamine has been found to induce a similar dose-dependent glutamatergic response to that observed with EtOH. More specifically, at low subanesthetic doses, ketamine induces glutamate release in the PFC, whereas at a high anesthetic dose, it suppresses glutamatergic transmission (Moghaddam *et al.*, 1997). The NMDA antagonist effect of ketamine is thought to be mediated *via* activation of AMPA receptors (Maeng *et al.*, 2008), by predominately decreasing the activity of inhibitory GABA interneurons (Homayoun & Moghaddam, 2007).

4.1.3. [^{11}C]ABP688-MicroPET Findings

In our simultaneous dual-technique study, PET imaging data revealed that EtOH administration led to a significant reduction in striatal [^{11}C]ABP688 BP_{ND} compared to saline, with a percentage change of 6.8 ± 9.6%. These changes in radiotracer binding were not due to variations in injected radioactivity, volume or mass, molar activity of the radioligand, or time of the day of the scan. These findings indicate the EtOH-induced rises in extracellular glutamate concentrations, as observed with the microdialysis technique, are associated with a reduction in [^{11}C]ABP688 binding, suggesting the sensitivity of this radioligand to fluctuations in synaptic glutamate levels.

However, changes in [^{11}C]ABP688 binding caused by EtOH administration is drastically less than those reported in response to ceftriaxone, an activator of GLP-1 transporter (6.8% *vs*. 41%) (Zimmer *et al.*, 2015). The higher ceftriaxone-induced changes in [^{11}C]ABP688 binding might be attributed to the stronger glutamatergic effect of ceftriaxone or, alternatively, to the shorter exposure to isoflurane in comparison with our study (100 min *vs*. >360 min). This, in turn, suggests a greater isoflurane-mediated suppression of glutamate release in the present study. Furthermore, our study showed lower EtOH-induced reductions in [^{11}C]ABP688 binding than those reported with ketamine in healthy human participants (6.8% *vs*. 19-21% on average) (DeLorenzo *et al.*, 2015; Esterlis *et al.*, 2018). This could also be attributed to the glutamate-suppressive effect of isoflurane in our study, which could also explain why no change in [^{11}C]ABP688 binding was observed in anesthetized rats following ketamine administration, reflecting the isoflurane-mediated abolition of the glutamatergic transmission (Kosten *et al.*, 2018). Interestingly, the glutamate release enhancer *N*-acetylcysteine (NAC) caused decreases in [^{11}C]ABP688 binding in NHPs (Miyake *et al.*, 2011; Sandiego *et al.*, 2013), but not in rats (Wyckhuys *et al.*, 2013). Notably, this was observed despite all these studies using isoflurane as anesthetic. The authors have attributed this lack of reproducibility in rodents to species differences and variations in methodologies (Wyckhuys *et al.*, 2013). However, the use of an initial sedative dose of ketamine in NHPs (Miyake *et al.*, 2011; Sandiego *et al.*, 2013), but not in rodents (Wyckhuys *et al.*, 2013), cannot be overlooked. Both ketamine and NAC elicit glutamate release through different mechanisms, with ketamine acting as a competitive NMDA antagonist and NAC as an activator of cystine-glutamate antiporter. Together, ketamine and NAC could potentially have a synergistic glutamate-releasing effect that counteracts the glutamate-suppressive effect of isoflurane in NHPs. Collectively, we suspect that that EtOH-induced increases in extracellular

glutamate concentrations were limited in our dual-technique study due to the prolonged exposure of rodents to isoflurane.

Although EtOH-induced changes in extracellular glutamate concentrations and [^{11}C]ABP688 BP_{ND} were limited in the study, the ratio of the percentage increase of glutamate during the first post-EtOH dialysate fraction to percent reduction in [^{11}C]ABP688 BP_{ND} was surprisingly small (4:1). This ratio compares very favorably to the ratio of dopamine release to [^{11}C]raclopride binding of 44:1 and 64:1 in response to 0.2 and 0.4 mg/kg of *d*-amphetamine, respectively (Breier *et al.*, 1997). Notwithstanding this, contrary to the findings of [^{11}C]raclopride binding sensitivity to dopamine release, EtOH-induced alternations in extracellular glutamate concentrations in ventral striatum did not correlate with percent change in striatal [^{11}C]ABP688 BP_{ND} (r = 0.25, p = 0.46). This may be attributed to the limited increases in EtOH-induced glutamate release (~27%), which in turn could have a minimal effect on [^{11}C]ABP688 displacement from mGlu5 receptors. Indeed, the percent change in EtOH-induced decreases in [^{11}C]ABP688 BP_{ND} is in the range of test-retest variability for the striatum previously reported in rodents (Elmenhorst *et al.*, 2012) (6.8% *vs*. 4.8%). In comparison, *d*-amphetamine (0.2 and 0.4 mg/kg) induces larger effects on both [^{11}C]raclopride binding (10.5% and 21.3%) and dopamine release (459% and 1365%), respectively (Breier *et al.*, 1997). Taken together, the present study indicates that [^{11}C]ABP688 does not exhibit sufficient sensitivity to moderate *in vivo* fluctuations of glutamate concentrations. This highlights the need for more rigorous study designs in PET imaging of mGlu5 receptors.

4.1.3.1. Other PET Radiotracers for Measuring Glutamate Release

Developing PET radiotracers for non-invasive quantification of extracellular glutamate concentrations remains a relevant area of inquiry. Besides [^{11}C]ABP688, other glutamatergic PET radiotracers, such as [^{18}F]FPEB and [^{18}F]PSS232, have also been investigated for their susceptibility to measure fluctuations in glutamate release, at both preclinical and clinical levels. However, neither of these radioligands demonstrated superior sensitivity over [^{11}C]ABP688 for acute fluctuations in glutamate release.

A preclinical study in rodents with [^{18}F]FPEB did not reveal any significant changes in radiotracer binding in response to NAC-induced fluctuations of glutamate levels (maximum percent changes in standardized uptake value ratio; $\Delta SUVR_{max}$ = ~2%) (Dupont *et al.*, 2021). These findings are consistent with those reported using [^{11}C]ABP688 in response to NAC challenge in rodents, as discussed in more details in section 4.1.3 (Wyckhuys *et al.*, 2013). Nevertheless, in clinical settings, [^{18}F]FPEB was found to be inferior to [^{11}C]ABP688 in detecting fluctuations in extracellular glutamate. Indeed, ketamine infusion in healthy volunteers resulted in ~10% global reduction in [^{18}F]FPEB binding (Holmes *et al.*, 2020). In comparison, global [^{11}C]ABP688 binding decreased by ~20% in response to ketamine infusion in healthy human participants (DeLorenzo *et al.*, 2015). The variability in binding sensitivity between [^{11}C]ABP688 and [^{18}F]FPEB cannot be attributed to differences in the binding site. This has been demonstrated in a cross-sectional study where bindings of [^{11}C]ABP688 and [^{18}F]FPEB were reduced to the levels of cerebellar reference region following blocking with the non-radioactive counterpart of other radiotracer (*i.e.*, [^{11}C]ABP688 *vs*. FPEB, and [^{18}F]FPEB *vs*. ABP688) (Glorie *et al.*, 2022). This in turn indicates that both radiotracers have similar binding sites. Collectively, these findings

suggest that [^{11}C]ABP688 is more sensitive than [^{18}F]FPEB to glutamate release fluctuations in pharmacological challenge paradigms.

Furthermore, compared to [^{11}C]ABP688, [^{18}F]FPEB shows superior test-retest reproducibility in humans (Leurquin-Sterk *et al.*, 2016; Park *et al.*, 2015) along with greater peak uptake in mGlu5-rich regions, which may indicate higher signal-to-noise ratio. This suggests that [^{18}F]FPEB could detect minor differences in mGlu5 receptor expression. Nevertheless, these hypothetical superior characteristics of [^{18}F]FPEB have not been manifested in clinical settings. For instance, several [^{11}C]ABP688 studies in MDD patients showed a reduction in radiotracer binding (Deschwanden *et al.*, 2011; Esterlis *et al.*, 2018), a finding that was confirmed in a post-mortem study (Deschwanden *et al.*, 2011). In contrast, no changes in [^{18}F]FPEB binding were observed between MDD and control groups (Abdallah *et al.*, 2017; Davis *et al.*, 2019).

The fluorinated derivative of ABP688, [^{18}F]PSS232, is another glutamatergic PET radioligand that has been investigated as a probe in quantifying drug-induced acute extracellular glutamate fluctuations. Neither increased glutamate levels with ketamine challenge nor reduced glutamate concentrations following ceftriaxone administration result in changes in [^{18}F]PSS232 binding (Müller Herde *et al.*, 2018). Likewise, NAC-induced increases in extracellular glutamate in healthy participants did not yield variations in [^{18}F]PSS232 binding (O'Gorman Tuura *et al.*, 2019), suggesting the lack of radioligand sensitivity to acute fluctuations in endogenous glutamate levels. As it stands, [^{11}C]ABP688 appears to be the most sensitive radiotracer to acute fluctuations in synaptic glutamate levels in comparison with other glutamatergic PET radioligands, although it is not suitable for quantifying moderate alterations in glutamate release.

4.1.3.2. Mechanisms Underlying EtOH-Induced Decreased [^{11}C]ABP688 BP_{ND}

Contrary to the well-established neurotransmitter-quantifying PET radioligands that bind to the orthosteric site on their respective receptors, such as [^{11}C]raclopride, [^{18}F]fallypride (for dopamine) and [^{11}C]CIMBI-36 (for serotonin), [^{11}C]ABP688 binds to the allosteric site of mGlu5 receptors. Accordingly, endogenous glutamate does not directly compete with [^{11}C]ABP688 for its binding site. Indeed, *in vitro* autoradiography studies have shown that exogenous glutamate does not influence the mGlu5 receptor binding of [^{18}F]PSS232, a fluorinated derivative of ABP688, (Müller Herde *et al.*, 2018). One possible mechanism underlying EtOH-induced reduction in [^{11}C]ABP688 binding is glutamate release-induced conformational changes in mGlu5 receptors, which reduces the likelihood of radiotracer binding at the allosteric site. Alternatively, glutamate binding to the active orthosteric site could lead to internalization of mGlu5 receptors, preventing [^{11}C]ABP688 binding to these receptors. Indeed, it has been shown that both [^{11}C]ABP688 and [^{18}F]FPEB only bind to mGlu5 receptors on the cell surface and are unable to penetrate cell membrane to bind to the internalized receptors (Asch *et al.*, 2023; Lin *et al.*, 2015). Furthermore, receptor internalization is thought to account for long-lasting decreases in the binding of D_2 receptor radioligands, such as [^{11}C]raclopride and [^{123}I]IBZM, following dopamine release (Laruelle, 2012; Laruelle *et al.*, 1997). Similarly, rapid receptor internalization has also been reported following stimulation of 5-HT_{2A} receptors (Berry *et al.*, 1996; Gray & Roth, 2001), the binding site of [^{11}C]CIMBI-36 radioligand. This noted, although both [^{11}C]ABP688 and [^{18}F]FPEB bind to the same sites on mGlu5 receptors (Glorie *et al.*, 2022) and both cannot bind to internalized mGlu5 receptors (Asch *et al.*, 2023; Lin *et al.*, 2015), [^{11}C]ABP688 continues to display higher binding sensitivity to *in vivo* fluctuations of glutamate levels (as discussed in section

4.1.3.1). This indicates the involvement of other [^{11}C]ABP688 displacing mechanisms that remain unclear.

4.2. Other Factors Affecting [^{11}C]ABP688 Binding

In addition to fluctuations in synaptic glutamate levels, [^{11}C]ABP688 binding has been shown to be influenced by other factors, such as age and sex. In clinical settings, the radiotracer binding was found to significantly decline with age (Joo *et al.*, 2021). These findings are in agreement with those observed with [^{18}F]FPEB (Esterlis *et al.*, 2022), which has largely been ascribed to gray matter tissue loss (Mecca *et al.*, 2021). Although there was a statistically significant difference in age between [^{11}C]ABP688 baseline and challenge scans in our animal study (paired *t*-test, $p < 0.05$), the age gap between the scans was very small to cause an impact on radiotracer binding (mean age difference: 4.36 days, range: 2-7 days). Indeed, previous research has not demonstrated significant reductions in striatal [^{11}C]ABP688 binding between scans conducted 3 months apart in rodents (Bertoglio *et al.*, 2018). Accordingly, age was not considered a covariant in our study.

Beyond age, sex differences in [^{11}C]ABP688 binding have been reported in healthy human participants, with higher mGlu5 receptor expression in males than females (Smart *et al.*, 2019b). Other studies, however, found no significant effect of sex on [^{11}C]ABP688 binding (Akkus *et al.*, 2016; DuBois *et al.*, 2016), which could be attributed to the lack of correction for *Z*-isomer content and/or small sample size being recruited. Sex differences in [^{11}C]ABP688 binding could be ascribed to the functional coupling of mGlu5 to estrogen receptors (Grove-Strawser, Boulware, & Mermelstein, 2010). Taken together, it appears that changes in [^{11}C]ABP688 BP_{ND} following low-

dose EtOH administration could not be attributed to age or sex differences, particularly since only male rats were used in our study.

4.3. Comparison with PET Radioligands for Other Neurotransmitter Systems

To date, only a few PET radiotracers exist for the measurement of extracellular levels of endogenous neurotransmitters. Over the last two decades, the sensitivity of [^{11}C]raclopride to dopamine release has been well documented using simultaneous PET and microdialysis in NHPs, where changes in radiotracer binding are proportional to alterations in extracellular dopamine concentrations (Breier *et al.*, 1997; Endres *et al.*, 1997). This noted, *in vivo* changes in [^{11}C]raclopride binding does not simply reflect synaptic dopamine concentrations since various neuronal manipulations can affect radioligand binding differently (Tsukada *et al.*, 1999).

Given the low affinity of [^{11}C]raclopride to $D_{2/3}$ receptors, it is mainly used for imaging of striatal dopamine release (Liu *et al.*, 2019). Contrary to that, [^{18}F]fallypride exhibits high affinity to $D_{2/3}$ receptors, which makes it more suitable for imaging of extra-striatal brain regions with lower receptor density, such as PFC (Liu *et al.*, 2019). In NHPs, [^{18}F]fallypride binding in the striatum and extra-striatal regions has been negatively correlated with rising doses of *d*-amphetamine, a dopamine release inducer (Slifstein *et al.*, 2004). Nonetheless, there has been no research in the literature to date examining the direct correlation between [^{18}F]fallypride binding and dopamine release, using combined PET and microdialysis. Hence, the ratio of percentage changes in dopamine concentrations to [^{18}F]fallypride binding remains unknown.

The binding sensitivity of [^{11}C]FLB 457, another high-affinity $D_{2/3}$ receptor radioligand, has been examined in response to *d*-amphetamine-induced dopamine release, using simultaneous PET and microdialysis in NHPs (Narendran *et al.*, 2014). Findings demonstrated that changes in

[^{11}C]FLB 457 binding were linearly correlated to changes in cortical dopamine levels. Furthermore, the ratio of percent changes of dopamine release to [^{11}C]FLB 457 BP_{ND} in the frontal cortex ranges from 83:1 to 167:1 in response to various doses of *d*-amphetamine (Narendran *et al.*, 2014). This ratio compares poorly to that of EtOH-induced changes in glutamate release and [^{11}C]ABP688 binding (4:1).

Regarding serotonergic neurotransmission, the 5-HT_{2A} receptor agonist [^{11}C]CIMBI-36 has shown sensitivity in detecting changes to endogenous serotonin levels in response to several pharmacological interventions, using combined PET and microdialysis in pigs (Jorgensen *et al.*, 2017). In Jørgensen *et al*, the pharmacological interventions caused significant increases in serotonin release of 217-1123% of baseline level in mPFC, which significantly correlated with reductions in cortical [^{11}C]CIMBI-36 binding of 19-44% (Jorgensen *et al.*, 2017). In comparison, administration of low-dose EtOH in the present research resulted in a lower increase in glutamate release (~27%), accompanied with smaller changes in [^{11}C]ABP688 BP_{ND} (6.8%). Furthermore, the ratio of percent changes in serotonin release to [^{11}C]CIMBI-36 binding varied from 11:1 to 16:1, depending on the pharmacological intervention used (Jorgensen *et al.*, 2017), which is inferior to that of glutamate release and [^{11}C]ABP688 BP_{ND} (4:1). Noteworthy, the findings of Jørgensen and colleagues are underpowered by the small sample size of animals used in the study (2-3 pigs per group), which makes the reliability of these results inconclusive. Additionally, conducting both scans (*i.e.*, baseline and challenge) on the same day could affect the number of 5-HT_{2A} receptors available for binding. For instance, agonist stimulation of 5-HT_{2A} receptors has been shown to cause internalization of these receptors (Berry *et al.*, 1996), which could last 2.5 hr before returning to normal surface level *in vitro* (Bhattacharyya *et al.*, 2002). This could explain why saline administration during the second (*i.e.*, challenge) [^{11}C]CIMBI-36 scan on the same day

caused a significant reduction in cortical radiotracer binding (17%), but without any changes in extracellular serotonin levels (Jorgensen *et al.,* 2017). Accordingly, reduction in [^{11}C]CIMBI-36 signals in response to pharmacological interventions in Jørgensen *et al* might not only reflect radioligand displacement from 5-HT$_{2A}$ receptors, but also receptor internalization.

Very recently, the alpha 2 (α2)-adrenergic receptor antagonist [^{11}C]yohimbine has been investigated as a non-invasive PET tool to quantify norepinephrine (*i.e.*, noradrenaline) release *in vivo* (Landau *et al.*, 2023). Indeed, combined PET and microdialysis studies in pigs showed a significant correlation between percent reductions in [^{11}C]yohimbine binding and percent increases in extracellular norepinephrine levels in response to various doses of the non-specific norepinephrine releaser *l*-amphetamine. The ratio of percent changes in norepinephrine release to radioligand binding was 24:1 to 30:1, depending on the dose of *l*-amphetamine used (Landau *et al.*, 2023). Nonetheless, the sample size used in this study was very small (1-2 animals per group), and the baseline and challenge scans were conducted sequentially during the same day. Although the effect of α2-adrenergic antagonists on receptor availability is not widely investigated, agonists of α2-adrenoceptors lead to internalization of these receptors (Saunders & Limbird, 1999). As with Jørgensen *et al* (2017), the results of Landau *et al* (2023) need to be interpreted with caution as the reduction in [^{11}C]yohimbine binding in response to amphetamine might reflect a combined effect of radioligand displacement, as well as receptor internalization. These findings suggest that baseline and challenge scans should be conducted on separate days, as done in our study. Furthermore, it is recommended that future studies make use of a larger sample size to confirm the findings of [^{11}C]CIMBI-36 and [^{11}C]yohimbine studies.

Taken together, PET radioligands developed for other neurotransmission systems (*i.e.*, dopaminergic, serotonergic and noradrenergic) bind to the orthosteric sites of their target receptors

and compete directly with the corresponding endogenous neurotransmitter. On the contrary, [^{11}C]ABP688 binds to the allosteric sites so it does not directly compete for the binding site of glutamate on mGlu5 receptors. Additionally, the ratio of percent changes in neurotransmitter levels to radioligand binding has been shown to be the highest with glutamate and [^{11}C]ABP688 binding. Unlike with PET radioligands for other neurotransmission systems, [^{11}C]ABP688 binding has been challenged with only a single dose of the neurotransmitter release inducer (*i.e.*, EtOH). Future studies will need to examine [^{11}C]ABP688 binding in response to various doses of EtOH or other glutamate release inducers.

4.4. Limitations

In terms of [^{11}C]ABP688 radiosynthesis, the retention time of the (*E*)-[^{11}C]ABP688 in our study was relatively longer than that reported by Kawamura *et al* (Kawamura *et al.*, 2014) and Lee (Lee, 2020) (18.5 min *vs*. 10.4 min *vs*. 10.8 min, respectively). Considering the short half-life of carbon-11 (20.4 min), a long retention time could negatively impact the molar activity of the final product. Accordingly, reducing the retention time of (*E*)-[^{11}C]ABP688 isomer in our study would further enhance the molar activity. This noted, the interval between the retention times of the (*Z*)-[^{11}C]ABP688 and (*E*)-[^{11}C]ABP688 diastereomers in our study is sufficient (3 min) to permit the use of a higher flow rate (e.g., 6 or 7 mL/min). This in turn would reduce the retention time of the *E*-isomer, without potentially merging the peaks of both isomers.

The use of the anesthetic isoflurane to maintain rats in the same position within the field of view of the microPET scanner constitutes a limitation to our animal study. Hence, omitting the use of isoflurane during the simultaneous dual-technique study, or using a stronger trigger of glutamate release that could overcome the glutamate-suppressing effect of isoflurane are warranted.

Another limitation of our animal study is that the microdialysis measurements represent fluctuations in ventral striatal glutamate concentrations, whereas the PET signal represents the full striatum. This noted, it has been hypothesized that low-dose EtOH (*i.e.*, 0.5 g/kg) would increase glutamate release throughout the entire striatum (*i.e.*, dorsal and ventral striatum) (Fliegel *et al.*, 2013).

Additionally, to study the proportionality between changes in neurotransmitter release and changes in radioligand binding, different doses of neurotransmitter release inducer are required. Notwithstanding this, only one dose of EtOH (*i.e.*, 0.5 g/kg) was used in our animal study to induce glutamate release, which makes it challenging to construct a correlation between [^{11}C]ABP688 binding and glutamate release. Finally, only male rats were used in our study, which does not fully represent the general population. Future studies will be needed to examine [^{11}C]ABP688 sensitivity to glutamate release in female animals.

4.5. Future Directions

To overcome the negative glutamatergic influence of isoflurane, future research could use a stronger trigger of glutamate release. This would allow for testing [^{11}C]ABP688 sensitivity to greater *in vivo* fluctuations of glutamate levels. Indeed, local perfusion of melatonin (500 µM) in freely moving rodents increased striatal glutamate concentrations to 896% of the baseline values during darkness (*i.e.*, awake period) (Marquez de Prado *et al.*, 2000). In comparison, our group showed that low-dose EtOH (*i.e.*, 0.5 g/kg) in awake rats increases glutamate concentrations in the ventral striatum to 190% of the baseline levels (Planche, 2018). This noted, it remains unknown whether local perfusion of melatonin will stimulate a greater release of extracellular glutamate than low-dose EtOH in anesthetized rats. Another option is to use ceftriaxone as a trigger for *in*

vivo glutamate release, since it induces higher extracellular glutamate levels compared to EtOH in anesthetized animals. The disadvantages of these challenges are that they cannot be used in humans or would yield a difficult to interpret feature of human glutamate release.

An alternative approach to overcome the effect of isoflurane is to conduct the simultaneous microdialysis and PET imaging in awake animals, thereby omitting the use of isoflurane. Though uncommon given its complexity, conducting PET scans in awake and freely moving rats inside the human HRRT PET scanner has been reported (Miranda *et al.*, 2019). This noted, the literature has yet to examine simultaneous microdialysis and PET scans in awake animals. The author of this thesis has recently succeeded in conducting these two techniques simultaneously in awake rats, using the human HRRT PET scanner (unpublished data). Future investigators may wish to pursue this further.

4.6. Conclusion

We have reported the development of an optimized radiosynthesis method that produces >99% radiochemically pure (*E*)-[^{11}C]ABP688 diastereomer via the use a widely available, versatile reverse-phase Phenomenex Luna C18(2) column. In anesthetized rats, we have shown that a low dose of 20% EtOH (*i.e.*, 0.5 g/kg) causes significant increases in ventral striatal glutamate release. However, these EtOH-induced increases in glutamate release response were less pronounced than those observed in awake rats (127% *vs*. 190%). This smaller increase in ventral striatal glutamate release was accompanied by a significant reduction in striatal [^{11}C]ABP688 BP_{ND} with a ratio of 4:1. Nevertheless, a significant correlation was not observed between changes in ventral striatum glutamate release and striatal [^{11}C]ABP688 binding,

highlighting the need for highly controlled testing conditions during PET imaging of mGlu5 receptor availability.

REFERENCES

Abdallah, C. G., Hannestad, J., Mason, G. F., Holmes, S. E., DellaGioia, N., Sanacora, G., . . . Esterlis, I. (2017). Metabotropic Glutamate Receptor 5 and Glutamate Involvement in Major Depressive Disorder: A Multimodal Imaging Study. *Biol Psychiatry Cogn Neurosci Neuroimaging, 2*(5), 449-456.

Abe, T., Sugihara, H., Nawa, H., Shigemoto, R., Mizuno, N., & Nakanishi, S. (1992). Molecular characterization of a novel metabotropic glutamate receptor mGluR5 coupled to inositol phosphate/Ca2+ signal transduction. *Journal of Biological Chemistry, 267*(19), 13361-13368.

Abraham, W. C., & Bear, M. F. (1996). Metaplasticity: the plasticity of synaptic plasticity. *Trends in Neurosciences, 19*(4), 126-130.

Abraham, W. C., & Mason, S. E. (1988). Effects of the NMDA receptor/channel antagonists CPP and MK801 on hippocampal field potentials and long-term potentiation in anesthetized rats. *Brain Research, 462*(1), 40-46.

Akkus, F., Ametamey, S. M., Treyer, V., Burger, C., Johayem, A., Umbricht, D., . . . Hasler, G. (2013). Marked global reduction in mGluR5 receptor binding in smokers and ex-smokers determined by [11C]ABP688 positron emission tomography. *Proceedings of the National Academy of Sciences of the United States of America, 110*(2), 737-742.

Akkus, F., Mihov, Y., Treyer, V., Ametamey, S. M., Johayem, A., Senn, S., . . . Hasler, G. (2018). Metabotropic glutamate receptor 5 binding in male patients with alcohol use disorder. *Transl Psychiatry, 8*(1), 17.

Akkus, F., Terbeck, S., Ametamey, S. M., Rufer, M., Treyer, V., Burger, C., . . . Hasler, G. (2014). Metabotropic glutamate receptor 5 binding in patients with obsessive-compulsive disorder. *International Journal of Neuropsychopharmacology, 17*(12), 1915-1922.

Akkus, F., Treyer, V., Ametamey, S. M., Johayem, A., Buck, A., & Hasler, G. (2017). Metabotropic glutamate receptor 5 neuroimaging in schizophrenia. *Schizophrenia Research, 183*, 95-101.

Akkus, F., Treyer, V., Johayem, A., Ametamey, S. M., Mancilla, B. G., Sovago, J., . . . Hasler, G. (2016). Association of Long-Term Nicotine Abstinence With Normal Metabotropic Glutamate Receptor-5 Binding. *Biological Psychiatry, 79*(6), 474-480.

Aksoy-Aksel, A., & Manahan-Vaughan, D. (2015). Synaptic strength at the temporoammonic input to the hippocampal CA1 region in vivo is regulated by NMDA receptors, metabotropic glutamate receptors and voltage-gated calcium channels. *Neuroscience, 309*, 191-199.

Alcohol and Drug Use in Canada. (2019). Retrieved from https://www150.statcan.gc.ca/n1/daily-quotidien/211220/dq211220c-eng.htm

Ametamey, S. M., Bruehlmeier, M., Kneifel, S., Kokic, M., Honer, M., Arigoni, M., . . . Schubiger, P. A. (2002). PET studies of 18F-memantine in healthy volunteers. *Nuclear Medicine and Biology, 29*(2), 227-231.

Ametamey, S. M., Kessler, L. J., Honer, M., Wyss, M. T., Buck, A., Hintermann, S., . . . Schubiger, P. A. (2006). Radiosynthesis and Preclinical Evaluation of 11C-ABP688 as a Probe for Imaging the Metabotropic Glutamate Receptor Subtype 5. *Journal of Nuclear Medicine, 47*(4), 698-705.

Ametamey, S. M., Samnick, S., Leenders, K. L., Vontobel, P., Quack, G., Parsons, C. G., & Schubiger, P. A. (1999). Fluorine-18 radiolabelling, biodistribution studies and preliminary PET evaluation of a new memantine derivative for imaging the NMDA receptor. *Journal of Receptor and Signal Transduction Research, 19*(1-4), 129-1**41**.

Ametamey, S. M., Treyer, V., Streffer, J., Wyss, M. T., Schmidt, M., Blagoev, M., . . . Buck, A. (2007). Human PET Studies of Metabotropic Glutamate Receptor Subtype 5 with 11C-ABP688. *Journal of Nuclear Medicine, 48*(2), 247.

Andersson, J. D., Seneca, N., Truong, P., Wensbo, D., Raboisson, P., Farde, L., & Halldin, C. (2013). Palladium mediated 11C-cyanation and characterization in the non-human primate brain of the novel mGluR5 radioligand [11C]AZD9272. *Nuclear Medicine and Biology, 40*(4), 547-553.

Anwyl, R. (2009). Metabotropic glutamate receptor-dependent long-term potentiation. *Neuropharmacology, 56*(4), 735-740.

Arisawa, T., Kimura, K., Miyazaki, T., Takada, Y., Nakajima, W., Ota, W., . . . Takahashi, T. (2022). Synthesis of [18F] fluorine-labeled K-2 derivatives as radiotracers for AMPA receptors. *Nuclear Medicine and Biology, 110-111*, 47-58.

Arisawa, T., Miyazaki, T., Ota, W., Sano, A., Suyama, K., Takada, Y., & Takahashi, T. (2021). [11C]K-2 image with positron emission tomography represents cell surface AMPA receptors. *Neuroscience Research, 173*, 106-113.

Aronica, E., Gorter, J. A., Ijlst-Keizers, H., Rozemuller, A. J., Yankaya, B., Leenstra, S., & Troost, D. (2003). Expression and functional role of mGluR3 and mGluR5 in human astrocytes and glioma cells: opposite regulation of glutamate transporter proteins. *European Journal of Neuroscience, 17*(10), 2106-2118.

Arstad, E., Gitto, R., Chimirri, A., Caruso, R., Constanti, A., Turton, D., . . . Luthra, S. K. (2006). Closing in on the AMPA receptor: synthesis and evaluation of 2-acetyl-1-(4'-chlorophenyl)-6-methoxy-7-[11C]methoxy-1,2,3,4-tetrahydroisoquinoline as a potential PET tracer. *Bioorg Med Chem, 14*(14), 4712-4717.

Awad, H., Hubert, G. W., Smith, Y., Levey, A. I., & Conn, P. J. (2000). Activation of metabotropic glutamate receptor 5 has direct excitatory effects and potentiates NMDA receptor currents in neurons of the subthalamic nucleus. *Journal of Neuroscience, 20*(21), 7871-7879.

Ayala, J. E., Chen, Y., Banko, J. L., Sheffler, D. J., Williams, R., Telk, A. N., . . . Conn, P. J. (2009). mGluR5 positive allosteric modulators facilitate both hippocampal LTP and LTD and enhance spatial learning. *Neuropsychopharmacology, 34*(9), 2057-2071.

Backstrom, P., Bachteler, D., Koch, S., Hyytia, P., & Spanagel, R. (2004). mGluR5 antagonist MPEP reduces ethanol-seeking and relapse behavior. *Neuropsychopharmacology, 29*(5), 921-928.

Bak, L. K., Schousboe, A., & Waagepetersen, H. S. (2006). The glutamate/GABA-glutamine cycle: aspects of transport, neurotransmitter homeostasis and ammonia transfer. *Journal of Neurochemistry, 98*(3), 641-653.

Barthel, H. (2020). First Tau PET Tracer Approved: Toward Accurate In Vivo Diagnosis of Alzheimer Disease. *Journal of Nuclear Medicine, 61*(10), 1409-1410.

Bdair, H., Kang, M. S., Ottoy, J., Arturo., A., Kunach, P., Singleton, T. A., . . . Kostikov, A. (2023). Brain PET Imaging in Small Animals: Tracer Formulation, Data Acquisition, Image Reconstruction, and Data Analysis. In T. H. Witney & A. J. Shuhendler (Eds.), *Positron Emission Tomography.* (Vol. 2729): Methods in Molecular Biology.

Bdair, H., Tsai, I. H., Smart, K., Benkelfat, C., Leyton, M., & Kostikov, A. (2019). Radiosynthesis of the diastereomerically pure (E)-[11 C]ABP688. *J Labelled Comp Radiopharm, 62*(12), 860-864.

Berry, S. A., Shah, M. C., Khan, N., & Roth, B. L. (1996). Rapid agonist-induced internalization of the 5-hydroxytryptamine2A receptor occurs via the endosome pathway in vitro. *Molecular Pharmacology, 50*(2), 306-313.

Berthele, A., Platzer, S., Laurie, D. J., Weis, S., Sommer, B., Zieglgansberger, W., . . . Tolle, T. R. (1999). Expression of metabotropic glutamate receptor subtype mRNA (mGluR1-8) in human cerebellum. *Neuroreport, 10*(18), 3861-3867.

Bertoglio, D., Kosten, L., Verhaeghe, J., Thomae, D., Wyffels, L., Stroobants, S., . . . Staelens, S. (2018). Longitudinal Characterization of mGluR5 Using 11C-ABP688 PET Imaging in the Q175 Mouse Model of Huntington Disease. *Journal of Nuclear Medicine, 59*(11), 1722-1727.

Besheer, J., Faccidomo, S., Grondin, J. J., & Hodge, C. W. (2008). Regulation of motivation to self-administer ethanol by mGluR5 in alcohol-preferring (P) rats. *Alcoholism, Clinical and Experimental Research, 32*(2), 209-221.

Bhattacharyya, S., Puri, S., Miledi, R., & Panicker, M. M. (2002). Internalization and recycling of 5-HT2A receptors activated by serotonin and protein kinase C-mediated mechanisms. *Proceedings of the National Academy of Sciences of the United States of America, 99*(22), 14470-14475.

Blin, J., Denis, A., Yamaguchi, T., Crouzel, C., MacKenzie, E. T., & Baron, J. C. (1991). PET studies of [18F]methyl-MK-801, a potential NMDA receptor complex radioligand. *Neuroscience Letters, 121*(1-2), 183-186.

Bodzeta, A., Scheefhals, N., & MacGillavry, H. D. (2021). Membrane trafficking and positioning of mGluRs at presynaptic and postsynaptic sites of excitatory synapses. *Neuropharmacology, 200*, 108799.

Bollmann, J. H., Sakmann, B., & Borst, J. G. (2000). Calcium sensitivity of glutamate release in a calyx-type terminal. *Science, 289*(5481), 953-957.

Bortolotto, Z. A., Bashir, Z. I., Davies, C. H., & Collingridge, G. L. (1994). A molecular switch activated by metabotropic glutamate receptors regulates induction of long-term potentiation. *Nature, 368*(6473), 740-743.

Bortolotto, Z. A., Collett, V. J., Conquet, F., Jia, Z., van der Putten, H., & Collingridge, G. L. (2005). The regulation of hippocampal LTP by the molecular switch, a form of metaplasticity, requires mGlu5 receptors. *Neuropharmacology, 49 Suppl 1*, 13-25.

Breier, A., Su, T.-P., Saunders, R., Carson, R. E., Kolachana, B. S., de Bartolomeis, A., . . . Pickar, D. (1997). Schizophrenia is associated with elevated amphetamine-induced synaptic dopamine concentrations: Evidence from a novel positron emission tomography method. *PNAS, 94*(6), 2569-2574.

Brickley, S. G., & Mody, I. (2012). Extrasynaptic GABAA receptors: their function in the CNS and implications for disease. *Neuron, 73*(1), 23-34.

Brown, A. K., Kimura, Y., Zoghbi, S. S., Simeon, F. G., Liow, J. S., Kreisl, W. C., . . . Innis, R. B. (2008). Metabotropic glutamate subtype 5 receptors are quantified in the human brain with a novel radioligand for PET. *Journal of Nuclear Medicine, 49*(12), 2042-2048.

Chen, J., Gan, J., Sun, J., Chen, Z., Fu, H., Rong, J., . . . Liang, S. H. (2020). Radiosynthesis and preliminary evaluation of 11C-labeled 4-cyclopropyl-7-(3-methoxyphenoxy)-3,4-dihydro-2H-benzo[e] [1,2,4] thiadiazine 1,1-dioxide for PET imaging AMPA receptors. *Tetrahedron Letters, 61*(12), 151635.

Choi, H., Kim, Y. K., Oh, S. W., Im, H. J., Hwang, D. W., Kang, H., . . . Lee, D. S. (2014). In vivo imaging of mGluR5 changes during epileptogenesis using [11C]ABP688 PET in pilocarpine-induced epilepsy rat model. *PloS One, 9*(3), e92765.

Coan, E. J., Irving, A. J., & Collingridge, G. L. (1989). Low-frequency activation of the NMDA receptor system can prevent the induction of LTP. *Neuroscience Letters, 105*(1-2), 205-210.

Collett, V. J., & Collingridge, G. L. (2004). Interactions between NMDA receptors and mGlu5 receptors expressed in HEK293 cells. *British Journal of Pharmacology, 142*(6), 991-1001.

Conn, P. J. (2003). Physiological roles and therapeutic potential of metabotropic glutamate receptors. *Annals of the New York Academy of Sciences, 1003*(1), 12-21.

Cox, S. M. L., Tippler, M., Jaworska, N., Smart, K., Castellanos-Ryan, N., Durand, F., . . . Leyton, M. (2020). mGlu5 receptor availability in youth at risk for addictions: effects of vulnerability traits and cannabis use. *Neuropsychopharmacology, 45*(11), 1817-1825.

D'Ascenzo, M., Fellin, T., Terunuma, M., Revilla-Sanchez, R., Meaney, D. F., Auberson, Y. P., . . . Haydon, P. G. (2007). mGluR5 stimulates gliotransmission in the nucleus accumbens. *Proceedings of the National Academy of Sciences of the United States of America, 104*(6), 1995-2000.

Dahchour, A., Quertemont, E., & De Witte, P. (1996). Taurine increases in the nucleus accumbens microdialysate after acute ethanol administration to naive and chronically alcoholised rats. *Brain Research, 735*(1), 9-19.

Davis, M. T., Hillmer, A., Holmes, S. E., Pietrzak, R. H., DellaGioia, N., Nabulsi, N., . . . Esterlis, I. (2019). In vivo evidence for dysregulation of mGluR5 as a biomarker of suicidal ideation. *Proceedings of the National Academy of Sciences of the United States of America, 116*(23), 11490-11495.

Davis, S., Bliss, T. V., Dutrieux, G., Laroche, S., & Errington, M. L. (1997). Induction and duration of long-term potentiation in the hippocampus of the freely moving mouse. *Journal of Neuroscience Methods, 75*(1), 75-80.

DeLorenzo, C., DellaGioia, N., Bloch, M., Sanacora, G., Nabulsi, N., Abdallah, C., . . . Esterlis, I. (2015a). In vivo ketamine-induced changes in [11C]ABP688 binding to metabotropic glutamate receptor subtype 5. *Biological Psychiatry, 77*(3), 266-275.

DeLorenzo, C., Gallezot, J. D., Gardus, J., Yang, J., Planeta, B., Nabulsi, N., . . . Esterlis, I. (2017). In vivo variation in same-day estimates of metabotropic glutamate receptor subtype 5 binding using [11C]ABP688 and [18F]FPEB. *Journal of Cerebral Blood Flow and Metabolism, 37*(8), 2716-2727.

DeLorenzo, C., Kumar, J. S., Mann, J. J., & Parsey, R. V. (2011a). In vivo variation in metabotropic glutamate receptor subtype 5 binding using positron emission tomography and [11C]ABP688. *Journal of Cerebral Blood Flow and Metabolism, 31*(11), 2169-2180.

DeLorenzo, C., Milak, M. S., Brennan, K. G., Kumar, J. S., Mann, J. J., & Parsey, R. V. (2011b). In vivo positron emission tomography imaging with [11C]ABP688: binding variability and specificity for the metabotropic glutamate receptor subtype 5 in baboons. *European Journal of Nuclear Medicine and Molecular Imaging, 38*(6), 1083-1094.

DeLorenzo, C., Sovago, J., Gardus, J., Xu, J., Yang, J., Behrje, R., . . . Parsey, R. V. (2015b). Characterization of brain mGluR5 binding in a pilot study of late-life major depressive

disorder using positron emission tomography and [11C]ABP688. *Transl Psychiatry, 5*(12), e693.

Derrick, B. E., Weinberger, S. B., & Martinez, J. L., Jr. (1991). Opioid receptors are involved in an NMDA receptor-independent mechanism of LTP induction at hippocampal mossy fiber-CA3 synapses. *Brain Research Bulletin, 27*(2), 219-223.

Deschwanden, A., Karolewicz, B., Feyissa, A. M., Treyer, V., Ametamey, S. M., Johayem, A., . . . Hasler, G. (2011). Reduced metabotropic glutamate receptor 5 density in major depression determined by [11C]ABP688 PET and postmortem study. *American Journal of Psychiatry, 168*(7), 727-734.

Dhawan, V., Niethammer, M., Lesser, M., Pappas, K., Hellman, M., Fitzpatrick, T., . . . Chlay, T. (2020). Prospective FDOPA PET imaging study in human PD :our final step towards NDA approval. *Journal of Nuclear Medicine, 61*(supplement 1), 1565.

DuBois, J. M., Rousset, O. G., Guiot, M. C., Hall, J. A., Reader, A. J., Soucy, J. P., . . . Kobayashi, E. (2016). Metabotropic Glutamate Receptor Type 5 (mGluR5) Cortical Abnormalities in Focal Cortical Dysplasia Identified In Vivo With [11C]ABP688 Positron-Emission Tomography (PET) Imaging. *Cerebral Cortex, 26*(11), 4170-4179.

DuBois, J. M., Rousset, O. G., Rowley, J., Porras-Betancourt, M., Reader, A. J., Labbe, A., . . . Kobayashi, E. (2016). Characterization of age/sex and the regional distribution of mGluR5 availability in the healthy human brain measured by high-resolution [11C]ABP688 PET. *European Journal of Nuclear Medicine and Molecular Imaging, 43*(1), 152-162.

Eckelman, W. C., & Mathis, C. A. (2006). Targeting proteins in vivo: in vitro guidelines. *Nuclear Medicine and Biology, 33*(2), 161-164.

Elmenhorst, D., Mertens, K., Kroll, T., Oskamp, A., Ermert, J., Elmenhorst, E. M., . . . Bauer, A. (2016). Circadian variation of metabotropic glutamate receptor 5 availability in the rat brain. *Journal of Sleep Research, 25*(6), 754-761.

Elmenhorst, D., Minuzzi, L., Aliaga, A., Rowley, J., Massarweh, G., Diksic, M., . . . Rosa-Neto, P. (2010). In vivo and in vitro validation of reference tissue models for the mGluR5 ligand [11C]ABP688. *Journal of Cerebral Blood Flow and Metabolism, 30*(8), 1538-1549.

Endres, C. J., Kolachana, B. S., Saunders, R. C., Su, T., Weinberger, D., Breier, A., . . . Carson, R. E. (1997). Kinetic modeling of [11C]raclopride: combined PET-microdialysis studies. *Journal of Cerebral Blood Flow and Metabolism, 17*(9), 932-942.

Erritzoe, D., Ashok, A. H., Searle, G. E., Colasanti, A., Turton, S., Lewis, Y., . . . Rabiner, E. A. (2020). Serotonin release measured in the human brain: a PET study with [11C]CIMBI-36 and d-amphetamine challenge. *Neuropsychopharmacology, 45*(5), 804-810.

Esterlis, I., DeBonee, S., Cool, R., Holmes, S., Baldassari, S. R., Maruff, P., . . . Davis, M. T. (2022). Differential Role of mGluR5 in Cognitive Processes in Posttraumatic Stress Disorder and Major Depression. *Chronic Stress (Thousand Oaks), 6*, 24705470221105804.

Esterlis, I., DellaGioia, N., Pietrzak, R. H., Matuskey, D., Nabulsi, N., Abdallah, C. G., . . . DeLorenzo, C. (2018). Ketamine-induced reduction in mGluR5 availability is associated with an antidepressant response: an [11C]ABP688 and PET imaging study in depression. *Molecular Psychiatry, 23*(4), 824-832.

Faas, G. C., Adwanikar, H., Gereau, R. W. t., & Saggau, P. (2002). Modulation of presynaptic calcium transients by metabotropic glutamate receptor activation: a differential role in acute depression of synaptic transmission and long-term depression. *Journal of Neuroscience, 22*(16), 6885-6890.

Fatemi, S. H., Wong, D. F., Brasic, J. R., Kuwabara, H., Mathur, A., Folsom, T. D., . . . Lee, S. (2018). Metabotropic glutamate receptor 5 tracer [18F]-FPEB displays increased binding potential in postcentral gyrus and cerebellum of male individuals with autism: a pilot PET study. *Cerebellum Ataxias, 5*(1), 3.

Fliegel, S., Brand, I., Spanagel, R., & Noori, H. R. (2013). Ethanol-induced alterations of amino acids measured by in vivo microdialysis in rats: a meta-analysis. *In Silico Pharmacol, 1*(1), 7.

Fonnum, F. (1984). Glutamate: a neurotransmitter in mammalian brain. *Journal of Neurochemistry, 42*(1), 1-11.

Fujinaga, M., Yamasaki, T., Nengaki, N., Ogawa, M., Kumata, K., Shimoda, Y., . . . Zhang, M. R. (2016). Radiosynthesis and evaluation of 5-methyl-N-(4-[11C]methylpyrimidin-2-yl)-4-(1H-pyrazol-4-yl)thiazol-2-amine ([11C]ADX88178) as a novel radioligand for

imaging of metabotropic glutamate receptor subtype 4 (mGluR4). *Bioorg Med Chem Lett, 26*(2), 370-374.

Gao, M., Kong, D., Clearfield, A., & Zheng, Q. H. (2006). Synthesis of carbon-11 and fluorine-18 labeled N-acetyl-1-aryl-6,7-dimethoxy-1,2,3,4-tetrahydroisoquinoline derivatives as new potential PET AMPA receptor ligands. *Bioorg Med Chem Lett, 16*(8), 2229-2233.

Garber, K. (2012). First FDA-approved beta-amyloid diagnostic hits the market. *Nature Biotechnology, 30*(7), 575.

Gasparini, F., Lingenhohl, K., Stoehr, N., Flor, P. J., Heinrich, M., Vranesic, I., . . . Kuhn, R. (1999). 2-Methyl-6-(phenylethynyl)-pyridine (MPEP), a potent, selective and systemically active mGlu5 receptor antagonist. *Neuropharmacology, 38*(10), 1493-1503.

Gitto, R., Barreca, M. L., De Luca, L., De Sarro, G., Ferreri, G., Quartarone, S., . . . Chimirri, A. (2003). Discovery of a novel and highly potent noncompetitive AMPA receptor antagonist. *Journal of Medicinal Chemistry, 46*(1), 197-200.

Glasgow, N. G., Siegler Retchless, B., & Johnson, J. W. (2015). Molecular bases of NMDA receptor subtype-dependent properties. *Journal of Physiology, 593*(1), 83-95.

Glorie, D., Verhaeghe, J., Miranda, A., De Lombaerde, S., Stroobants, S., & Staelens, S. (2022). Quantification of Metabotropic Glutamate Receptor 5 Availability With Both [11C]ABP688 and [18F]FPEB Positron Emission Tomography in the Sapap3 Knockout Mouse Model for Obsessive-Compulsive-like Behavior. *Biol Psychiatry Cogn Neurosci Neuroimaging, 7*(6), 607-615.

Glorie, D., Verhaeghe, J., Miranda, A., Kertesz, I., Wyffels, L., Stroobants, S., & Staelens, S. (2020). Progression of obsessive compulsive disorder-like grooming in Sapap3 knockout mice: A longitudinal [11C]ABP688 PET study. *Neuropharmacology, 177*, 108160.

Goffin, E., Drapier, T., Larsen, A. P., Geubelle, P., Ptak, C. P., Laulumaa, S., . . . Francotte, P. (2018). 7-Phenoxy-Substituted 3,4-Dihydro-2H-1,2,4-benzothiadiazine 1,1-Dioxides as Positive Allosteric Modulators of alpha-Amino-3-hydroxy-5-methyl-4-isoxazolepropionic Acid (AMPA) Receptors with Nanomolar Potency. *Journal of Medicinal Chemistry, 61*(1), 251-264.

Goh, J. J., & Manahan-Vaughan, D. (2013). Endogenous hippocampal LTD that is enabled by spatial object recognition requires activation of NMDA receptors and the metabotropic glutamate receptor, mGlu5. *Hippocampus, 23*(2), 129-138.

Gray, J. A., & Roth, B. L. (2001). Paradoxical trafficking and regulation of 5-HT2A receptors by agonists and antagonists. *Brain Research Bulletin, 56*(5), 441-451.

Grove-Strawser, D., Boulware, M. I., & Mermelstein, P. G. (2010). Membrane estrogen receptors activate the metabotropic glutamate receptors mGluR5 and mGluR3 to bidirectionally regulate CREB phosphorylation in female rat striatal neurons. *Neuroscience, 170*(4), 1045-1055.

Gruetter, R., Weisdorf, S. A., Rajanayagan, V., Terpstra, M., Merkle, H., Truwit, C. L., . . . Ugurbil, K. (1998). Resolution improvements in in vivo 1H NMR spectra with increased magnetic field strength. *Journal of Magnetic Resonance, 135*(1), 260-264.

Gubellini, P., Saulle, E., Centonze, D., Costa, C., Tropepi, D., Bernardi, G., . . . Calabresi, P. (2003). Corticostriatal LTP requires combined mGluR1 and mGluR5 activation. *Neuropharmacology, 44*(1), 8-16.

Gussew, A., Rzanny, R., Erdtel, M., Scholle, H. C., Kaiser, W. A., Mentzel, H. J., & Reichenbach, J. R. (2010). Time-resolved functional 1H MR spectroscopic detection of glutamate concentration changes in the brain during acute heat pain stimulation. *Neuroimage, 49*(2), 1895-1902.

Haider, A., Herde, A. M., Kramer, S. D., Varisco, J., Keller, C., Frauenknecht, K., . . . Ametamey, S. M. (2019). Preclinical Evaluation of Benzazepine-Based PET Radioligands (R)- and (S)-11C-Me-NB1 Reveals Distinct Enantiomeric Binding Patterns and a Tightrope Walk Between GluN2B- and sigma(1)-Receptor-Targeted PET Imaging. *Journal of Nuclear Medicine, 60*(8), 1167-1173.

Hamill, T. G., Krause, S., Ryan, C., Bonnefous, C., Govek, S., Seiders, T. J., . . . Burns, H. D. (2005). Synthesis, characterization, and first successful monkey imaging studies of metabotropic glutamate receptor subtype 5 (mGluR5) PET radiotracers. *Synapse, 56*(4), 205-216.

Haradahira, T., Zhang, M., Maeda, J., Okauchi, T., Kawabe, K., Kida, T., . . . Suhara, T. (2000). A strategy for increasing the brain uptake of a radioligand in animals: use of a drug that inhibits plasma protein binding. *Nuclear Medicine and Biology, 27*(4), 357-360.

Hascup, E. R., Hascup, K. N., Stephens, M., Pomerleau, F., Huettl, P., Gratton, A., & Gerhardt, G. A. (2010). Rapid microelectrode measurements and the origin and regulation of

extracellular glutamate in rat prefrontal cortex. *Journal of Neurochemistry, 115*(6), 1608-1620.

Hashimoto, A., Oka, T., & Nishikawa, T. (1995). Extracellular concentration of endogenous free D-serine in the rat brain as revealed by in vivo microdialysis. *Neuroscience, 66*(3), 635-643.

Hasler, G., van der Veen, J. W., Grillon, C., Drevets, W. C., & Shen, J. (2010). Effect of acute psychological stress on prefrontal GABA concentration determined by proton magnetic resonance spectroscopy. *American Journal of Psychiatry, 167*(10), 1226-1231.

Heidbreder, C. A., Andreoli, M., Marcon, C., Hutcheson, D. M., Gardner, E. L., & Ashby, C. R., Jr. (2007). Evidence for the role of dopamine D3 receptors in oral operant alcohol self-administration and reinstatement of alcohol-seeking behavior in mice. *Addiction Biology, 12*(1), 35-50.

Hennrich, U., & Kopka, K. (2019). Lutathera®: The First FDA- and EMA-Approved Radiopharmaceutical for Peptide Receptor Radionuclide Therapy. *Pharmaceuticals, 12*(3). doi:10.3390/ph12030114

Hill, M. N., McLaughlin, R. J., Bingham, B., Shrestha, L., Lee, T. T., Gray, J. M., . . . Viau, V. (2010). Endogenous cannabinoid signaling is essential for stress adaptation. *Proceedings of the National Academy of Sciences of the United States of America, 107*(20), 9406-9411.

Hintermann, S., Vranesic, I., Allgeier, H., Brulisauer, A., Hoyer, D., Lemaire, M., . . . Auberson, Y. P. (2007). ABP688, a novel selective and high affinity ligand for the labeling of mGlu5 receptors: identification, in vitro pharmacology, pharmacokinetic and biodistribution studies. *Bioorg Med Chem, 15*(2), 903-914.

Holmes, S. E., Girgenti, M. J., Davis, M. T., Pietrzak, R. H., DellaGioia, N., Nabulsi, N., . . . Traumatic Stress Brain Study, G. (2017). Altered metabotropic glutamate receptor 5 markers in PTSD: In vivo and postmortem evidence. *Proceedings of the National Academy of Sciences of the United States of America, 114*(31), 8390-8395.

Homayoun, H., Stefani, M. R., Adams, B. W., Tamagan, G. D., & Moghaddam, B. (2004). Functional Interaction Between NMDA and mGlu5 Receptors: Effects on Working Memory, Instrumental Learning, Motor Behaviors, and Dopamine Release. *Neuropsychopharmacology, 29*(7), 1259-1269.

Honer, M., Stoffel, A., Kessler, L. J., Schubiger, P. A., & Ametamey, S. M. (2007). Radiolabeling and in vitro and in vivo evaluation of [18F]-FE-DABP688 as a PET radioligand for the metabotropic glutamate receptor subtype 5. *Nuclear Medicine and Biology, 34*(8), 973-980.

Hostetler, E. D., Eng, W., Joshi, A. D., Sanabria-Bohorquez, S., Kawamoto, H., Ito, S., . . . Hargreaves, R. (2011). Synthesis, characterization, and monkey PET studies of [(1)(8)F]MK-1312, a PET tracer for quantification of mGluR1 receptor occupancy by MK-5435. *Synapse, 65*(2), 125-135.

Huang, Y. Y., Colino, A., Selig, D. K., & Malenka, R. C. (1992). The influence of prior synaptic activity on the induction of long-term potentiation. *Science, 255*(5045), 730-733.

Huang, Y., Narendran, R., Bischoff, F., Guo, N., Bae, S. A., Hwang, D. R., . . . Laruelle, M. (2012). Synthesis and characterization of two PET radioligands for the metabotropic glutamate 1 (mGlu1) receptor. *Synapse, 66*(12), 1002-1014.

Huang, Y., Narendran, R., Bischoff, F., Guo, N., Zhu, Z., Bae, S. A., . . . Laruelle, M. (2005). A positron emission tomography radioligand for the in vivo labeling of metabotropic glutamate 1 receptor: (3-ethyl-2-[11C]methyl-6-quinolinyl)(cis- 4-methoxycyclohexyl)methanone. *Journal of Medicinal Chemistry, 48*(16), 5096-5099.

Hubert, G. W., Paquet, M., & Smith, Y. (2001). Differential subcellular localization of mGluR1a and mGluR5 in the rat and monkey Substantia nigra. *Journal of Neuroscience, 21*(6), 1838-1847.

Hulka, L. M., Treyer, V., Scheidegger, M., Preller, K. H., Vonmoos, M., Baumgartner, M. R., . . . Quednow, B. B. (2014). Smoking but not cocaine use is associated with lower cerebral metabotropic glutamate receptor 5 density in humans. *Molecular Psychiatry, 19*(5), 625-632.

Innis, R. B., Cunningham, V. J., Delforge, J., Fujita, M., Gjedde, A., Gunn, R. N., . . . Carson, R. E. (2007). Consensus nomenclature for in vivo imaging of reversibly binding radioligands. *Journal of Cerebral Blood Flow and Metabolism, 27*(9), 1533-1539.

Ishibashi, K., Miura, Y., Toyohara, J., Ishii, K., & Ishiwata, K. (2017). Comparison of imaging using 11C-ITMM and 18F-FDG for the detection of cerebellar ataxia. *Journal of the Neurological Sciences, 375*, 97-102.

Ishibashi, K., Miura, Y., Toyohara, J., Ishiwata, K., & Ishii, K. (2019). Unchanged type 1 metabotropic glutamate receptor availability in patients with Alzheimer's disease: A study using 11C-ITMM positron emission tomography. *Neuroimage Clin, 22*, 101783.

Ishibashi, K., Miura, Y., Wagatsuma, K., Kameyama, M., & Ishii, K. (2021). Brain 11C-ITMM PET to longitudinally assess type 1 metabotropic glutamate receptor availability in Alzheimer's disease. *Journal of Neuroimaging, 31*(5), 864-868.

Iyo, A. H., Feyissa, A. M., Chandran, A., Austin, M. C., Regunathan, S., & Karolewicz, B. (2010). Chronic corticosterone administration down-regulates metabotropic glutamate receptor 5 protein expression in the rat hippocampus. *Neuroscience, 169*(4), 1567-1574.

Jia, Z., Lu, Y., Henderson, J., Taverna, F., Romano, C., Abramow-Newerly, W., . . . Roder, J. (1998). Selective abolition of the NMDA component of long-term potentiation in mice lacking mGluR5. *Learning and Memory, 5*(4-5), 331-343.

Joo, Y. H., Kim, J. H., Kim, H. K., Son, Y. D., Cumming, P., & Kim, J. H. (2021). Functional Analysis of Brain Imaging Suggests Changes in the Availability of mGluR5 and Altered Connectivity in the Cerebral Cortex of Long-Term Abstaining Males with Alcohol Dependence: A Preliminary Study. *Life, 11*(6), 506.

Jorgensen, L. M., Weikop, P., Villadsen, J., Visnapuu, T., Ettrup, A., Hansen, H. D., . . . Knudsen, G. M. (2017). Cerebral 5-HT release correlates with [11C]Cimbi36 PET measures of 5-HT2A receptor occupancy in the pig brain. *Journal of Cerebral Blood Flow and Metabolism, 37*(2), 425-434.

Kagedal, M., Cselenyi, Z., Nyberg, S., Raboisson, P., Stahle, L., Stenkrona, P., . . . Karlsson, M. O. (2013). A positron emission tomography study in healthy volunteers to estimate mGluR5 receptor occupancy of AZD2066 - estimating occupancy in the absence of a reference region. *Neuroimage, 82*, 160-169.

Kanazawa, M., Furuta, K., Doi, H., Mori, T., Minami, T., Ito, S., & Suzuki, M. (2011). Synthesis of an acromelic acid A analog-based 11C-labeled PET tracer for exploration of the site of action of acromelic acid A in allodynia induction. *Bioorg Med Chem Lett, 21*(7), 2017-2020.

Kang, J. H., Lee, M., Ryu, Y. H., Lyoo, C. H., Kim, C. H., Lee, K. C., . . . Choi, J. Y. (2015). [18F]FPEB and [18F]FDEGPECO comparative study of mGlu5 quantification in rodent brain. *Appl Radiat Isot, 98*, 103-107.

Kang, M. S., Hamadjida, A., Bedard, D., Nuara, S. G., Gourdon, J. C., Frey, S., . . . Huot, P. (2023). Distribution of [11C]-JNJ-42491293 in the marmoset brain: a positron emission tomography study. *Naunyn-Schmiedebergs Archives of Pharmacology*.

Kang, Y., Henchcliffe, C., Verma, A., Vallabhajosula, S., He, B., Kothari, P. J., . . . Mozley, P. D. (2019). 18F-FPEB PET/CT Shows mGluR5 Upregulation in Parkinson's Disease. *Journal of Neuroimaging, 29*(1), 97-103.

Kashkin, V. A., & De Witte, P. (2004). Ethanol but not acetaldehyde induced changes in brain taurine: a microdialysis study. *Amino Acids, 26*(2), 117-124.

Kawamura, K., Yamasaki, T., Kumata, K., Furutsuka, K., Takei, M., Wakizaka, H., . . . Zhang, M. R. (2014). Binding potential of (E)-[11C]ABP688 to metabotropic glutamate receptor subtype 5 is decreased by the inclusion of its 11C-labelled Z-isomer. *Nuclear Medicine and Biology, 41*(1), 17-23.

Kenji, I., Tetsuro, T., Kei, W., Muneyuki, S., Jun, T., & Kenji, I. (2018). Type 1 metabotropic glutamate receptors measured with a novel PET ligand, 11C-ITMM, in patients with cerebellar ataxia. *Journal of Nuclear Medicine, 59*(supplement 1), 1696.

Kerner, J. A., Standaert, D. G., Penney, J. B., Jr., Young, A. B., & Landwehrmeyer, G. B. (1997). Expression of group one metabotropic glutamate receptor subunit mRNAs in neurochemically identified neurons in the rat neostriatum, neocortex, and hippocampus. *Brain Research: Molecular Brain Research, 48*(2), 259-269.

Kessler, L. J. (2004). *Development of novel ligands for PET imaging of the metabotropic glutamate receptor subtype 5 (mGluR5).* ETH Zurich,

Kil, K. E., Poutiainen, P., Zhang, Z., Zhu, A., Choi, J. K., Jokivarsi, K., & Brownell, A. L. (2014). Radiosynthesis and evaluation of an 18F-labeled positron emission tomography (PET) radioligand for metabotropic glutamate receptor subtype 4 (mGlu4). *Journal of Medicinal Chemistry, 57*(21), 9130-9138.

Kil, K. E., Poutiainen, P., Zhang, Z., Zhu, A., Kuruppu, D., Prabhakar, S., . . . Brownell, A. L. (2016). Synthesis and evaluation of N-(methylthiophenyl)picolinamide derivatives as PET radioligands for metabotropic glutamate receptor subtype 4. *Bioorg Med Chem Lett, 26*(1), 133-139.

Kil, K. E., Zhang, Z., Jokivarsi, K., Gong, C., Choi, J. K., Kura, S., & Brownell, A. L. (2013). Radiosynthesis of N-(4-chloro-3-[11C]methoxyphenyl)-2-picolinamide ([11C]ML128) as

a PET radiotracer for metabotropic glutamate receptor subtype 4 (mGlu4). *Bioorg Med Chem, 21*(19), 5955-5962.

Kim, J. H., Joo, Y. H., Son, Y. D., Kim, H. K., & Kim, J. H. (2022). Differences in mGluR5 Availability Depending on the Level of Social Avoidance in Drug-Naive Young Patients with Major Depressive Disorder. *Neuropsychiatric Disease and Treatment, 18*, 2041-2053.

Kim, J. H., Joo, Y. H., Son, Y. D., Kim, J. H., Kim, Y. K., Kim, H. K., . . . Ido, T. (2019). In vivo metabotropic glutamate receptor 5 availability-associated functional connectivity alterations in drug-naive young adults with major depression. *European Neuropsychopharmacology, 29*(2), 278-290.

Kobayashi, T., Ikeda, K., Kojima, H., Niki, H., Yano, R., Yoshioka, T., & Kumanishi, T. (1999). Ethanol opens G-protein-activated inwardly rectifying K+ channels. *Nature Neuroscience, 2*(12), 1091-1097.

Kokic, M., Honer, M., Kessler, L. J., Grauert, M., Schubiger, P. A., & Ametamey, S. M. (2002). Synthesis and in vitro and in vivo evaluation of [11C]methyl-BIII277CL for imaging the PCP-binding site of the NMDA receptor by pet. *Journal of Receptor and Signal Transduction Research, 22*(1-4), 123-139.

Kotecha, S. A., Jackson, M. F., Al-Mahrouki, A., Roder, J. C., Orser, B. A., & MacDonald, J. F. (2003). Co-stimulation of mGluR5 and N-methyl-D-aspartate receptors is required for potentiation of excitatory synaptic transmission in hippocampal neurons. *Journal of Biological Chemistry, 278*(30), 27742-27749.

Kramer, S. D., Betzel, T., Mu, L., Haider, A., Herde, A. M., Boninsegni, A. K., . . . Ametamey, S. M. (2018). Evaluation of 11C-Me-NB1 as a Potential PET Radioligand for Measuring GluN2B-Containing NMDA Receptors, Drug Occupancy, and Receptor Cross Talk. *Journal of Nuclear Medicine, 59*(4), 698-703.

Krishnamoorthy, S., Schmall, J. P., & Surti, S. (2017). PET Physics and Instrumentation. In M. M. Khalil (Ed.), *Basic Science of PET Imaging* (pp. 173-197). Cham: Springer International Publishing.

Kronenberg, U. B., Drewes, B., Sihver, W., & Coenen, H. H. (2007). N-2-(4-N-(4-[18F]Fluorobenzamido)phenyl)-propyl-2-propanesulphonamide: synthesis and

radiofluorination of a putative AMPA receptor ligand. *Journal of Labelled Compounds and Radiopharmaceuticals, 50*(13), 1169-1175.

Kumata, K., Hatori, A., Yamasaki, T., Zhang, Y., Mori, W., Fujinaga, M., . . . Zhang, M. R. (2019). Synthesis and evaluation of 4-(2-fluoro-4-[11C]methoxyphenyl)-5-((2-methylpyridin-4-yl)methoxy)picolinamide for PET imaging of the metabotropic glutamate receptor 2 in the rat brain. *Bioorg Med Chem, 27*(3), 483-491.

Kunishima, N., Shimada, Y., Tsuji, Y., Sato, T., Yamamoto, M., Kumasaka, T., . . . Morikawa, K. (2000). Structural basis of glutamate recognition by a dimeric metabotropic glutamate receptor. *Nature, 407*(6807), 971-977.

Lam, J., DuBois, J. M., Rowley, J., Gonzalez-Otarula, K. A., Soucy, J. P., Massarweh, G., . . . Kobayashi, E. (2019). In vivo metabotropic glutamate receptor type 5 abnormalities localize the epileptogenic zone in mesial temporal lobe epilepsy. *Annals of Neurology, 85*(2), 218-228.

Lammertsma, A. A., & Hume, S. P. (1996). Simplified reference tissue model for PET receptor studies. *Neuroimage, 4*(3 Pt 1), 153-158.

Landau, A. M., Jakobsen, S., Thomsen, M. B., Alstrup, A. K. O., Orlowski, D., Jacobsen, J., . . . Doudet, D. J. (2023). Combined In Vivo Microdialysis and PET Studies to Validate [11C]Yohimbine Binding as a Marker of Noradrenaline Release. *Biomolecules, 13*(4), 674.

Leurquin-Sterk, G., Celen, S., Van Laere, K., Koole, M., Bormans, G., Langlois, X., . . . Schmidt, M. E. (2017). What We Observe In Vivo Is Not Always What We See In Vitro: Development and Validation of 11C-JNJ-42491293, A Novel Radioligand for mGluR2. *Journal of Nuclear Medicine, 58*(1), 110-116.

Leurquin-Sterk, G., Crunelle, C., Ceccarini, J., de Laat, B., Peuskens, H., Bormans, G., & Van Laere, K. (2016). Alcohol addiction is associated with decreased limbic mGluR5 availability: a 18F-FPEB PET study in human. In: Soc Nuclear Med.

Leurquin-Sterk, G., Postnov, A., de Laat, B., Casteels, C., Celen, S., Crunelle, C. L., . . . Van Laere, K. (2016). Kinetic modeling and long-term test-retest reproducibility of the mGluR5 PET tracer 18F-FPEB in human brain. *Synapse, 70*(4), 153-162.

Leuzy, A., Zimmer, E. R., Dubois, J., Pruessner, J., Cooperman, C., Soucy, J. P., . . . Rosa-Neto, P. (2016). In vivo characterization of metabotropic glutamate receptor type 5 abnormalities in behavioral variant FTD. *Brain Struct Funct, 221*(3), 1387-1402.

Liu, C., Yang, T. Q., Zhou, Y. D., & Shen, Y. (2022). Reduced astrocytic mGluR5 in the hippocampus is associated with stress-induced depressive-like behaviors in mice. *Neuroscience Letters, 784*, 136766.

Liu, H., Zakiniaeiz, Y., Cosgrove, K. P., & Morris, E. D. (2019). Toward whole-brain dopamine movies: a critical review of PET imaging of dopamine transmission in the striatum and cortex. *Brain Imaging Behav, 13*(2), 314-322.

Lohith, T. G., Tsujikawa, T., Simeon, F. G., Veronese, M., Zoghbi, S. S., Lyoo, C. H., . . . Innis, R. B. (2017). Comparison of two PET radioligands, [11C]FPEB and [11C]SP203, for quantification of metabotropic glutamate receptor 5 in human brain. *Journal of Cerebral Blood Flow and Metabolism, 37*(7), 2458-2470.

Lovinger, D. M. (1999). 5-HT3 receptors and the neural actions of alcohols: an increasingly exciting topic. *Neurochemistry International, 35*(2), 125-130.

Lovinger, D. M., White, G., & Weight, F. F. (1989). Ethanol inhibits NMDA-activated ion current in hippocampal neurons. *Science, 243*(4899), 1721-1724.

Lu, Y. M., Jia, Z., Janus, C., Henderson, J. T., Gerlai, R., Wojtowicz, J. M., & Roder, J. C. (1997). Mice lacking metabotropic glutamate receptor 5 show impaired learning and reduced CA1 long-term potentiation (LTP) but normal CA3 LTP. *Journal of Neuroscience, 17*(13), 5196-5205.

Lucatelli, C., Honer, M., Salazar, J. F., Ross, T. L., Schubiger, P. A., & Ametamey, S. M. (2009). Synthesis, radiolabeling, in vitro and in vivo evaluation of [18F]-FPECMO as a positron emission tomography radioligand for imaging the metabotropic glutamate receptor subtype 5. *Nuclear Medicine and Biology, 36*(6), 613-622.

Lupinsky, D., Moquin, L., & Gratton, A. (2010). Interhemispheric regulation of the medial prefrontal cortical glutamate stress response in rats. *Journal of Neuroscience, 30*(22), 7624-7633.

Ma, Y., Kumata, K., Yui, J., Zhang, Y., Yamasaki, T., Hatori, A., . . . Zhang, M. R. (2017). Synthesis and evaluation of 1-(cyclopropylmethyl)-4-(4-[11C]methoxyphenyl)-piperidin-

1-yl-2-oxo-1,2-dihydropyridine-3-carbonitrile ([11C]CMDC) for PET imaging of metabotropic glutamate receptor 2 in the rat brain. *Bioorg Med Chem, 25*(3), 1014-1021.

Majo, V. J., Prabhakaran, J., Mann, J. J., & Kumar, J. S. (2013). PET and SPECT tracers for glutamate receptors. *Drug Discovery Today, 18*(3-4), 173-184.

Marquez de Prado, B., Castaneda, T. R., Galindo, A., del Arco, A., Segovia, G., Reiter, R. J., & Mora, F. (2000). Melatonin disrupts circadian rhythms of glutamate and GABA in the neostriatum of the awake rat: a microdialysis study. *Journal of Pineal Research, 29*(4), 209-216.

Martinez, D., Slifstein, M., Nabulsi, N., Grassetti, A., Urban, N. B., Perez, A., . . . Huang, Y. (2014). Imaging glutamate homeostasis in cocaine addiction with the metabotropic glutamate receptor 5 positron emission tomography radiotracer [11C]ABP688 and magnetic resonance spectroscopy. *Biological Psychiatry, 75*(2), 165-171.

Masu, M., Tanabe, Y., Tsuchida, K., Shigemoto, R., & Nakanishi, S. (1991). Sequence and expression of a metabotropic glutamate receptor. *Nature, 349*(6312), 760-765.

Matsumoto, R., Haradahira, T., Ito, H., Fujimura, Y., Seki, C., Ikoma, Y., . . . Suhara, T. (2007). Measurement of glycine binding site of N-methyl-D-asparate receptors in living human brain using 4-acetoxy derivative of L-703,717, 4-acetoxy-7-chloro-3-[3-(4-[11c] methoxybenzyl) phenyl]-2(1H)-quinolone (AcL703) with positron emission tomography. *Synapse, 61*(10), 795-800.

Matta, J. A., Ashby, M. C., Sanz-Clemente, A., Roche, K. W., & Isaac, J. T. (2011). mGluR5 and NMDA receptors drive the experience- and activity-dependent NMDA receptor NR2B to NR2A subunit switch. *Neuron, 70*(2), 339-351.

Mecca, A. P., Rogers, K., Jacobs, Z., McDonald, J. W., Michalak, H. R., DellaGioia, N., . . . van Dyck, C. H. (2021). Effect of age on brain metabotropic glutamate receptor subtype 5 measured with [18F]FPEB PET. *Neuroimage, 238*, 118217.

Meldrum, B. S. (2000). Glutamate as a neurotransmitter in the brain: review of physiology and pathology. *Journal of Nutrition, 130*(4S Suppl), 1007S-1015S.

Miao, C., Dong, F., Jia, L., Li, W., Wang, M., Zheng, Q. H., & Xu, Z. (2019). Radiosynthesis of a carbon-11-labeled AMPAR allosteric modulator as a new PET radioligand candidate for imaging of Alzheimer's disease. *Bioorg Med Chem Lett, 29*(10), 1177-1181.

Mihic, S. J., Ye, Q., Wick, M. J., Koltchine, V. V., Krasowski, M. D., Finn, S. E., . . . Harrison, N. L. (1997). Sites of alcohol and volatile anaesthetic action on GABA(A) and glycine receptors. *Nature, 389*(6649), 385-389.

Milella, M. S., Marengo, L., Larcher, K., Fotros, A., Dagher, A., Rosa-Neto, P., . . . Leyton, M. (2014). Limbic system mGluR5 availability in cocaine dependent subjects: a high-resolution PET [11C]ABP688 study. *Neuroimage, 98*, 195-202.

Milella, M. S., Reader, A. J., Albrechtsons, D., Minuzi, L., Soucy, J. P., & Benkelfat, C. (2011). *Human PET validation study of reference tissue models for the mGluR5 ligand [11C] ABP688.* Paper presented at the Society for Neuroscience Annual Meeting. Washington, DC.

Minakami, R., Katsuki, F., Yamamoto, T., Nakamura, K., & Sugiyama, H. (1994). Molecular cloning and the functional expression of two isoforms of human metabotropic glutamate receptor subtype 5. *Biochem Biophys Res Commun, 199*(3), 1136-1143.

Miyake, N., Skinbjerg, M., Easwaramoorthy, B., Kumar, D., Girgis, R. R., Xu, X., . . . Abi-Dargham, A. (2011). Imaging changes in glutamate transmission in vivo with the metabotropic glutamate receptor 5 tracer [11C]ABP688 and N-acetylcysteine challenge. *Biological Psychiatry, 69*(9), 822-824.

Miyazaki, T., Nakajima, W., Hatano, M., Shibata, Y., Kuroki, Y., Arisawa, T., . . . Takahashi, T. (2020). Visualization of AMPA receptors in living human brain with positron emission tomography. *Nature Medicine, 26*(2), 281-288.

Moghaddam, B. (1993). Stress preferentially increases extraneuronal levels of excitatory amino acids in the prefrontal cortex: comparison to hippocampus and basal ganglia. *Journal of Neurochemistry, 60*(5), 1650-1657.

Morris, R. G., Anderson, E., Lynch, G. S., & Baudry, M. (1986). Selective impairment of learning and blockade of long-term potentiation by an N-methyl-D-aspartate receptor antagonist, AP5. *Nature, 319*(6056), 774-776.

Moss, G. P. (1996). Basic terminology of stereochemistry (IUPAC Recommendations 1996). *Pure and Applied Chemistry, 68*(12), 2193-2222.

Müller Herde, A., Boss, S. D., He, Y., Schibli, R., Mu, L., & Ametamey, S. M. (2018). Ketamine and Ceftriaxone-Induced Alterations in Glutamate Levels Do Not Impact the Specific

Binding of Metabotropic Glutamate Receptor Subtype 5 Radioligand [18F]PSS232 in the Rat Brain. *Pharmaceuticals, 11*(3), 83.

Muller, P. (1994). Glossary of terms used in physical organic chemistry (IUPAC Recommendations 1994). *Pure and Applied Chemistry, 66*(5), 1077-1184.

Musazzi, L., Milanese, M., Farisello, P., Zappettini, S., Tardito, D., Barbiero, V. S., . . . Popoli, M. (2010). Acute stress increases depolarization-evoked glutamate release in the rat prefrontal/frontal cortex: the dampening action of antidepressants. *PloS One, 5*(1), e8566.

Musazzi, L., Racagni, G., & Popoli, M. (2011). Stress, glucocorticoids and glutamate release: effects of antidepressant drugs. *Neurochemistry International, 59*(2), 138-149.

Nag, S., Varnas, K., Arakawa, R., Jahan, M., Schou, M., Farde, L., & Halldin, C. (2020). Synthesis, Biodistribution, and Radiation Dosimetry of a Novel mGluR5 Radioligand: 18F-AZD9272. *ACS Chemical Neuroscience, 11*(7), 1048-1057.

Naisbitt, S., Kim, E., Tu, J. C., Xiao, B., Sala, C., Valtschanoff, J., . . . Sheng, M. (1999). Shank, a novel family of postsynaptic density proteins that binds to the NMDA receptor/PSD-95/GKAP complex and cortactin. *Neuron, 23*(3), 569-582.

Narahashi, T., Aistrup, G. L., Marszalec, W., & Nagata, K. (1999). Neuronal nicotinic acetylcholine receptors: a new target site of ethanol. *Neurochemistry International, 35*(2), 131-141.

Narendran, R., Jedema, H. P., Lopresti, B. J., Mason, N. S., Gurnsey, K., Ruszkiewicz, J., . . . Bradberry, C. W. (2014). Imaging dopamine transmission in the frontal cortex: a simultaneous microdialysis and [11C]FLB 457 PET study. *Molecular Psychiatry, 19*(3), 302-310.

Niciu, M. J., Kelmendi, B., & Sanacora, G. (2012). Overview of glutamatergic neurotransmission in the nervous system. *Pharmacol Biochem Behav, 100*(4), 656-664.

O'Gorman Tuura, R., Warnock, G., Ametamey, S., Treyer, V., Noeske, R., Buck, A., & Sommerauer, M. (2019). Imaging glutamate redistribution after acute N-acetylcysteine administration: A simultaneous PET/MR study. *Neuroimage, 184*, 826-833.

O'Shea, R. D. (2002). Roles and regulation of glutamate transporters in the central nervous system. *Clin Exp Pharmacol Physiol, 29*(11), 1018-1023.

Oi, N., Tokunaga, M., Suzuki, M., Nagai, Y., Nakatani, Y., Yamamoto, N., . . . Higuchi, M. (2015). Development of Novel PET Probes for Central 2-Amino-3-(3-hydroxy-5-methyl-

4-isoxazolyl)propionic Acid Receptors. *Journal of Medicinal Chemistry, 58*(21), 8444-8462.

Olmo, I. G., Ferreira-Vieira, T. H., & Ribeiro, F. M. (2016). Dissecting the Signaling Pathways Involved in the Crosstalk between Metabotropic Glutamate 5 and Cannabinoid Type 1 Receptors. *Molecular Pharmacology, 90*(5), 609-619.

Pang, Z. P., & Sudhof, T. C. (2010). Cell biology of Ca2+-triggered exocytosis. *Current Opinion in Cell Biology, 22*(4), 496-505.

Paoletti, P., Bellone, C., & Zhou, Q. (2013). NMDA receptor subunit diversity: impact on receptor properties, synaptic plasticity and disease. *Nature Reviews: Neuroscience, 14*(6), 383-400.

Paquet, M., & Smith, Y. (2003). Group I metabotropic glutamate receptors in the monkey striatum: subsynaptic association with glutamatergic and dopaminergic afferents. *Journal of Neuroscience, 23*(20), 7659-7669.

Park, E., Sullivan, J. M., Planeta, B., Gallezot, J. D., Lim, K., Lin, S. F., . . . Carson, R. E. (2015). Test-retest reproducibility of the metabotropic glutamate receptor 5 ligand [18F]FPEB with bolus plus constant infusion in humans. *European Journal of Nuclear Medicine and Molecular Imaging, 42*(10), 1530-1541.

Patel, S., Ndubizu, O., Hamill, T., Chaudhary, A., Burns, H. D., Hargreaves, R., & Gibson, R. E. (2005). Screening cascade and development of potential Positron Emission Tomography radiotracers for mGluR5: in vitro and in vivo characterization. *Molecular Imaging and Biology, 7*(4), 314-323.

Perkins, J. J., McQuade, P., Bungard, C. J., Diamond, T. L., Gantert, L. T., Gotter, A. L., . . . Meissner, R. S. (2023). Discovery of [11C]MK-8056: A Selective PET Imaging Agent for the Study of mGluR2 Negative Allosteric Modulators. *ACS Medicinal Chemistry Letters, 14*(7), 986-992.

Pin, J. P., Galvez, T., & Prezeau, L. (2003). Evolution, structure, and activation mechanism of family 3/C G-protein-coupled receptors. *Pharmacol Ther, 98*(3), 325-354.

Pinheiro, P. S., & Mulle, C. (2008). Presynaptic glutamate receptors: physiological functions and mechanisms of action. *Nature Reviews: Neuroscience, 9*(6), 423-436.

Pisani, A., Gubellini, P., Bonsi, P., Conquet, F., Picconi, B., Centonze, D., . . . Calabresi, P. (2001). Metabotropic glutamate receptor 5 mediates the potentiation of N-methyl-D-aspartate responses in medium spiny striatal neurons. *Neuroscience, 106*(3), 579-587.

Popkirov, S. G., & Manahan-Vaughan, D. (2011). Involvement of the metabotropic glutamate receptor mGluR5 in NMDA receptor-dependent, learning-facilitated long-term depression in CA1 synapses. *Cerebral Cortex, 21*(3), 501-509.

Popoli, M., Yan, Z., McEwen, B. S., & Sanacora, G. (2011). The stressed synapse: the impact of stress and glucocorticoids on glutamate transmission. *Nature Reviews: Neuroscience, 13*(1), 22-37.

Prabhakaran, J., Majo, V. J., Milak, M. S., Kassir, S. A., Palner, M., Savenkova, L., . . . Kumar, J. S. (2010). Synthesis, in vitro and in vivo evaluation of [11C]MMTP: a potential PET ligand for mGluR1 receptors. *Bioorg Med Chem Lett, 20*(12), 3499-3501.

Ramadan, S., Lin, A., & Stanwell, P. (2013). Glutamate and glutamine: a review of in vivo MRS in the human brain. *NMR in Biomedicine, 26*(12), 1630-1646.

Rassnick, S., Pulvirenti, L., & Koob, G. F. (1992). Oral ethanol self-administration in rats is reduced by the administration of dopamine and glutamate receptor antagonists into the nucleus accumbens. *Psychopharmacology, 109*(1-2), 92-98.

Raymond, C. R., Thompson, V. L., Tate, W. P., & Abraham, W. C. (2000). Metabotropic Glutamate Receptors Trigger Homosynaptic Protein Synthesis to Prolong Long-Term Potentiation. *The Journal of Neuroscience, 20*(3), 969-976.

Regio Brambilla, C., Scheins, J., Tellmann, L., Issa, A., Herzog, H., Shah, N. J., . . . Lerche, C. W. (2023). Impact of framing scheme optimization and smoking status on binding potential analysis in dynamic PET with [11C]ABP688. *EJNMMI Res, 13*(1), 11.

Rischka, L., Vraka, C., Pichler, V., Rasul, S., Nics, L., Gryglewski, G., . . . Ametamey, S. M. (2022). First-in-Humans Brain PET Imaging of the GluN2B-Containing N-methyl-d-aspartate Receptor with (R)-11C-Me-NB1. *Journal of Nuclear Medicine, 63*(6), 936-941.

Romano, C., Sesma, M. A., McDonald, C. T., O'Malley, K., Van den Pol, A. N., & Olney, J. W. (1995). Distribution of metabotropic glutamate receptor mGluR5 immunoreactivity in rat brain. *Journal of Comparative Neurology, 355*(3), 455-469.

Romano, C., Yang, W. L., & O'Malley, K. L. (1996). Metabotropic glutamate receptor 5 is a disulfide-linked dimer. *Journal of Biological Chemistry, 271*(45), 28612-28616.

Sakata, M., Toyohara, J., Ishibashi, K., Wagatsuma, K., Ishii, K., Zhang, M. R., & Ishiwata, K. (2017). Age and gender effects of 11C-ITMM binding to metabotropic glutamate receptor type 1 in healthy human participants. *Neurobiology of Aging, 55*, 72-77.

Sandiego, C. M., Nabulsi, N., Lin, S. F., Labaree, D., Najafzadeh, S., Huang, Y., . . . Carson, R. E. (2013). Studies of the metabotropic glutamate receptor 5 radioligand [11C]ABP688 with N-acetylcysteine challenge in rhesus monkeys. *Synapse, 67*(8), 489-501.

Saunders, C., & Limbird, L. E. (1999). Localization and trafficking of alpha2-adrenergic receptor subtypes in cells and tissues. *Pharmacol Ther, 84*(2), 193-205.

Scala, S. (2023). *A multimodal neuroimaging study of mGluR5 availability, cue reactivity, and cognitive regulation in recreational cocaine users.* (Doctoral). McGill University,

Schoenberger, M., Schroeder, F. A., Placzek, M. S., Carter, R. L., Rosen, B. R., Hooker, J. M., & Sander, C. Y. (2018). In Vivo [18F]GE-179 Brain Signal Does Not Show NMDA-Specific Modulation with Drug Challenges in Rodents and Nonhuman Primates. *ACS Chemical Neuroscience, 9*(2), 298-305.

Schroeder, J. P., Overstreet, D. H., & Hodge, C. W. (2005). The mGluR5 antagonist MPEP decreases operant ethanol self-administration during maintenance and after repeated alcohol deprivations in alcohol-preferring (P) rats. *Psychopharmacology, 179*(1), 262-270.

Selim, M., & Bradberry, C. W. (1996). Effect of ethanol on extracellular 5-HT and glutamate in the nucleus accumbens and prefrontal cortex: comparison between the Lewis and Fischer 344 rat strains. *Brain Research, 716*(1-2), 157-164.

Sephton, S. M., Dennler, P., Leutwiler, D. S., Mu, L., Schibli, R., Kramer, S. D., & Ametamey, S. M. (2012). Development of [18F]-PSS223 as a PET tracer for imaging of metabotropic glutamate receptor subtype 5 (mGluR5). *Chimia (Aarau), 66*(4), 201-204.

Sephton, S. M., Dragic, M., Krämer, S., Schibli, R., & Ametamey, S. M. (2013). Synthesis and In Vitro Evaluation of E- and Z-Geometrical Isomers of PSS232 as Potential Metabotropic Glutamate Receptors Subtype 5 (mGlu5) Binders. *Synthesis, 45*(13), 1877-1885.

Sephton, S. M., Herde, A. M., Mu, L., Keller, C., Rudisuhli, S., Auberson, Y., . . . Ametamey, S. M. (2015). Preclinical evaluation and test-retest studies of [18F]PSS232, a novel

radioligand for targeting metabotropic glutamate receptor 5 (mGlu5). *European Journal of Nuclear Medicine and Molecular Imaging, 42*(1), 128-137.

Severance, A. J., Parsey, R. V., Kumar, J. S., Underwood, M. D., Arango, V., Majo, V. J., . . . Mann, J. J. (2006). In vitro and in vivo evaluation of [11C]MPEPy as a potential PET ligand for mGlu5 receptors. *Nuclear Medicine and Biology, 33*(8), 1021-1027.

Shen, J., Petersen, K. F., Behar, K. L., Brown, P., Nixon, T. W., Mason, G. F., . . . Rothman, D. L. (1999). Determination of the rate of the glutamate/glutamine cycle in the human brain by in vivo 13C NMR. *Proceedings of the National Academy of Sciences of the United States of America, 96*(14), 8235-8240.

Shigemoto, R., Nomura, S., Ohishi, H., Sugihara, H., Nakanishi, S., & Mizuno, N. (1993). Immunohistochemical localization of a metabotropic glutamate receptor, mGluR5, in the rat brain. *Neuroscience Letters, 163*(1), 53-57.

Siessmeier, T., Zhou, Y., Buchholz, H. G., Landvogt, C., Vernaleken, I., Piel, M., . . . Bartenstein, P. (2005). Parametric mapping of binding in human brain of D2 receptor ligands of different affinities. *Journal of Nuclear Medicine, 46*(6), 964-972.

Simeon, F. G., Brown, A. K., Zoghbi, S. S., Patterson, V. M., Innis, R. B., & Pike, V. W. (2007). Synthesis and simple 18F-labeling of 3-fluoro-5-(2-(2-(fluoromethyl)thiazol-4-yl)ethynyl)benzonitrile as a high affinity radioligand for imaging monkey brain metabotropic glutamate subtype-5 receptors with positron emission tomography. *Journal of Medicinal Chemistry, 50*(14), 3256-3266.

Simeon, F. G., Liow, J. S., Zhang, Y., Hong, J., Gladding, R. L., Zoghbi, S. S., . . . Pike, V. W. (2012). Synthesis and characterization in monkey of [11C]SP203 as a radioligand for imaging brain metabotropic glutamate 5 receptors. *European Journal of Nuclear Medicine and Molecular Imaging, 39*(12), 1949-1958.

Slifstein, M., Narendran, R., Hwang, D. R., Sudo, Y., Talbot, P. S., Huang, Y., & Laruelle, M. (2004). Effect of amphetamine on [18F]fallypride in vivo binding to D(2) receptors in striatal and extrastriatal regions of the primate brain: Single bolus and bolus plus constant infusion studies. *Synapse, 54*(1), 46-63.

Smart, K., Cox, S. M. L., Kostikov, A., Shalai, A., Scala, S. G., Tippler, M., . . . Leyton, M. (2019a). Effect of (Z)-isomer content on [11C]ABP688 binding potential in humans. *European Journal of Nuclear Medicine and Molecular Imaging, 46*(5), 1175-1178.

Smart, K., Cox, S. M. L., Scala, S. G., Tippler, M., Jaworska, N., Boivin, M., . . . Leyton, M. (2019b). Sex differences in [11C]ABP688 binding: a positron emission tomography study of mGlu5 receptors. *European Journal of Nuclear Medicine and Molecular Imaging, 46*(5), 1179-1183.

Smart, K., Nagano-Saito, A., Milella, M. S., Sakae, D. Y., Favier, M., Vigneault, E., . . . Benkelfat, C. (2021). Metabotropic glutamate type 5 receptor binding availability during dextroamphetamine sensitization in mice and humans. *Journal of Psychiatry and Neuroscience, 46*(1), E1-E13.

Smart, K., Scala, S. G., El Mestikawy, S., Benkelfat, C., & Leyton, M. (2017). Cocaine addiction and mGluR5. In V. R. Preedy (Ed.), *The Neuroscience of Cocaine* (pp. 269-278). San Diego: Academic Press.

Smart, K., Worhunsky, P. D., Scheinost, D., Angarita, G. A., Esterlis, I., Carson, R. E., . . . Hillmer, A. T. (2022a). Multimodal neuroimaging of metabotropic glutamate 5 receptors and functional connectivity in alcohol use disorder. *Alcoholism, Clinical and Experimental Research, 46*(5), 770-782.

Smart, K., Zheng, M. Q., Ahmed, H., Fang, H., Xu, Y., Cai, L., . . . Carson, R. E. (2022b). Comparison of three novel radiotracers for GluN2B-containing NMDA receptors in non-human primates: (R)-[11C]NR2B-Me, (R)-[18F]of-Me-NB1, and (S)-[18F]of-NB1. *Journal of Cerebral Blood Flow and Metabolism, 42*(8), 1398-1409.

Smith, F. L., Smith, P. A., Dewey, W. L., & Javed, R. R. (2004). Effects of mGlu1 and mGlu5 metabotropic glutamate antagonists to reverse morphine tolerance in mice. *European Journal of Pharmacology, 492*(2-3), 137-142.

Stefani, M. R., & Moghaddam, B. (2010). Activation of type 5 metabotropic glutamate receptors attenuates deficits in cognitive flexibility induced by NMDA receptor blockade. *European Journal of Pharmacology, 639*(1-3), 26-32.

Sun, H., Su, R., Zhang, X., Wen, J., Yao, D., Gao, X., . . . Li, H. (2017). Hippocampal GR- and CB1-mediated mGluR5 differentially produces susceptibility and resilience to acute and chronic mild stress in rats. *Neuroscience, 357*, 295-302.

Sun, J. Y., Kumata, K., Chen, Z., Zhang, Y. D., Chen, J. H., Hatori, A., . . . Liang, S. H. (2021). Synthesis and preliminary evaluation of novel 11C-labeled GluN2B-selective NMDA receptor negative allosteric modulators. *Acta Pharmacologica Sinica, 42*(3), 491-498.

Sun, Y., Xu, Y., Cheng, X., Chen, X., Xie, Y., Zhang, L., . . . Gao, Z. (2018). The differences between GluN2A and GluN2B signaling in the brain. *Journal of Neuroscience Research, 96*(8), 1430-1443.

Takahata, K., Kimura, Y., Seki, C., Tokunaga, M., Ichise, M., Kawamura, K., . . . Higuchi, M. (2017). A human PET study of [11C]HMS011, a potential radioligand for AMPA receptors. *EJNMMI Res, 7*(1), 63.

Takamori, S. (2006). VGLUTs: 'exciting' times for glutamatergic research? *Neuroscience Research, 55*(4), 343-351.

Takano, A., Nag, S., Jia, Z., Jahan, M., Forsberg, A., Arakawa, R., . . . Charvin, D. (2019). Characterization of [11C]PXT012253 as a PET Radioligand for mGlu(4) Allosteric Modulators in Nonhuman Primates. *Molecular Imaging and Biology, 21*(3), 500-508.

Tang, Y. P., Shimizu, E., Dube, G. R., Rampon, C., Kerchner, G. A., Zhuo, M., . . . Tsien, J. Z. (1999). Genetic enhancement of learning and memory in mice. *Nature, 401*(6748), 63-69.

Testa, C. M., Standaert, D. G., Young, A. B., & Penney, J. B., Jr. (1994). Metabotropic glutamate receptor mRNA expression in the basal ganglia of the rat. *Journal of Neuroscience, 14*(5 Pt 2), 3005-3018.

Thandi, S., Blank, J. L., & Challiss, R. A. (2002). Group-I metabotropic glutamate receptors, mGlu1a and mGlu5a, couple to extracellular signal-regulated kinase (ERK) activation via distinct, but overlapping, signalling pathways. *Journal of Neurochemistry, 83*(5), 1139-1153.

Tkac, I., Andersen, P., Adriany, G., Merkle, H., Ugurbil, K., & Gruetter, R. (2001). In vivo 1H NMR spectroscopy of the human brain at 7 T. *Magnetic Resonance in Medicine, 46*(3), 451-456.

Toyohara, J., Sakata, M., Oda, K., Ishii, K., Ito, K., Hiura, M., . . . Ishiwata, K. (2013). Initial human PET studies of metabotropic glutamate receptor type 1 ligand 11C-ITMM. *Journal of Nuclear Medicine, 54*(8), 1302-1307.

Treyer, V., Streffer, J., Wyss, M. T., Bettio, A., Ametamey, S. M., Fischer, U., . . . Buck, A. (2007). Evaluation of the metabotropic glutamate receptor subtype 5 using PET and 11C-ABP688: assessment of methods. *Journal of Nuclear Medicine, 48*(7), 1207-1215.

Tsukada, H., Nishiyama, S., Kakiuchi, T., Ohba, H., Sato, K., & Harada, N. (1999). Is synaptic dopamine concentration the exclusive factor which alters the in vivo binding of

[11C]raclopride?: PET studies combined with microdialysis in conscious monkeys. *Brain Research, 841*(1-2), 160-169.

Tu, J. C., Xiao, B., Naisbitt, S., Yuan, J. P., Petralia, R. S., Brakeman, P., . . . Worley, P. F. (1999). Coupling of mGluR/Homer and PSD-95 complexes by the Shank family of postsynaptic density proteins. *Neuron, 23*(3), 583-592.

van den Pol, A. N., Romano, C., & Ghosh, P. (1995). Metabotropic glutamate receptor mGluR5 subcellular distribution and developmental expression in hypothalamus. *Journal of Comparative Neurology, 362*(1), 134-150.

Varnas, K., Cselenyi, Z., Arakawa, R., Nag, S., Stepanov, V., Moein, M. M., . . . Farde, L. (2020). The pro-psychotic metabotropic glutamate receptor compounds fenobam and AZD9272 share binding sites with monoamine oxidase-B inhibitors in humans. *Neuropharmacology, 162*, 107809.

Varnas, K., Jureus, A., Finnema, S. J., Johnstrom, P., Raboisson, P., Amini, N., . . . Farde, L. (2018). The metabotropic glutamate receptor 5 radioligand [11C]AZD9272 identifies unique binding sites in primate brain. *Neuropharmacology, 135*, 455-463.

Vengeliene, V., Bilbao, A., Molander, A., & Spanagel, R. (2008). Neuropharmacology of alcohol addiction. *British Journal of Pharmacology, 154*(2), 299-315.

Vibholm, A. K., Landau, A. M., Alstrup, A. K. O., Jacobsen, J., Vang, K., Munk, O. L., . . . Brooks, D. J. (2020). Activation of NMDA receptor ion channels by deep brain stimulation in the pig visualised with [18F]GE-179 PET. *Brain Stimul, 13*(4), 1071-1078.

Vieira, M., Yong, X. L. H., Roche, K. W., & Anggono, V. (2020). Regulation of NMDA glutamate receptor functions by the GluN2 subunits. *Journal of Neurochemistry, 154*(2), 121-143.

Wang, J. Q., Tueckmantel, W., Zhu, A., Pellegrino, D., & Brownell, A. L. (2007). Synthesis and preliminary biological evaluation of 3-[18F]fluoro-5-(2-pyridinylethynyl)benzonitrile as a PET radiotracer for imaging metabotropic glutamate receptor subtype 5. *Synapse, 61*(12), 951-961.

Wang, J. Q., Zhang, Z., Kuruppu, D., & Brownell, A. L. (2012). Radiosynthesis of PET radiotracer as a prodrug for imaging group II metabotropic glutamate receptors in vivo. *Bioorg Med Chem Lett, 22*(5), 1958-1962.

Wang, J., Qu, X., Shoup, T. M., Yuan, G., Afshar, S., Pan, C., . . . Brownell, A.-L. (2020). Synthesis and Characterization of Fluorine-18-Labeled N-(4-Chloro-3-((fluoromethyl-d2)thio)phenyl)picolinamide for Imaging of mGluR4 in Brain. *Journal of Medicinal Chemistry, 63*(6), 3381-3389.

Wang, X., Wang, G., Lemos, J. R., & Treistman, S. N. (1994). Ethanol directly modulates gating of a dihydropyridine-sensitive Ca2+ channel in neurohypophysial terminals. *Journal of Neuroscience, 14*(9), 5453-5460.

Wanger-Baumann, C. A., Mu, L., Honer, M., Belli, S., Alf, M. F., Schubiger, P. A., . . . Ametamey, S. M. (2011). In vitro and in vivo evaluation of [18F]-FDEGPECO as a PET tracer for imaging the metabotropic glutamate receptor subtype 5 (mGluR5). *Neuroimage, 56*(3), 984-991.

Warnock, G., Sommerauer, M., Mu, L., Pla Gonzalez, G., Geistlich, S., Treyer, V., . . . Ametamey, S. M. (2018). A first-in-man PET study of [18F]PSS232, a fluorinated ABP688 derivative for imaging metabotropic glutamate receptor subtype 5. *European Journal of Nuclear Medicine and Molecular Imaging, 45*(6), 1041-1051.

Waterhouse, R. N. (2003). Determination of lipophilicity and its use as a predictor of blood-brain barrier penetration of molecular imaging agents. *Molecular Imaging and Biology, 5*(6), 376-389.

Waterhouse, R. N., Slifstein, M., Dumont, F., Zhao, J., Chang, R. C., Sudo, Y., . . . Laruelle, M. (2004). In vivo evaluation of [11C]N-(2-chloro-5-thiomethylphenyl)-N'-(3-methoxy-phenyl)-N'-methylguanidine ([11C]GMOM) as a potential PET radiotracer for the PCP/NMDA receptor. *Nuclear Medicine and Biology, 31*(7), 939-948.

Waterhouse, R. N., Sultana, A., & Laruelle, M. (2002). In vivo evaluation of [11C]-3-[2-[(3-methoxyphenylamino)carbonyl]ethenyl]-4,6-dichloroindole-2-carboxylic acid ([11C]3MPICA) as a PET radiotracer for the glycine site of the NMDA ion channel. *Nuclear Medicine and Biology, 29*(8), 791-794.

Wurzer, A., Di Carlo, D., Herz, M., Richter, A., Robu, S., Schirrmacher, R., . . . Wester, H. J. (2021). Automated synthesis of [18F]Ga-rhPSMA-7/ -7.3: results, quality control and experience from more than 200 routine productions. *EJNMMI Radiopharm Chem, 6*(1), 4.

Wyckhuys, T., Verhaeghe, J., Wyffels, L., Langlois, X., Schmidt, M., Stroobants, S., & Staelens, S. (2013). N-acetylcysteine- and MK-801-induced changes in glutamate levels do not affect in vivo binding of metabotropic glutamate 5 receptor radioligand 11C-ABP688 in rat brain. *Journal of Nuclear Medicine, 54*(11), 1954-1961.

Wyss, M. T., Ametamey, S. M., Treyer, V., Bettio, A., Blagoev, M., Kessler, L. J., . . . Buck, A. (2007). Quantitative evaluation of 11C-ABP688 as PET ligand for the measurement of the metabotropic glutamate receptor subtype 5 using autoradiographic studies and a beta-scintillator. *Neuroimage, 35*(3), 1086-1092.

Xiao, C., Shao, X. M., Olive, M. F., Griffin, W. C., 3rd, Li, K. Y., Krnjevic, K., . . . Ye, J. H. (2009). Ethanol facilitates glutamatergic transmission to dopamine neurons in the ventral tegmental area. *Neuropsychopharmacology, 34*(2), 307-318.

Xie, L., Yui, J., Fujinaga, M., Hatori, A., Yamasaki, T., Kumata, K., . . . Zhang, M. R. (2014). Molecular imaging of ectopic metabotropic glutamate 1 receptor in melanoma with a positron emission tomography radioprobe 18F-FITM. *International Journal of Cancer, 135*(8), 1852-1859.

Xu, R., Zanotti-Fregonara, P., Zoghbi, S. S., Gladding, R. L., Woock, A. E., Innis, R. B., & Pike, V. W. (2013). Synthesis and evaluation in monkey of [18F]4-fluoro-N-methyl-N-(4-(6-(methylamino)pyrimidin-4-yl)thiazol-2-yl)benzamide ([18F]FIMX): a promising radioligand for PET imaging of brain metabotropic glutamate receptor 1 (mGluR1). *Journal of Medicinal Chemistry, 56*(22), 9146-9155.

Yamasaki, T., Fujinaga, M., Maeda, J., Kawamura, K., Yui, J., Hatori, A., . . . Zhang, M. R. (2012). Imaging for metabotropic glutamate receptor subtype 1 in rat and monkey brains using PET with [18F]FITM. *European Journal of Nuclear Medicine and Molecular Imaging, 39*(4), 632-641.

Yamasaki, T., Zhang, X., Kumata, K., Zhang, Y., Deng, X., Fujinaga, M., . . . Zhang, M. R. (2020). Identification and Development of a New Positron Emission Tomography Ligand 4-(2-Fluoro-4-[11C]methoxyphenyl)-5-((1-methyl-1H-pyrazol-3-yl)methoxy)picolinamide for Imaging Metabotropic Glutamate Receptor Subtype 2 (mGlu(2)). *Journal of Medicinal Chemistry, 63*(20), 11469-11483.

Yan, Q. S., Reith, M. E., Yan, S. G., & Jobe, P. C. (1998). Effect of systemic ethanol on basal and stimulated glutamate releases in the nucleus accumbens of freely moving Sprague-Dawley rats: a microdialysis study. *Neuroscience Letters, 258*(1), 29-32.

Yanamoto, K., Konno, F., Odawara, C., Yamasaki, T., Kawamura, K., Hatori, A., . . . Zhang, M. R. (2010). Radiosynthesis and evaluation of [11C]YM-202074 as a PET ligand for imaging the metabotropic glutamate receptor type 1. *Nuclear Medicine and Biology, 37*(5), 615-624.

Yu, M., Tueckmantel, W., Wang, X., Zhu, A., Kozikowski, A. P., & Brownell, A. L. (2005). Methoxyphenylethynyl, methoxypyridylethynyl and phenylethynyl derivatives of pyridine: synthesis, radiolabeling and evaluation of new PET ligands for metabotropic glutamate subtype 5 receptors. *Nuclear Medicine and Biology, 32*(6), 631-640.

Yuan, G., Dhaynaut, M., Guehl, N. J., Afshar, S., Huynh, D., Moon, S. H., . . . Brownell, A. L. (2022a). Design, Synthesis, and Characterization of [18F]mG2P026 as a High-Contrast PET Imaging Ligand for Metabotropic Glutamate Receptor 2. *Journal of Medicinal Chemistry, 65*(14), 9939-9954.

Yuan, G., Dhaynaut, M., Guehl, N. J., Neelamegam, R., Moon, S. H., Qu, X., . . . Brownell, A. L. (2023). PET imaging studies to investigate functional expression of mGluR2 using [11C]mG2P001. *Journal of Cerebral Blood Flow and Metabolism, 43*(2), 296-308.

Yuan, G., Dhaynaut, M., Lan, Y., Guehl, N. J., Huynh, D., Iyengar, S. M., . . . Brownell, A. L. (2022b). Synthesis and Characterization of 5-(2-Fluoro-4-[11C]methoxyphenyl)-2,2-dimethyl-3,4-dihydro-2H-pyrano[2,3-b]pyridine-7-carboxamide as a PET Imaging Ligand for Metabotropic Glutamate Receptor 2. *Journal of Medicinal Chemistry, 65*(3), 2593-2609.

Yuan, G., Jones, G. B., Vasdev, N., & Liang, S. H. (2016). Radiosynthesis and preliminary PET evaluation of 18F-labeled 2-(1-(3-fluorophenyl)-2-oxo-5-(pyrimidin-2-yl)-1,2-dihydropyridin-3-yl)benzonitrile for imaging AMPA receptors. *Bioorg Med Chem Lett, 26*(19), 4857-4860.

Yuan, G., Qu, X., Zheng, B., Neelamegam, R., Afshar, S., Iyengar, S., . . . Brownell, A. L. (2020). Design, Synthesis, and Characterization of Benzimidazole Derivatives as Positron Emission Tomography Imaging Ligands for Metabotropic Glutamate Receptor 2. *Journal of Medicinal Chemistry, 63*(20), 12060-12072.

Yuksel, C., & Ongur, D. (2010). Magnetic resonance spectroscopy studies of glutamate-related abnormalities in mood disorders. *Biological Psychiatry, 68*(9), 785-794.

Zanotti-Fregonara, P., Barth, V. N., Zoghbi, S. S., Liow, J. S., Nisenbaum, E., Siuda, E., . . . Innis, R. B. (2013). 11C-LY2428703, a positron emission tomographic radioligand for the metabotropic glutamate receptor 1, is unsuitable for imaging in monkey and human brains. *EJNMMI Res, 3*(1), 47.

Zanotti-Fregonara, P., Xu, R., Zoghbi, S. S., Liow, J. S., Fujita, M., Veronese, M., . . . Innis, R. B. (2016). The PET Radioligand 18F-FIMX Images and Quantifies Metabotropic Glutamate Receptor 1 in Proportion to the Regional Density of Its Gene Transcript in Human Brain. *Journal of Nuclear Medicine, 57*(2), 242-247.

Zhang, X., Kumata, K., Yamasaki, T., Cheng, R., Hatori, A., Ma, L., . . . Liang, S. H. (2017). Synthesis and Preliminary Studies of a Novel Negative Allosteric Modulator, 7-((2,5-Dioxopyrrolidin-1-yl)methyl)-4-(2-fluoro-4-[11C]methoxyphenyl) quinoline-2-carboxamide, for Imaging of Metabotropic Glutamate Receptor 2. *ACS Chemical Neuroscience, 8*(9), 1937-1948.

Zimmer, E. R., Parent, M. J., Leuzy, A., Aliaga, A., Aliaga, A., Moquin, L., . . . Rosa-Neto, P. (2015). Imaging in vivo glutamate fluctuations with [11C]ABP688: a GLT-1 challenge with ceftriaxone. *Journal of Cerebral Blood Flow and Metabolism, 35*(7), 1169-1174.

Zuo, G. C., Yang, J. Y., Hao, Y., Dong, Y. X., & Wu, C. F. (2007). Ethanol and acetaldehyde induce similar changes in extracellular levels of glutamate, taurine and GABA in rat anterior cingulate cortex. *Toxicology Letters, 169*(3), 253-258.